12-2014

Allosteric Regulation of Bacterial and Fungal Xylulose 5-phosphate/ Fructose 6-phosphate Phosphoketolases (Xfps)

Katie Glenn
Clemson University, kglenn456@gmail.com

ALLOSTERIC REGULATION OF BACTERIAL AND FUNGAL XYLULOSE 5-PHOSPHATE/FRUCTOSE 6-PHOSOPHATE PHOSPHOKETOLASES (XFPs)

A Dissertation
Presented to
the Graduate School of
Clemson University

In Partial Fulfillment
of the Requirements for the Degree
Doctor of Philosophy
Biochemistry and Molecular Biology

---

by
Katie Frances Glenn
December 2014

Accepted by
Kerry S. Smith, Committee Chair
William R. Marcotte, Jr.
James C. Morris
Kimberly S. Paul

ABSTRACT

Acetate is excreted as a metabolic end product in many microbes. Acetate production has primarily been studied in bacteria and archaea but is known to occur in eukaryotic organisms as well. For example, acetate is one of the most abundant metabolites excreted by the fungal pathogen *Cryptococcus neoformans* during cryptococcosis suggesting that acetate production may be important during pathogenesis. One possible pathway for acetate production in *C. neoformans* involves the enzymes xylulose 5-phosphate/ fructose 6-phosphate phosphoketolase (Xfp), which can generate acetyl phosphate from either fructose 6-phosphate (F6P) or xylulose 5-phosphate (X5P), and acetate kinase (Ack), which can then convert acetyl phosphate to acetate. *C. neoformans* has an *ACK* and two *XFP* open reading frames that we've designated as *XFP1* and *XFP2*, and several studies indicate that these transcripts are expressed and/or upregulated under infectious conditions. However, until now, the Xfp-Ack pathway in *C. neoformans* has not been studied.

Here I describe the first characterization of a eukaryotic Xfp, the *C. neoformans* Xfp2. *C. neoformans* Xfp2 was found to display both substrate cooperativity and allosteric regulation. *C. neoformans* Xfp2 showed positive cooperativity in regards to F6P and X5P binding and negative cooperativity for P_i binding. Activity was inhibited by ATP, phosphenolpyruvate (PEP), oxaloacetic acid (OAA) and glyoxylate and activated by AMP. Both PEP and OAA were found to bind at the same or possess overlapping allosteric sites on the enzyme.

Prior to this characterization of *C. neoformans* Xfp2 the only other phosphoketolases characterized have been from bacteria, and none report the presence of substrate cooperativity or allosteric regulation. Therefore, *Lactobacillus plantarum* Xfp was re-characterized to determine if the enzyme showed substrate cooperativity and/or allosteric regulation. *L. plantarum* Xfp displayed negative cooperativity for P_i binding and was also allosterically inhibited by PEP, OAA and glyoxylate, but activity was unaffected by the presence of AMP or ATP. Like *C. neoformans* Xfp2, PEP and OAA were found to share the same or overlapping allosteric sites on *L. plantarum* Xfp. This study proved that substrate cooperativity and allosteric regulation exist for at least some bacterial Xfps.

Models of *C. neoformans* Xfp2 monomer and dimer were generated from existing bacterial Xfp crystal structures. Since bacterial and eukaryotic Xfps may share the PEP/OAA allosteric site, ligand docking simulations were performed with PEP and OAA in various proposed binding sites on the *C. neoformans* Xfp2 model. Site-directed mutagenesis was performed on residues predicted to hydrogen bond with PEP and OAA within these sites. However, these studies have yet to reveal the location of the PEP/OAA allosteric site. More recently the Xfp2 dimer model has revealed new sites formed between monomers that could serve as the PEP/OAA allosteric site.

DEDICATION

I would like to dedicate this dissertation to my mother, Cathy, father, Gary, and sister, Hannah. I feel blessed to have such a close, loving family. I am grateful for all of their support through this long and difficult journey. None of my accomplishments would have been possible without them. To mom, dad and Hannah: I love you very much and thank you for all that you do.

ACKNOWLEDGMENTS

First I would like to thank my advisor Dr. Kerry Smith for his guidance and support throughout these years. He showed enormous faith in me by accepting me directly into his lab, and I have been very grateful for this opportunity. I would also like to thank Dr. Cheryl Ingram-Smith for all of her assistance, insight, and knowledge which have been essential to my transition into biochemistry research.

I also thank my committee members Dr. Jim Morris, Dr. Bill Marcotte, and Dr. Kim Paul. I have appreciated all of your advice and support throughout my graduate career here at Clemson University.

I thank all former and present lab members of both the Smith and Ingram-Smith labs for their assistance and advice in matters of science and life, particularly Tonya Taylor, Grace Kisirkoi, Jessica Tumolo, Ann Guggisberg and Dr. Matt Fowler from the Smith lab and Cheryl Jones and Thanh Dang from the Ingram-Smith lab. You have all made graduate school a much more pleasant and enjoyable experience. I must give a special thank you to Tonya Taylor who has been by my side as my friend and comrade in the Smith lab literately from the very beginning of this journey.

I would also like to thank the faculty, graduate students and staff of both the Genetics and Biochemistry Department of Clemson University and the Eukaryotic Pathogens Innovation Center. You have all contributed in many ways to my success in this program, and I am thankful to be associated with such wonderful colleagues.

Finally I thank my family (mom, dad and sister) and friends (especially my PC girls). Without your love and support I would have never made it this far. I am blessed to have each and every one of you in my life.

TABLE OF CONTENTS

PAGE

TITLE PAGE i

ABSTRACT ii

DEDICATION iv

ACKNOWLEDGMENTS v

LIST OF TABLES ix

LIST OF FIGURES x

CHAPTER

I. LITERATURE REVIEW 1

Introduction 1
Acetate Production 3
Xylulose 5-phosphate/Fructose 6-phosphate Phosphoketolase (Xfp) 12
Cryptococcus neoformans 15
Possible Roles of Acetate Producing Pathways in Fungi 19
References 23

II. BIOCHEMICAL AND KINETICH CHARACTERIZATION OF XYLULOSE 5-PHOSPHATE FRUCTOSE 6-PHOSPHATE PHOSPHOKETOLASE 2 (XFP2) FROM *CRYPTOCOCCUS NEOFORMANS* 40

Abstract 40
Introduction 42
Materials and Methods 44
Results 47
Discussion 52
Acknowledgments 57
References 58

III. ALLOSTERIC REGULATION OF LACTOBACILLUS PLANTARUM XYLULOSE 5-PHOSPHATE/ FRUCTOSE 6-PHOSPHATE PHOSPHOKETOLASE 70

Table of Contents (Continued)

Abstract 70
Introduction 72
Materials and Methods 74
Results 78
Discussion 84
Acknowledgments 89
References 90

IV. INVESTIGATIONS INTO THE LOCATION OF C. NEOFORMANS XFP2 ALLOSTERIC SITES THROUGH COMPUTATIONAL MODELING AND SITE-DIRECTED MUTAGENESIS 99

Abstract 99
Introduction 101
Materials and Methods 103
Results 106
Discussion 113
Acknowledgments 118
References 119

V. CONCLUSIONS 135

APPENDICES 140

A. A MUTATION OF CRE1 IN MEDICAGO TRUNCATULA THAT SUPPRESSES SUPERNODULATION AND ROOT GROWTH WITH MINIMAL EFFECT ON CYTOKIN RESPONSES 140

LIST OF TABLES

Table		Page
1.1	Kinetic parameters for *B. breve* Xfp wild type and variants	31
2.1	Apparent kinetic parameters for *C. neoformans* Xfp2	61
2.2	Half maximal inhibitory (IC_{50}) concentrations	62
3.1	Apparent kinetic parameters for *L. plantarum* Xfp and *C. neoformans* Xfp2	92
3.2	Half maximal inhibitory concentrations (IC_{50}s)	93
4.1	*C. neoformans* Xfp2 enzyme variants	121
4.2	Apparent kinetic parameters for *C. neoformans* Xfp2 R66A variant	122

LIST OF FIGURES

Figure		Page
1.1	*S. enterica* PtaII function and regulation	32
1.2	Glucose fermentation in *Lactobacillus plantarum*	33
1.3	Xfp reaction mechanism	34
1.4	Crystal structure of B. breve Xfp homodimer (A) and monomer (B) with bound TPP	35
1.5	Comparison of the estimated number of deaths in Sub-Saharan Africa due to various infectious diseases	36
1.6	Infection pathway of *Cryptococcus neoformans* from the environment to the host	37
1.7	Sources of acetate in *C. neoformans*	38
1.8	Comparison of *C. neoformans* WT, Acs1 deletion (*acs1*), and Acs1 recomplementation (*acs1 + ACS1*) strains	39
2.1	Optimization of Xfp2 reaction conditions	63
2.2	Effect of various ligands on Xfp2 activity	64
2.3	Effect of ATP on substrate progress curves	65
2.4	Effect of PEP on substrate progress curves	66
2.5	Effect of OAA on substrate progress curves	67
2.6	Effect of AMP on substrate progress curves	68
2.7	AMP activates Xfp2 activity and alleviates inhibition by allosteric inhibitors	69
3.1	Effect of pH on *L. plantarum* Xfp and *C. neoformans* Xfp2 percent activity	94
3.2	Effect of various ligands on *L. plantarum* Xfp activity	95

List of Figures (Continued)

Figure Page

3.3 Effect of non-phosphorylated PEP analogs on *L. plantarum* Xfp (A) and C. neoformans Xfp2 (B) activity 96

3.4 Inhibition of L. plantarum Xfp by OAA, PEP and glyoxylate 97

3.5 Effect of PEP on L. plantarum Xfp substrate progress curves 98

4.1 Model of C. neoformans Xfp2 monomer 123

4.2 Location of the predicted PEP binding sites 13 and 35 124

4.3 AMP activation of *C. neoformans* Xfp2 R66A variant 125

4.4 Effect of PEP on *C. neoformans* Xfp2 R66A variant activity in the presence of AMP 126

4.5 Model predicting structural effects of R66A mutation 127

4.6 Effect of pH on *C. neoformans* Xfp2 activity in the presence and absence of AMP 128

4.7 Location of sites on the *C. neoformans* Xfp2 model in which PEP interacts with arginine residues 129

4.8 *C. neoformans* Xfp2 dimer model 130

4.9 Effect of adenosine and AMP-PCP on *C. neoformans* Xfp2 activity compared to ATP inhibition 131

4.10 Effect of AMP-PCP on *C. neoformans* Xfp2 activity at pH 5.5 (grey) and pH 7.0 (black) 132

4.11 Effect of the presence of both AMP-PCP and ATP on *C. neoformans* Xfp2 activity 133

4.12 Location of R571 residue on the *C. neoformans* Xfp2 dimer model 134

5.1 Model of how Xfp2 fits into C. neoformans cellular metabolism 139

List of Figures (Continued)

Figure Page

A.1 The amino acid change in the *cre1-4* mutant does not effect the cytokinin binding pocket.....143

CHAPTER 1

LITERATURE REVIEW OF XYLULOSE 5-PHOSPHATE/ FRUCTOSE 6-PHOSPHATE PHOSPHOKETOLASES FROM BACTERIA AND FUNGI

I. INTRODUCTION

Acetate is excreted from the cell as a metabolic end product in many microbes of the Bacteria, Archaea and Eukarya. Acetate excretion allows for the regeneration of NAD^+ consumed during glycolysis, recycling of coenzyme A (CoASH) required for generating the central metabolic intermediate acetyl-CoA, and production of ATP under conditions in which the TCA cycle is not fully operational (1). However, extracellular acetate dissociates, posing a problem to the cell by acidifying the surrounding environment, but one way the cell can overcome this problem is by importing extracellular acetate and utilizing it as a carbon source (2,3). Therefore, cells must maintain a balance between acetate excretion and utilization. The studies presented in this dissertation suggest that the regulation of this process is far more complex than anticipated.

The primary pathways for acetate production in bacteria typically involve the enzyme acetate kinase (Ack) which converts acetyl phosphate to acetate and energy in the form of ATP (4). Ack primarily partners with the acetyl phosphate producing

enzyme phosphotransacetylase (Pta), found in bacteria, one genus of methane producing archaea, and green algae, which generates acetyl phosphate from excess acetyl-CoA. Ack can also partner with xylulose 5-phosphate/ fructose 6-phosphate phosphoketolase (Xfp), which is found in lactic acid bacteria and fungi that generate acetyl phosphate from pentose phosphate pathway end products xylulose 5-phosphate (X5P) or fructose 6-phosphate (F6P) (4). Additionally, both the Pta-Ack and Xfp-Ack pathways provide mechanisms for controlling cellular concentrations of acetyl-phosphate, which plays an important role in signal transduction (1). Some bacteria including *Escherichia coli* have an acetate forming pyruvate oxidase (PoxB) that generates acetate from pyruvate (1).

Most studies of enzymes involved in acetate production have been in bacteria. However, acetate is a major metabolic end product in eukaryotic microbes as well, and many of the enzymes and pathways involved in acetate production in bacteria can be found in eukaryotic organisms (4-6). This chapter begins with a review of acetate production in bacteria, archaea, and eukaryotes. Literature describing acetate production via the Xfp-Ack pathway (which until now had not been studied in eukaryotic microbes) will be focused on in this chapter and is the central theme throughout this dissertation. Also, a brief overview will be given on the pathogenic fungus *Cryptococcus neoformans* highlighting evidence of the utilization of the Xfp-Ack pathway during cryptococcal infections.

II. ACETATE PRODUCTION

Acetate Production in Bacteria

Many studies have focused on the production and utilization of acetate in bacteria. Bacterial cells perform what is referred to as the "acetate switch" in which cells transition from a condition of rapid growth, where acetate is excreted, to a period of slow growth following the depletion of essential carbon sources, where cells begin to scavenge, import and utilize acetate as a carbon source, allowing growth to continue (1). Acetogenesis, the excretion of acetate, occurs as a result of the needs to regenerate coenzyme A (CoASH) for acetyl-CoA production and NAD^+ for glycolysis, and it provides a mechanism for generating ATP under conditions in which the TCA cycle is not fully functioning (1). The accumulation of both intracellular and extracellular acetate can be toxic to the cell (2,3). Therefore, it is essential for cells to maintain a proper balance between the benefits of acetate production and excretion and the uptake and utilization of acetate as a carbon source when necessary.

E. coli produces acetate aerobically during periods of rapid growth on glucose, which ultimately inhibits respiration, and anaerobically during mixed-acid fermentation (1,7). Acetate is produced in *E. coli* through a pathway involving Pta (EC 2.3.1.8; Eq. 1.1]) and Ack (EC 2.7.2.1; Eq. 1.2) (1,4,8) or by the enzyme pyruvate oxidase (PoxB, EC 1.2.5.1; Eq. 1.3) (1). In the absence of oxygen the Pta-Ack pathway also serves as a source of ATP when a branched form of the tricarboxylic acid (TCA) cycle is utilized

that does not generate energy (1). Deletion of the Pta-Ack pathway in *E. coli* results in highly reduced acetate production but increased levels of formate and lactate (3) while deletion of PoxB primarily causes a reduction in biomass and growth efficiency under aerobic conditions (3,9) . Therefore, the Pta-Ack pathway primarily contributes to acetate production during anaerobic fermentation while PoxB functions primarily under aerobic conditions. In addition to redirecting acetyl-CoA overflow and generating ATP under hypoxic conditions, the Pta-Ack pathway also serves as the primary influence over intracellular acetyl phosphate concentrations. Acetyl phosphate is a high-energy form of phosphate that plays important roles in signal transduction (1,10,11). For example, signal transduction in bacteria often involves a two component signal transduction pathway. These two component signaling pathways typically involve the phosphorylation of a histidine kinase that in turn phosphorylates various response regulators resulting in the activation of the signaling pathway process (12-14). It has been shown that acetyl phosphate can act as the phosphoryl donor for two component response regulators via direct phosphoryl transfer (14). Additionally, acetyl phosphate has been found to regulate other important bacterial processes such as biofilm development (11) and flagellar expression (15).

$$\text{acetyl-CoA} + P_i \leftrightarrow \text{CoA} + \text{acetyl phosphate} \qquad \text{[Eq. 1.1]}$$

$$\text{acetyl phosphate} + \text{ADP} \leftrightarrow \text{acetate} + \text{ATP} \qquad \text{[Eq. 1.2]}$$

$$\text{pyruvate} + \text{ubiquinone} + H_2O \rightarrow \text{acetate} + \text{ubiquinol} + CO_2 \qquad \text{[Eq. 1.3]}$$

In addition to Pta, Ack can also partner with Xfp in lactic acid bacteria (16) and bifidobacteria (17). Xfp generates acetyl phosphate from the pentose phosphate pathway end products X5P (EC 4.1.2.9; Eq. 1.4) and F6P (EC 4.1.2.22; Eq. 1.5) which can then be converted to acetate and ATP by Ack (Eq. 1.2) (4,17). The Xfp-Ack pathway will be discussed in greater detail later on in this chapter. Other enzymes that produce the Ack substrate acetyl phosphate include glycine reductase (EC 1.21.4.2; Eq. 1.6), and related enzymes sarcosine reductase (EC 1.21.4.3) and betaine reductase (EC 1.21.4.4), sulfoacetaldehyde acetyltransferase (Xsc; EC 2.3.3.15; Eq. 1.7), and acetyl phosphate forming pyruvate oxidase (Pox; EC 1.2.3.3; Eq. 1.8). These enzymes are present in various bacteria but are not found in *E. coli*, archaea, or eukaryotes.

xylulose 5-phosphate + P_i → acetyl phosphate + glyceraldehyde 3-phosphate [Eq. 1.4]

fructose 6-phosphate + P_i → acetyl phosphate + erythrose 4-phosphate [Eq. 1.5]

glycine + P_i + thioredoxin → acetyl phosphate + NH_3 + thioredoxin disulfide [Eq. 1.6]

2-sulfoacetaldehyde + P_i → acetyl phosphate + sulfite [Eq. 1.7]

pyruvate + P_i + O_2 → acetyl phosphate + CO_2 + H_2O_2 [Eq. 1.8]

Acetate Production in Archaea

The Pta-Ack pathway is also found in one genera of methane producing archaea, *Methanosarcina*, where acetate is utilized to produce methane (18). It has been shown in *Methanosarcina thermophila* that Ack and Pta are produced in greater quantities in cells grown on acetate versus methanol (19,20). Since *M. thermophila* is a thermophile, the

Ack and Pta enzymes from this organism have been shown to be active at temperatures up to 70°C, but activity is greatly reduced at higher temperatures (19,20). Additionally, gene knockouts of either Ack or Pta in *Methanosarcina acetivorans* prevents growth on acetate and carbon monoxide suggesting that both Ack and Pta are essential (21). Therefore, in *Methanosarcina* the Pta-Ack pathway primarily acts in the direction of acetate activation to acetyl-CoA rather than acetate production (22). However, acetate and formate rather than methane are the primary metabolic end products of *M. acetivorans* grown on carbon monoxide suggesting that under this condition the Pta-Ack pathway acts in the direction of acetate and ATP production (21).

Pyrococcus furiosus, a hyperthermophilic archaeon, has an ADP-forming acetyl-CoA synthetase (Acd; EC 6.2.1.13; Eq. 1.9) that catalyzes, under physiological conditions, the reversible conversion of acetyl-CoA to acetate and ATP (23). *P. furiosus* can grow at temperatures up to 105°C, and Acd from this organism shows optimal activity at 90°C. In addition to acetyl-CoA, Acd can also utilize propionyl-CoA (100%) and butyrl-CoA (92%) as substrates (23). Acd was first described in *P. furiosus* but has since been discovered and characterized in some other archaea, including *Archaeoglobus fulgidus* (24), *Methanococcus jannaschii* (24), *Haloarcula marismortui* (25) and *Pyrobaculum aerophilum* (25).

$$\text{acetyl-CoA} + P_i + \text{ADP} \rightarrow \text{acetate} + \text{ATP} + \text{CoA} \qquad \text{[Eq. 1.9]}$$

Acetate Production in Eukarya

Ack and partner enzymes were originally thought to exist only in bacteria and one genus of methane-producing archaea, but have more recently been identified in eukaryotic organisms as well (4,26). The Pta-Ack pathway has been discovered in green algae and the oomycete *Phytophthora* (4) but has thus far only been studied in the green alga *Chlamydomonas*. Acetate is a major fermentation product of *Chlamydomonas* grown under dark, anoxic conditions (27). *C. reinhardtii* has two Pta-Ack pathways, and it has been suggested that one may function in the direction of acetate activation while the other functions in the direction of acetate production (4), though more recent evidence contradicts this hypothesis (27). *Chlamydomonas* RNA levels of Ack1, Ack2, Pta1 and Pta2 are increased following growth in dark, anaerobic conditions suggesting they are involved in the production of acetate and ATP under these conditions (27). More recently, it has been discovered that Ack1 and Pta2 are localized to chloroplasts while Ack2 and Pta1 are localized to the mitochondria (Yang et al. Plant Cell *in press*). A reduction of excreted metabolites was observed in all of the double and single mutations of these enzymes except for an *ack2* single mutant suggesting that the *C. reinhardtii* chloroplast play the dominant role in acetate production under dark anoxic conditions. A double mutation of *ack1ack2* showed no acetate kinase activity; however acetate was still produced and excreted under anoxic conditions suggesting the presence of other acetate producing pathways in this organism (Yang et al., Plant Cell, in press). Additionally, none of the *C. reinhardtii* ack/pta knockouts show a growth defect on acetate suggesting

that neither of the two Pta-Ack pathways contribute to acetate utilization (Yang et al., Plant Cell, in press) as previously suggested (4).

Even though *ACK* open reading frames (ORFs) have been identified in both euascomycete and basidiomycete fungi, a *PTA* ORF has yet to be found (4). Instead, all fungi with a *ACK* ORF have at least one and in some cases two *XFP* ORFs suggesting that Ack partners with Xfp in fungi as in lactic acid bacteria and *Bifidobacteria* (4). Additionally, fungi can generate acetate from pyruvate via the pyruvate dehydrogenase bypass utilizing the enzymes pyruvate decarboxylase (Pdc; EC 4.1.1.1; Eq. 1.10) and acetaldehyde dehydrogenase (Ald; EC 1.2.1.5; Eq. 1.11) (28,29). A deletion of the acetaldehyde dehydrogenase genes *ALD6* and *ALD5* in *Saccharomyces cerevisiae* significantly decreases acetate production during anaerobic growth on glucose (29). Some fungi may also produce acetate using the AMP-forming acetyl-CoA synthetase (Acs; EC 6.2.1.1: Eq 1.12). In *Salmonella enterica* Acs activity is regulated through post translational modification of Lys609. Acetylation of this lysine residue reduced activity while activation of the acetylated enzyme required deacetylation by CobB, an NAD^+ dependent deacetylase of the sirtuin (Sir2) family (30). The same *S. enterica* Acs lysine residue is conserved in the fungal *Aspergillus nidulans* Acs. Analysis of Acs purified from *A. nidulans* under both aerobic and anaerobic conditions showed that under anaerobic conditions Acs had a higher kinetic affinity (K_m) for acetate over acetyl-CoA. Immunoblotting analysis of Acs from *A. nidulans* grown under anaerobic conditions with an anti-acetyl-lysine antibody showed it is acetylated on lysine residues, but the identity

of the acetylated lysine was not reported (31). Therefore, *A. nidulans* Acs may function in the direction of acetate production upon acetylation under anaerobic conditions (31)

$$\text{pyruvate} \rightarrow \text{acetaldehyde} + CO_2 \qquad \text{[Eq. 1.10]}$$

$$\text{acetaldehyde} + NADP^+ \rightarrow \text{acetate} + NADPH + H^+ \qquad \text{[Eq. 1.11]}$$

$$\text{acetate} + ATP + CoA \leftrightarrow \text{acetyl-CoA} + AMP + PP_i \qquad \text{[Eq. 1.12]}$$

Acd, originally identified in thermophilic archaea, which can generate acetate from acetyl-CoA (Eq. 1.9), has been found in two amitochondriate protists, *Giardia lamblia* and *Entamoeba histolytica* (32). *G. lamblia* Acd functions primarily in the direction of acetate formation, and despite utilizing various assays, acetyl-CoA forming activity has yet to be detected. Enzymatic properties of Acd indicate that it serves as a primary source of ATP in *G. lamblia* (32). Native *E. histolytica* Acd has also been characterized and found to require the presence of P_i, ADP and a divalent metal cation for activity. *E. histolytica* Acd prefers magnesium, iron or manganese for the divalent metal cation, and is unable to utilize AMP and PP_i in place of ADP and P_i (33).

Additional sources of acetate, other than those previously mentioned, have been identified in some parasitic helminthes (34), protists (34) and algae (35). An acetate:succinate CoA transferase (Asct; EC 2.8.3.8; Eq. 1.13), identified in some protists, including *Fasciola hepatica*, *Trichomonas vaginalis*, and *Trypanosoma brucei*, is responsible for acetate production in mitochondria-like organelles (34). Additionally

some eukaryotic microbes contain an acyl-CoA hydrolase (Ach; EC 3.1.2.1; Eq. 1.14), which has been found to be responsible for acetate production in peroxisomes (34,35).

acetyl-CoA + succinate → acetate + succinyl-CoA [Eq. 1.13]

acetyl-CoA + H_2O → acetate + CoA [Eq. 1.14]

Regulation of Acetate Producing Pathways

In some bacteria it has been shown that the Ack partner enzyme Pta is allosterically regulated. Allosteric enzymes are regulated by the binding of ligands that induce a conformational change influencing substrate binding and catalysis (36). There are two types of Pta enzymes designated as PtaI and PtaII. Only PtaII enzymes exhibit allosteric regulation. PtaII enzymes consist of two domains while PtaI has only one domain. Both PtaIs and PtaIIs share homology in their C-terminal domains, which contains the substrate binding site. The N-terminal domain, present in PtaII but not in PtaI, is the primary contributor to PtaII allostery (37,38). The allosteric nature of Pta has primarily been explored in *E. coli* (37) and *S. enterica* (38). In the direction of acetyl phosphate production, *E. coli* PtaII is inhibited by NADH and ATP and activated by pyruvate and phosphoenolpyruvate (PEP) (37). In the acetyl phosphate forming direction *S. enterica* PtaII is inhibited by NADH and ATP and activated by pyruvate, and studies suggest that the N-terminal domain serves as a sensor for these two ligands (38). The intricate regulation of Pta, as demonstrated in Figure 1.1 showing the influences and effects of *S. enterica* PtaII regulation as it fits with overall cellular metabolism (38), suggests that PtaII serves as an important sensor of cellular energy status.

Most of the characterized Ack enzymes have been shown to follow standard Michaelis-Menten kinetics; however a few studies suggest the presence of substrate cooperativity and allosteric regulation (39,40). An older study from 1979 stated that *Bacillus stearothermophilus* Ack displayed sigmoidal kinetics for ATP binding in the direction of acetyl phosphate formation, but this enzyme did not display sigmoidal kinetics for substrates in the direction of acetate formation (39). Additionally, *B. stearothermophilus* Ack activity in the acetyl phosphate forming direction was activated in the presence of fructose 1,6-bisphosphate (39). Very recently, both Ack enzymes (designated as AckA1 and AckA2) from *Lactococcus lactis* were reported to be allosterically regulated (40). In the direction of acetate formation, both *L. lactis* AckA1 and AckA2 are inhibited by fructose 1,6-bisphosphate with half maximal inhibitory concentrations (IC_{50}) of 17 mM and 43 mM, respectively. The cleavage of fructose 1,6-bisphosphate that occurs during glycolysis results in the products glyceraldehyde 3-phosphate (G3P) and dihydroxyacetone phosphate (DHAP). While DHAP had little effect on AckA1 and AckA2 activity, G3P inhibited both enzymes, but it inhibited AckA1 to a greater extent than AckA2. Additionally, the downstream glycolysis intermediate PEP inhibits both AckA1 and AckA2 with IC_{50}s of 15 mM and 18 mM, respectively (40). The authors conclude that allosteric control of AckA1 and AckA2 by major glycolytic intermediates provides a mechanism by which *L. lactis* can instantaneously switch between homolactic and mixed acid fermentation depending on the availability of quickly or slowly metabolized carbohydrate sources (40).

III. XYLULOSE 5-PHOSPHATE/ FRUCTOSE 6-PHOSPHATE PHOSPHOKETOLASE (XFP)

Xylulose 5-phosphate/ fructose 6-phosphate phosphoketolase (Xfp) is a thiamine pyrophosphate (TPP)-dependent enzyme that catalyzes the conversion of P_i and xylulose 5-phosphate (X5P) or fructose 6-phosphate (F6P) to acetyl phosphate and glyceraldehyde 3-phosphate (G3P) or erythrose 4-phosphate (E4P), respectively. Xfp functions as a key enzyme of the phosphoketolase pathway in lactic acid bacteria, shown in Figure 1.2, (41) and the fructose 6-phosphate shunt in bifidobacteria (17). Xfp was originally thought to exist only in bacteria, but *XFP* ORFs have more recently been identified in euscomycete and basidiomycete fungi as well (4). Until now only Xfp from bacteria have been biochemically and kinetically characterized. Native Xfp from *Bifidobacterium animalis* (17) along with recombinant Xfp from *Lactobacillus plantarum* (16), *Bifidobacterium breve* (42), *Lactococcus lactis* (43), *Leuconostoc mesenteroides* (43) and *Pseudomonas aeruginosa* (43) have been purified and characterized. All of these bacterial enzymes were reported to follow Michaelis-Menten kinetics and were found to possess dual substrate specificity for both F6P and X5P. Most bacterial Xfps, with the exception of *B. animalis* Xfp (17), display higher affinity for the substrate X5P over F6P (16,43) (kinetic parameters for X5P were not reported for *B. breve* Xfp).

An Xfp reaction mechanism originally proposed by Yevenes *et al.* (16) for *L. plantarum* Xfp has since been supported by the structure analysis of *B. longum* Xfp (44).

Yevenes *et al*. proposed that Xfp follows a ping pong bi bi kinetic mechanism depicted in Figure 1.3 (16). In this mechanism, the phosphoketose substrate, in this case X5P, first interacts with enzyme bound TPP. The TPP-X5P intermediate forms enzyme bound 2-α,β-dihydroxyethylidene-TPP (DHETPP) following the dissociation of G3P. DHETPP undergoes a dehydration reaction to form enzyme bound enolacetyl-TPP which undergoes ketonization to form enzyme bound 2-acetyl-thiamine pyrophosphate (AcTPP). Following nucleophilic attack by inorganic phosphate (P_i), acetyl phosphate is released, and enzyme bound TPP is free to interact with additional substrate. Interestingly the proposed reaction mechanism suggests that the formation of G3P or E4P from the substrates X5P or F6P respectively occurs in the absence of P_i.

To date only the structures of the *B. breve* Xfp (42) and the *Bifidobacterium longum* Xfp (44) have been reported. Figure 1.4 shows the dimer (a) and monomer (b) structures of *B. breve* Xfp (42). The Xfp structures show that the monomer consists of an N-terminal (PP domain), middle (PYR domain) and C-terminal domain with the active site located between the PP and PYR domain, and the minimum functional unit of the enzyme exists as a dimer. TPP binds within a deep, narrow channel in a V-conformation leaving the reactive C2 atom exposed to solvent. There are several active site residues conserved between Xfp and the related TPP dependent enzyme transketolase (TK), an enzyme of the pentose phosphate pathway that catalyzes the reversible reaction to convert X5P or ribose 5-phosphate to G3P or sedoheptulose 7-phosphate respectively. One residue, Glu479, is found in most TPP dependent enzymes and activates TPP through the formation of a hydrogen bond between the Glu479 side chain and TPP's N1' atom of

pyrimidine. Replacement of Glu479 with Ala in *B. breve* Xfp (42) or Asp in *B. longum* Xfp (44) completely abolished activity. Further analysis of conserved *B. breve* Xfp and *S. cerevisiae* TK histidine residues showed that alteration of these residues either severely reduced or completely abolished activity (Table 1.1) suggesting that at least the initial Xfp mechanism follows that of other TPP dependent enzymes (42). The Xfp reaction differs from that of TK primarily by the dehydration of DHETPP and nucleophilic attack of AcTPP by P_i neither of which occur in the TK reaction. A site is observed in the *B. breve* AcTPP intermediate Xfp structure that holds a water molecule believed to be derived from the dehydration of DHETPP. A similar site is also found in TK, but in TK this site is located at a greater distance away from the DHETPP intermediate which may be why dehydration of DHETPP in TK does not occur. Also, it has been proposed that the C-terminal domain of TK acts as a regulatory domain (45), and this could also be the case for the C-terminal domain of Xfp. In summary, studies of *B. breve* and *B. longum* Xfp active sites in comparison with the related enzyme TK from *S. cerevisiae* have provided important information on how the Xfp reaction proceeds.

IV. *CRYPTOCOCCUS NEOFORMANS*

Cryptococcus neoformans, a basidiomycete soil fungal pathogen, is the leading cause of fungal meningitis worldwide. It was clinically identified as a human pathogen in 1894. After undergoing several name changes, it was termed its current identification of *C. neoformans* around 1950 when many laboratory investigations of this organism began (46,47). The onset of the AIDS pandemic brought with it a surge of cryptococcal infections (48,49). The global burden of cryptococcal meningitis in 2006 was estimated to be around one million cases that resulted in approximately 625,000 deaths, most of which occurred in sub-Saharan Africa due to the heavy burden of HIV in this area (49). Cryptococcal meningitis causes more deaths in sub-Sarahan Africa than tuberculosis, which often receives far greater public attention (Figure 1.5) (49). Current treatments for cryptococcal infections often involve a combination of amphotericin B and fluconazole both of which target ergosterol, a component of fungal membranes not present in plants or animals. However, these drugs can exhibit potentially harmful side effects and treatment is often long term to prevent the reemergence of infection, especially in HIV patients (50).

Individuals come into contact with *C. neoformans* basidospores from environmental sources such as rotting trees and soil contaminated with bird guano, which is believed to provide a favorable growth environment for this fungus (48,51). Spores are inhaled into the lungs where they can cause an immediate infection that is often cleared

by host immune defenses, or the fungus can enter a dormant state while remaining in the host. If an individual's immune system later becomes compromised, the dormant form can re-emerge and potentially disseminate through the blood stream, cross the blood-brain barrier, and cause cryptococcal meningitis (Figure 1.6) (51). Originally *C. neoformans* was classified into four serotypes designated A, B, C and D, where serotype A was associated with *C. neoformans* var. grubii, serotype D was associated with *C. neoformans* var. *neoformans* and serotypes B and C were associated with *C. neoformans* var. *gatti* (47,51). More recently *C. neoformans* var *gatti* has been recognized as the separate species *C. gatti* (52,53). *C. neoformans* var. *grubii* and var. *neoformans* are encountered most often in isolates from infected AIDS patients (47,51). Originally considered less virulent, *C. gatti* has begun to emerge as a pathogen of even immunocompetent individuals and was the cause of a recent outbreak of cryptococcal infections on Vancouver Island in British Columbia, Canada (54). The progression of *C. gatti* as a pathogen of immunocompetent individuals is alarming considering it shares many characteristics known to contribute to pathogenicity in *C. neoformans* (55).

A number of factors have been identified that aid in *C. neoformans'* ability to combat and overcome host defenses. One factor essential for *C. neoformans* pathogenicity is its ability to grow at 37 °C, the temperature encountered during infection, which is an unusual characteristic for a soil fungus (56). For example, cryptococcal species *Cryptococcus podzolicus,* like *C. neoformans* and *C. gatti* possess other virulent attributes such as a protective capsule and melanin production, but it is incapable of growing at elevated temperatures and, therefore, does not cause infection

(56,57). *C. neoformans* is surrounded by a protective polysaccharide capsule that primarily protects the cell by limiting phagocytosis, the first line of host defense, and much research has been devoted towards understanding capsule synthesis and composition as drug targets for cryptococcal infections (58-61). Additionally, *C. neoformans* produces and excretes several extracellular enzymes such as laccase, phospholipase B, and urease that have also been shown to aid in virulence (55). Both laccase and phospholipase B are localized to the cell wall where laccase mediates melanin production and phospholipase B has been shown to aid in cell wall integrity (55). Additionally phospholipase B is secreted outside the cell and has been shown to aid in extracellular pulmonary dissemination by degrading lung surfactant and phagolysosomal membranes upon phagocytosis (55,62,63). *C. neoformans* produces large amounts of urease that catalyzes the breakdown of urea to ammonia and carbamate which may enhance central nervous system invasion (55,64,65).

In addition to mechanisms that aid in protection and defense from the hostile host environment, *C. neoformans* possesses a surprising tolerance to hostile environments as well. It has been shown that *C. neoformans* can reside inside the acidic environment of the phagolysosome of human macrophages. In fact, treatment of phagolysosomes containing *C. neoformans* with chloroquine, which increases lysosomal pH, resulted in antifungal activity, suggesting that *C. neoformans* is highly adaptable to acidic pH and less tolerant to alkaline pH (66). *C. neoformans* also produces and deposits melanin within its cell wall which provides a stable population of free radicals that is believed to confer protection from oxidative killing by macrophages (67). *C. neoformans*' ability to

reside within phagolysosomes has been proposed as a mechanism of crossing the blood brain barrier in what is termed a Trojan horse dissemination model (47). In support of the Trojan horse dissemination model, cryptococcal laden monocytes have been found in the brain suggesting that they can cross the blood brain barrier in this manner (68).

V. POSSIBLE ROLES OF ACETATE PRODUCING PATHWAYS IN FUNGI

Acetate has been identified as one of the two most abundant metabolites produced and excreted during cryptococcal infections (5,6); however, the role acetate plays particularly during infection remains unknown. In addition to the metabolic benefits of acetate production, such as the generation of ATP and regeneration of coenzyme A, there is evidence that *C. neoformans* may excrete acetate as a means of acidifying the extracellular environment. Alkaline pH has been attributed to the killing of *C. neoformans* within macrophages (66,69) suggesting that elevated pH may be harmful to *C. neoformans* cells. Additionally, the pH of cryptococcomas has been found to be between 5.4 and 5.6 in vivo (6) which could be a direct result of excreted acetate.

Several routes for acetate production exist in *C. neoformans* (Figure 1.7). The Xfp-Ack (Eq. 1.4, 1.5, and 1.1) pathway has been discovered as a possible source of acetate in basidiomycete and euscomycete fungi (4). All fungi lack Pta, therefore, Ack is believed to partner with Xfp as part of a modified pentose phosphate pathway to generate acetate from pentose phosphate pathway products X5P or F6P. Phylogenetic analysis of fungal Xfps shows that these sequences separate into two distinct clusters that have been designated as Xfp1 and Xfp2 (Ann Guggisburg, Tonya Taylor and Kerry Smith, unpublished data). All fungi that have an Ack have at least one and in some cases, such as *C. neoformans*, two Xfp ORFs (4). As with the yeast *S. cerevisiae*, acetate could be

produced in *C. neoformans* from pyruvate through the actions of Pdc (Eq. 1.10) and Ald (Eq. 1.11) (70).

Evidence for a role of an Xfp-Ack partnership in producing ATP under the hypoxic conditions encountered in infectious tissue in which oxidative phosphorylation is limited originates from RNA expression studies. Both *C. neoformans* Xfp2 and Ack have been shown to be upregulated under hypoxic conditions typically encountered in infectious tissue (71). Additionally Xfp2 has been shown to be expressed in *C. neoformans* cells collected from the lungs of infected mice; however this same study also shows elevated expression of Pdc, suggesting that the Pdc-Ald pathway could also be involved in acetate production under this condition (70). Ack has been found to be expressed in *C. neoformans* following macrophage engulfment (72) suggesting that acetate production and concomitant production of ATP by Ack may be advantageous in this harsh environment, which includes limiting oxygen and nutrient availability. All of these studies suggest that an Xfp-Ack partnership may play both an important nutritive and mechanistic role in controlling surrounding environmental conditions to aid in cell survival within infectious tissue.

Currently there have been no studies on the physiological role of Xfp in *C. neoformans*; however, a few studies provide some evidence of its role in other fungi. An Xfp2 homolog in the insect fungal pathogen *Metarhizium anisopliae* is required for full virulence (73), providing the first physiological evidence that Xfp2 may be important during fungal infections. The filamentous fungus *Aspergillus nidulans* has an Xfp1 and

Ack but no Xfp2. Overexpression of Xfp1 in *A. nidulans* resulted in increased specific growth rate on xylose, glycerol and ethanol but had no effect on growth on glucose (74). Therefore, Xfp1 was attributed to providing greater carbon metabolism flexibility in *A. nidulans* for growth on non-optimal carbon sources. The fission yeast *Schizosaccharomyces pombe* is the only yeast identified to have an Xfp, belonging to the Xfp1 family with no Ack, providing evidence of additional functions for Xfp besides acting as an Ack partner enzyme. Microarray studies have indicated increased Xfp RNA levels in *S. pombe* following exposure to environmental stresses such as oxidative stress due to hydrogen peroxide, heavy metal stress by cadmium sulfate, heat shock stress, osmotic stress by sorbitol, and alkylating stress (75). Additionally, a *S. pombe* Xfp mutant was capable of growing on rich YES (yeast extract-sucrose) medium containing glucose between 29 – 32 °C, however, the ability of this mutant to grow under stressful conditions has not been reported (76,77). As studies continue to shed light on the physiological role of acetate production and possible roles of Xfp1, Xfp2, and Ack in fungi, biochemical knowledge is lacking in regards to the function of any of these enzymes in eukaryotic organisms.

In addition to the production of acetate, the transport and utilization of acetate as an alternative carbon source is important during *C. neoformans* infection as well. The acetate transporter Ady2 along with the enzyme acetyl-CoA synthetase (Acs) have both been shown to be upregulated in *C. neoformans* cells collected from the lungs of infected mice (70), suggesting that *C. neoformans* takes up acetate and uses Acs to convert it to the central metabolic intermediate acetyl-CoA. Deletion of *C. neoformans* Acs results in

poor growth on acetate, ethanol and glycerol (Figure 1.8a). Also, Acs deletion mutants demonstrate attenuated virulence in a mouse inhalation model (Figure 1.8b) (70). Additionally, enzymes of the glyoxylate cycle, malate synthetase and isocitrate lyase, are also upregulated during infection (70,78). The primary role of the glyoxylate cycle is to produce energy from simple two carbon molecules such as acetate and ethanol when glucose availability is limiting. Further studies showed that *C. neoformans* isocitrate lyase deletion mutants were unable to grow on acetate as a sole carbon source yet demonstrated no defect in animal virulence models or a defect in growth within the macrophage. Therefore, even though glyoxylate cycle enzymes are upregulated during infection, these enzymes are not required for continued pathogenesis (78).

VI. REFERENCES

1. Wolfe, A. J. (2005) The acetate switch. *Microbiol. Mol. Biol. Rev.* **69**, 12-50

2. Peebo, K., Valgepea, K., Nahku, R., Riis, G., Õun, M., Adamberg, K., and Vilu, R. (2014) Coordinated activation of PTA-ACS and TCA cycles strongly reduces overflow metabolism of acetate in *Escherichia coli*. *Appl. Microbiol. Biotechnol.* **98**, 5131-5143

3. Valgepea, K., Adamberg, K., Nahku, R., Lahtvee, P.-J., Arike, L., and Vilu, R. (2010) Systems biology approach reveals that overflow metabolism of acetate in *Escherichia coli* is triggered by carbon catabolite repression of acetyl-CoA synthetase. *BMC Syst. Biol.* **4**, 166-179

4. Ingram-Smith, C., Martin, S. R., and Smith, K. S. (2006) Acetate kinase: not just a bacterial enzyme. *Trends Microbiol.* **14**, 249-253

5. Bubb, W. A., Wright, L. C., Cagney, M., Santangelo, R. T., Sorrell, T. C., and Kuchel, P. W. (1999) Heteronuclear NMR studies of metabolites produced by *Cryptococcus neoformans* in culture media: identification of possible virulence factors. *Magn. Reson. Med.* **42**, 442-453

6. Wright, L., Bubb, W., Davidson, J., Santangelo, R., Krockenberger, M., Himmelreich, U., and Sorrell, T. (2002) Metabolites released by *Cryptococcus neoformans* var. *neoformans* and var. *gattii* differentially affect human neutrophil function. *Microbes Infect.* **4**, 1427-1438

7. Åkesson, M., Karlsson, E. N., Hagander, P., Axelsson, J. P., and Tocaj, A. (1999) On-line detection of acetate formation in *Escherichia coli* cultures using dissolved oxygen responses to feed transients. *Biotechnol. Bioeng.* **64**, 590-598

8. el-Mansi, E. M., and Holms, W. H. (1989) Control of carbon flux to acetate excretion during growth of *Escherichia coli* in batch and continuous cultures. *J. Gen. Microbiol.* **135**, 2875-2883

9. Abdel-Hamid, A. M., Attwood, M. M., and Guest, J. R. (2001) Pyruvate oxidase contributes to the aerobic growth efficiency of *Escherichia coli*. *Microbiology* **147**, 1483-1498

10. Fredericks, C. E., Shibata, S., Aizawa, S., Reimann, S. A., and Wolfe, A. J. (2006) Acetyl phosphate-sensitive regulation of flagellar biogenesis and capsular biosynthesis depends on the Rcs phosphorelay. *Mol. Microbiol.* **61**, 734-747

11. Wolfe, A. J., Chang, D. E., Walker, J. D., Seitz-Partridge, J. E., Vidaurri, M. D., Lange, C. F., Pruss, B. M., Henk, M. C., Larkin, J. C., and Conway, T. (2003) Evidence that acetyl phosphate functions as a global signal during biofilm development. *Mol. Microbiol.* **48**, 977-988

12. West, A. H., and Stock, A. M. (2001) Histidine kinases and response regulator proteins in two-component signaling systems. *Trends Biochem. Sci.* **26**, 369-376

13. Lukat, G. S., McCleary, W. R., Stock, A. M., and Stock, J. B. (1992) Phosphorylation of bacterial response regulator proteins by low molecular weight phospho-donors. *Proc. Natl. Acad. Sci. U. S. A.* **89**, 718-722

14. Klein, A. H., Shulla, A., Reimann, S. A., Keating, D. H., and Wolfe, A. J. (2007) The intracellular concentration of acetyl phosphate in *Escherichia coli* is sufficient for direct phosphorylation of two-component response regulators. *J. Bacteriol.* **189**, 5574-5581

15. Pruss, B. M., and Wolfe, A. J. (1994) Regulation of acetyl phosphate synthesis and degradation, and the control of flagellar expression in *Escherichia coli*. *Mol. Microbiol.* **12**, 973-984

16. Yevenes, A., and Frey, P. A. (2008) Cloning, expression, purification, cofactor requirements, and steady state kinetics of phosphoketolase-2 from *Lactobacillus plantarum*. *Bioorg. Chem.* **36**, 121-127

17. Meile, L., Rohr, L. M., Geissmann, T. A., Herensperger, M., and Teuber, M. (2001) Characterization of the D-xylulose 5-phosphate/D-fructose 6-phosphate phosphoketolase gene (xfp) from *Bifidobacterium lactis*. *J. Bacteriol.* **183**, 2929-2936

18. Ferry, J. G. (1997) Enzymology of the fermentation of acetate to methane by *Methanosarcina thermophila*. *Biofactors* **6**, 25-35

19. Aceti, D. J., and Ferry, J. G. (1988) Purification and characterization of acetate kinase from acetate-grown *Methanosarcina thermophila*. Evidence for regulation of synthesis. *J. Biol. Chem.* **263**, 15444-15448

20. Lundie, L. L., Jr., and Ferry, J. G. (1989) Activation of acetate by *Methanosarcina thermophila*. Purification and characterization of phosphotransacetylase. *J. Biol. Chem.* **264**, 18392-18396

21. Rother, M., and Metcalf, W. W. (2004) Anaerobic growth of *Methanosarcina acetivorans C2A* on carbon monoxide: an unusual way of life for a methanogenic archaeon. *Proc. Natl. Acad. Sci. U. S. A.* **101**, 16929-16934

22. Ingram-Smith, C., Barber, R. D., and Ferry, J. G. (2000) The role of histidines in the acetate kinase from *Methanosarcina thermophila*. *J. Biol. Chem.* **275**, 33765-33770

23. Glasemacher, J., Bock, A. K., Schmid, R., and Schonheit, P. (1997) Purification and properties of acetyl-CoA synthetase (ADP-forming), an archaeal enzyme of acetate formation and ATP synthesis, from the hyperthermophile *Pyrococcus furiosus*. *Eur. J. Biochem.* **244**, 561-567

24. Musfeldt, M., and Schonheit, P. (2002) Novel type of ADP-forming acetyl coenzyme A synthetase in hyperthermophilic archaea: heterologous expression and characterization of isoenzymes from the sulfate reducer *Archaeoglobus fulgidus* and the methanogen *Methanococcus jannaschii*. *J. Bacteriol.* **184**, 636-644

25. Brasen, C., and Schonheit, P. (2004) Unusual ADP-forming acetyl-coenzyme A synthetases from the mesophilic halophilic euryarchaeon *Haloarcula marismortui* and from the hyperthermophilic crenarchaeon *Pyrobaculum aerophilum*. *Arch. Microbiol.* **182**, 277-287

26. Atteia, A., van Lis, R., Gelius-Dietrich, G., Adrait, A., Garin, J., Joyard, J., Rolland, N., and Martin, W. (2006) Pyruvate formate-lyase and a novel route of eukaryotic ATP synthesis in *Chlamydomonas* mitochondria. *J. Biol. Chem.* **281**, 9909-9918

27. Mus, F., Dubini, A., Seibert, M., Posewitz, M. C., and Grossman, A. R. (2007) Anaerobic acclimation in *Chlamydomonas reinhardtii* anoxic gene expression, hydrogenase induction, and metabolic pathways. *J. Biol. Chem.* **282**, 25475-25486

28. Postma, E., Verduyn, C., Scheffers, W. A., and Van Dijken, J. P. (1989) Enzymic analysis of the crabtree effect in glucose-limited chemostat cultures of *Saccharomyces cerevisiae*. *Appl. Environ. Microbiol.* **55**, 468-477

29. Saint-Prix, F., Bonquist, L., and Dequin, S. (2004) Functional analysis of the ALD gene family of *Saccharomyces cerevisiae* during anaerobic growth on glucose: the NADP+-dependent Ald6p and Ald5p isoforms play a major role in acetate formation. *Microbiology* **150**, 2209-2220

30. Starai, V. J., Celic, I., Cole, R. N., Boeke, J. D., and Escalante-Semerena, J. C. (2002) Sir2-dependent activation of acetyl-CoA synthetase by deacetylation of active lysine. *Science* **298**, 2390-2392

31. Takasaki, K., Shoun, H., Yamaguchi, M., Takeo, K., Nakamura, A., Hoshino, T., and Takaya, N. (2004) Fungal ammonia fermentation, a novel metabolic

mechanism that couples the dissimilatory and assimilatory pathways of both nitrate and ethanol. Role of acetyl CoA synthetase in anaerobic ATP synthesis. *J. Biol. Chem.* **279**, 12414-12420

32. Sanchez, L. B., and Muller, M. (1996) Purification and characterization of the acetate forming enzyme, acetyl-CoA synthetase (ADP-forming) from the amitochondriate protist, *Giardia lamblia*. *FEBS Lett.* **378**, 240-244

33. Reeves, R. E., Warren, L. G., Susskind, B., and Lo, H. S. (1977) An energy-conserving pyruvate-to-acetate pathway in *Entamoeba histolytica*. Pyruvate synthase and a new acetate thiokinase. *J. Biol. Chem.* **252**, 726-731

34. Tielens, A. G., van Grinsven, K. W., Henze, K., van Hellemond, J. J., and Martin, W. (2010) Acetate formation in the energy metabolism of parasitic helminths and protists. *Int. J. Parasitol.* **40**, 387-397

35. Atteia, A., van Lis, R., Tielens, A. G., and Martin, W. F. (2013) Anaerobic energy metabolism in unicellular photosynthetic eukaryotes. *Biochim. Biophys. Acta* **1827**, 210-223

36. Traut, T. (2008) *Allosteric regulatory enzymes*, Springer

37. Campos-Bermudez, V. A., Bologna, F. P., Andreo, C. S., and Drincovich, M. F. (2010) Functional dissection of *Escherichia coli* phosphotransacetylase structural domains and analysis of key compounds involved in activity regulation. *FEBS J.* **277**, 1957-1966

38. Brinsmade, S. R., and Escalante-Semerena, J. C. (2007) In vivo and in vitro analyses of single-amino acid variants of the *Salmonella enterica* phosphotransacetylase enzyme provide insights into the function of its N-terminal domain. *J. Biol. Chem.* **282**, 12629-12640

39. Nakajima, H., Suzuki, K., and Imahori, K. (1979) Studies on the allosteric nature of acetate kinase from *Bacillus stearothermophilus*. *J. Biochem.* **86**, 1169-1177

40. Puri, P., Goel, A., Bochynska, A., and Poolman, B. (2014) Regulation of Acetate Kinase Isozymes and Its Importance for Mixed-Acid Fermentation in *Lactococcus lactis*. *J. Bacteriol.* **196**, 1386-1393

41. Pieterse, B., Leer, R. J., Schuren, F. H., and van der Werf, M. J. (2005) Unravelling the multiple effects of lactic acid stress on *Lactobacillus plantarum* by transcription profiling. *Microbiology* **151**, 3881-3894

42. Suzuki, R., Katayama, T., Kim, B. J., Wakagi, T., Shoun, H., Ashida, H., Yamamoto, K., and Fushinobu, S. (2010) Crystal structures of phosphoketolase:

thiamine diphosphate-dependent dehydration mechanism. *J. Biol. Chem.* **285**, 34279-34287

43. Petrareanu, G., Balasu, M. C., Vacaru, A. M., Munteanu, C. V., Ionescu, A. E., Matei, I., and Szedlacsek, S. E. (2014) Phosphoketolases from *Lactococcus lactis*, *Leuconostoc mesenteroides* and *Pseudomonas aeruginosa*: dissimilar sequences, similar substrates but distinct enzymatic characteristics. *Appl. Microbiol. Biotechnol.*, 7855-7867

44. Takahashi, K., Tagami, U., Shimba, N., Kashiwagi, T., Ishikawa, K., and Suzuki, E. (2010) Crystal structure of *Bifidobacterium longum* phosphoketolase; key enzyme for glucose metabolism in Bifidobacterium. *FEBS Lett.* **584**, 3855-3861

45. Lindqvist, Y., Schneider, G., Ermler, U., and Sundström, M. (1992) Three-dimensional structure of transketolase, a thiamine diphosphate dependent enzyme, at 2.5 A resolution. *EMBO J.* **11**, 2373-2379

46. Casadevall, A., and Perfect, J. R. (1998) *Cryptococcus neoformans*, Amer Society for Microbiology

47. Sabiiti, W., and May, R. C. (2012) Mechanisms of infection by the human fungal pathogen *Cryptococcus neoformans*. *Future Microbiol.* **7**, 1297-1313

48. Idnurm, A., Bahn, Y. S., Nielsen, K., Lin, X., Fraser, J. A., and Heitman, J. (2005) Deciphering the model pathogenic fungus *Cryptococcus neoformans*. *Nat. Rev. Microbiol.* **3**, 753-764

49. Park, B. J., Wannemuehler, K. A., Marston, B. J., Govender, N., Pappas, P. G., and Chiller, T. M. (2009) Estimation of the current global burden of cryptococcal meningitis among persons living with HIV/AIDS. *AIDS* **23**, 525-530

50. Nelson, R., and Lodge, J. (2006) *Cryptococcus neoformans* pathogenicity. in *Fungal Genomics*, Springer. pp 237-266

51. Lin, X., and Heitman, J. (2006) The biology of the *Cryptococcus neoformans* species complex. *Annu. Rev. Microbiol.* **60**, 69-105

52. Kwon-Chung, K. J., Boekhout, T., Fell, J. W., and Diaz, M. (2002) (1557) Proposal to conserve the name *Cryptococcus gattii* against *C. hondurianus* and *C. bacillisporus* (Basidiomycota, Hymenomycetes, Tremellomycetidae). *Taxon.* **51**, 804-806

53. Boekhout, T., Van Belkum, A., Leenders, A. C., Verbrugh, H. A., Mukamurangwa, P., Swinne, D., and Scheffers, W. A. (1997) Molecular typing of

Cryptococcus neoformans: taxonomic and epidemiological aspects. *Int. J. Syst. Bacteriol.* **47**, 432-442

54. Kidd, S., Hagen, F., Tscharke, R., Huynh, M., Bartlett, K., Fyfe, M., Macdougall, L., Boekhout, T., Kwon-Chung, K., and Meyer, W. (2004) A rare genotype of *Cryptococcus gattii* caused the cryptococcosis outbreak on Vancouver Island (British Columbia, Canada). *Proc. Natl. Acad. Sci. U. S. A.* **101**, 17258-17263

55. Kronstad, J. W., Attarian, R., Cadieux, B., Choi, J., D'Souza, C. A., Griffiths, E. J., Geddes, J. M., Hu, G., Jung, W. H., Kretschmer, M., Saikia, S., and Wang, J. (2011) Expanding fungal pathogenesis: Cryptococcus breaks out of the opportunistic box. *Nat. Rev. Microbiol.* **9**, 193-203

56. Perfect, J. R. (2006) *Cryptococcus neoformans*: the yeast that likes it hot. *FEMS Yeast Res.* **6**, 463-468

57. Petter, R., Kang, B., Boekhout, T., Davis, B., and Kwon-Chung, K. (2001) A survey of heterobasidiomycetous yeasts for the presence of the genes homologous to virulence factors of *Filobasidiella neoformans*, CNLAC1 and CAP59. *Microbiology* **147**, 2029-2036

58. Bose, I., Reese, A. J., Ory, J. J., Janbon, G., and Doering, T. L. (2003) A yeast under cover: the capsule of *Cryptococcus neoformans*. *Eukaryot. Cell* **2**, 655-663

59. Bulmer, G., and Sans, M. (1968) *Cryptococcus neoformans* III. Inhibition of phagocytosis. *J. Bacteriol.* **95**, 5-8

60. Kozel, T. R., Pfrommer, G. S., Guerlain, A. S., Highison, B. A., and Highison, G. J. (1988) Role of the capsule in phagocytosis of *Cryptococcus neoformans*. *Clin. Infect. Dis.* **10**, 436-439

61. Hu, G., Caza, M., Cadieux, B., Chan, V., Liu, V., and Kronstad, J. (2013) *Cryptococcus neoformans* requires the ESCRT protein Vps23 for iron acquisition from heme, for capsule formation, and for virulence. *Infect. Immun.* **81**, 292-302

62. Siafakas, A. R., Sorrell, T. C., Wright, L. C., Wilson, C., Larsen, M., Boadle, R., Williamson, P. R., and Djordjevic, J. T. (2007) Cell wall-linked cryptococcal phospholipase B1 is a source of secreted enzyme and a determinant of cell wall integrity. *J. Biol. Chem.* **282**, 37508-37514

63. Cox, G. M., McDade, H. C., Chen, S. C., Tucker, S. C., Gottfredsson, M., Wright, L. C., Sorrell, T. C., Leidich, S. D., Casadevall, A., and Ghannoum, M. A. (2001) Extracellular phospholipase activity is a virulence factor for *Cryptococcus neoformans*. *Mol. Microbiol.* **39**, 166-175

64. Cox, G. M., Mukherjee, J., Cole, G. T., Casadevall, A., and Perfect, J. R. (2000) Urease as a virulence factor in experimental cryptococcosis. *Infect. Immun.* **68**, 443-448

65. Olszewski, M. A., Noverr, M. C., Chen, G.-H., Toews, G. B., Cox, G. M., Perfect, J. R., and Huffnagle, G. B. (2004) Urease Expression by *Cryptococcus neoformans* Promotes Microvascular Sequestration, Thereby Enhancing Central Nervous System Invasion. *Am. J. Path.* **164**, 1761-1771

66. Levitz, S. M., Nong, S.-H., Seetoo, K. F., Harrison, T. S., Speizer, R. A., and Simons, E. R. (1999) *Cryptococcus neoformans* resides in an acidic phagolysosome of human macrophages. *Infect. Immun.* **67**, 885-890

67. Wang, Y., Aisen, P., and Casadevall, A. (1995) Cryptococcus neoformans melanin and virulence: mechanism of action. *Infect. Immun.* **63**, 3131-3136

68. Charlier, C., Nielsen, K., Daou, S., Brigitte, M., Chretien, F., and Dromer, F. (2009) Evidence of a role for monocytes in dissemination and brain invasion by Cryptococcus neoformans. *Infect. Immun.* **77**, 120-127

69. Levitz, S. M., Harrison, T. S., Tabuni, A., and Liu, X. (1997) Chloroquine induces human mononuclear phagocytes to inhibit and kill *Cryptococcus neoformans* by a mechanism independent of iron deprivation. *J. Clin. Invest.* **100**, 1640-1646

70. Hu, G., Cheng, P. Y., Sham, A., Perfect, J. R., and Kronstad, J. W. (2008) Metabolic adaptation in *Cryptococcus neoformans* during early murine pulmonary infection. *Mol. Microbiol.* **69**, 1456-1475

71. Chun, C. D., Liu, O. W., and Madhani, H. D. (2007) A Link between Virulence and Homeostatic Responses to Hypoxia during Infection by the Human Fungal Pathogen *Cryptococcus neoformans PLoS Pathog.* **3**, 0225-0238

72. Fan, W., Kraus, P. R., Boily, M. J., and Heitman, J. (2005) *Cryptococcus neoformans* gene expression during murine macrophage infection. *Eukaryot. Cell* **4**, 1420-1433

73. Duan, Z., Shang, Y., Gao, Q., Zheng, P., and Wang, C. (2009) A phosphoketolase Mpk1 of bacterial origin is adaptively required for full virulence in the insect-pathogenic fungus *Metarhizium anisopliae*. *Environ. Microbiol.* **11**, 2351-2360

74. Panagiotou, G., Andersen, M. R., Grotkjær, T., Regueira, T. B., Hofmann, G., Nielsen, J., and Olsson, L. (2008) Systems analysis unfolds the relationship between the phosphoketolase pathway and growth in *Aspergillus nidulans*. *PLoS One* **3**, e3847

75. Chen, D., Toone, W. M., Mata, J., Lyne, R., Burns, G., Kivinen, K., Brazma, A., Jones, N., and Bähler, J. (2003) Global transcriptional responses of fission yeast to environmental stress. *Mol. Biol. Cell* **14**, 214-229

76. Kim, D.-U., Hayles, J., Kim, D., Wood, V., Park, H.-O., Won, M., Yoo, H.-S., Duhig, T., Nam, M., and Palmer, G. (2010) Analysis of a genome-wide set of gene deletions in the fission yeast *Schizosaccharomyces pombe*. *Nat. Biotechnol.* **28**, 617-623

77. Hayles, J., Wood, V., Jeffery, L., Hoe, K.-L., Kim, D.-U., Park, H.-O., Salas-Pino, S., Heichinger, C., and Nurse, P. (2013) A genome-wide resource of cell cycle and cell shape genes of fission yeast. *Open Biol.* **3**, 130053

78. Rude, T. H., Toffaletti, D. L., Cox, G. M., and Perfect, J. R. (2002) Relationship of the Glyoxylate Pathway to the Pathogenesis of *Cryptococcus neoformans*. *Infect. Immun.* **70**, 5684-5694

Enzyme	K_{cat}	Apparent K_m		Cofactor in mutant structures[a]
		F6P	P_i	
	min^{-1}	m_M		
WT[b]	1,540 ± 60	9.7 ± 0.3	1.2 ± 0.2	
H64A	NA[c]	NA	NA	Tricyclic ring form of ThDP
H64N	NA	NA	NA	
H97A	NA	NA	NA	(CDNG[d])
H97N	NA	NA	NA	(CDNG[d])
H142A	12.2 ± 0.9	7.4 ± 0.6	1.7 ± 0.2	AcThDP
H142N	39.2 ± 1.2	7.2 ± 0.8	2.6 ± 0.5	
H320A	NA	NA	NA	AcThDP
H320N	NA	NA	NA	
Q321A	59.5 ± 2.5	4.4 ± 0.3	1.6 ± 0.2	
S440A	350 ± 11	53.5 ± 1.8	0.57 ± 0.04	
E479A	NA	NA	NA	
Y501F	197 ± 4	1.4 ± 0.2	25.5 ± 1.7	
H548A	100 ± 3	2.3 ± 0.7	0.52 ± 0.16	
N549A	NA	NA	NA	
H553A	NA	NA	NA	ThDP
H553N	NA	NA	NA	
K605A	NA	NA	NA	

TABLE 1.1 Kinetic parameters for B. breve Xfp wild type and variants (Ref 42).

(Permission granted for the reuse of this table)

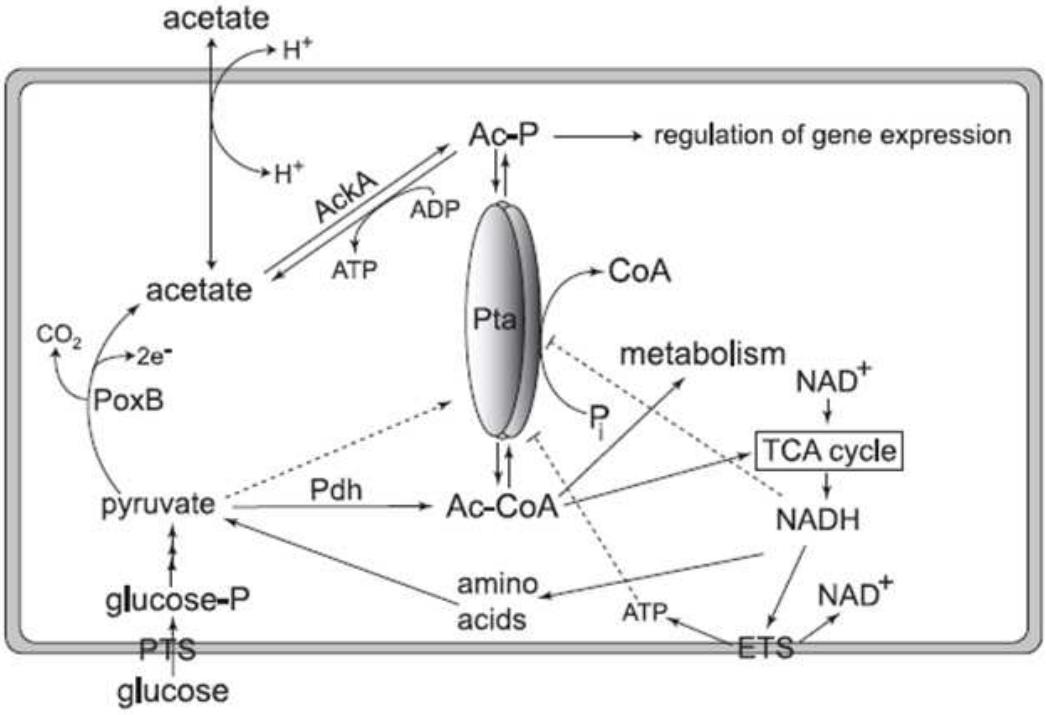

FIG 1.1 *S. enterica* PtaII function and regulation. This figure depicts the regulation of PtaII by various metabolites and how PtaII fits into cellular energy metabolism in *S. enterica*. Dashed lines with an arrow indicate a positive effect on PtaII activity while dashed lines with a blunt end indicate a negative effect. *S. enterica* PtaII is activated by pyruvate and inhibited by ATP and NADH (Ref 38). (Permission granted for reuse of this figure)

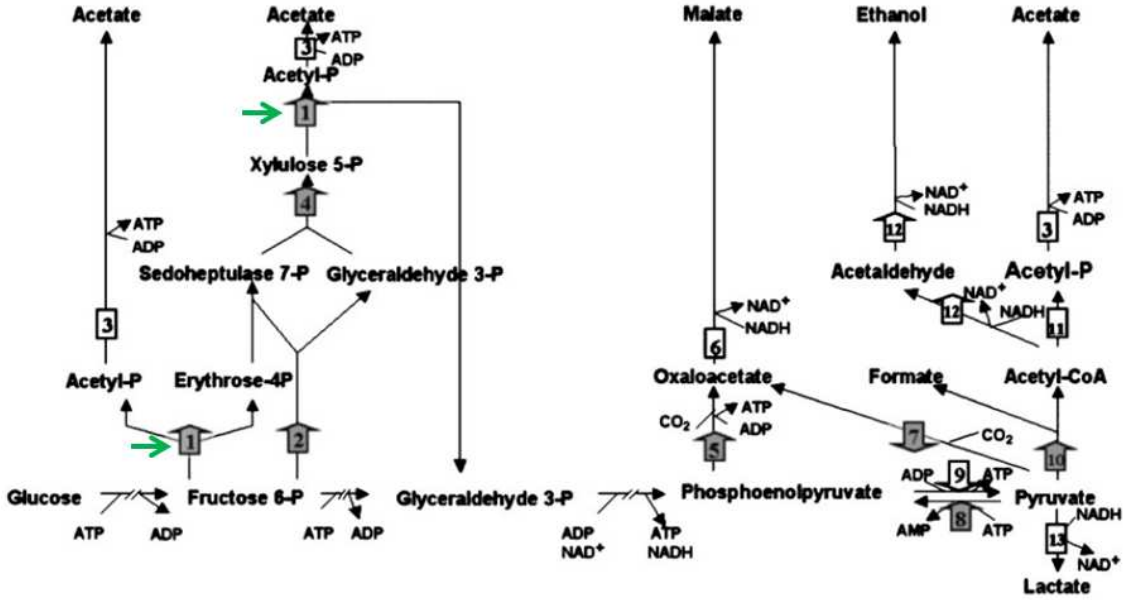

FIG 1.2 Glucose fermentation in *Lactobacillus plantarum*. Green arrows point towards the phosphoketolase enzyme within the phosphoketolase pathway of *L. plantarum* as a means of producing acetate during glucose fermentation. (1) phosphoketolase, (2) transaldolase, (3) acetate kinase, (4) transketolase, (5) phosphoenolpyruvate carboxykinase, (6) malate dehydrogenase, (7) pyruvate carboxylase, (8) phosphenolpyruvate synthase, (9) pyruvate kinase, (10) pyruvate formate-lyase, (11) phosphotransacetylase, (12) bifunctional alcohol dehydrogenase/ acetaldehyde dehydrogenase, (13) lactate dehydrogenase (Ref. 41). (Permission granted for the reuse of this figure).

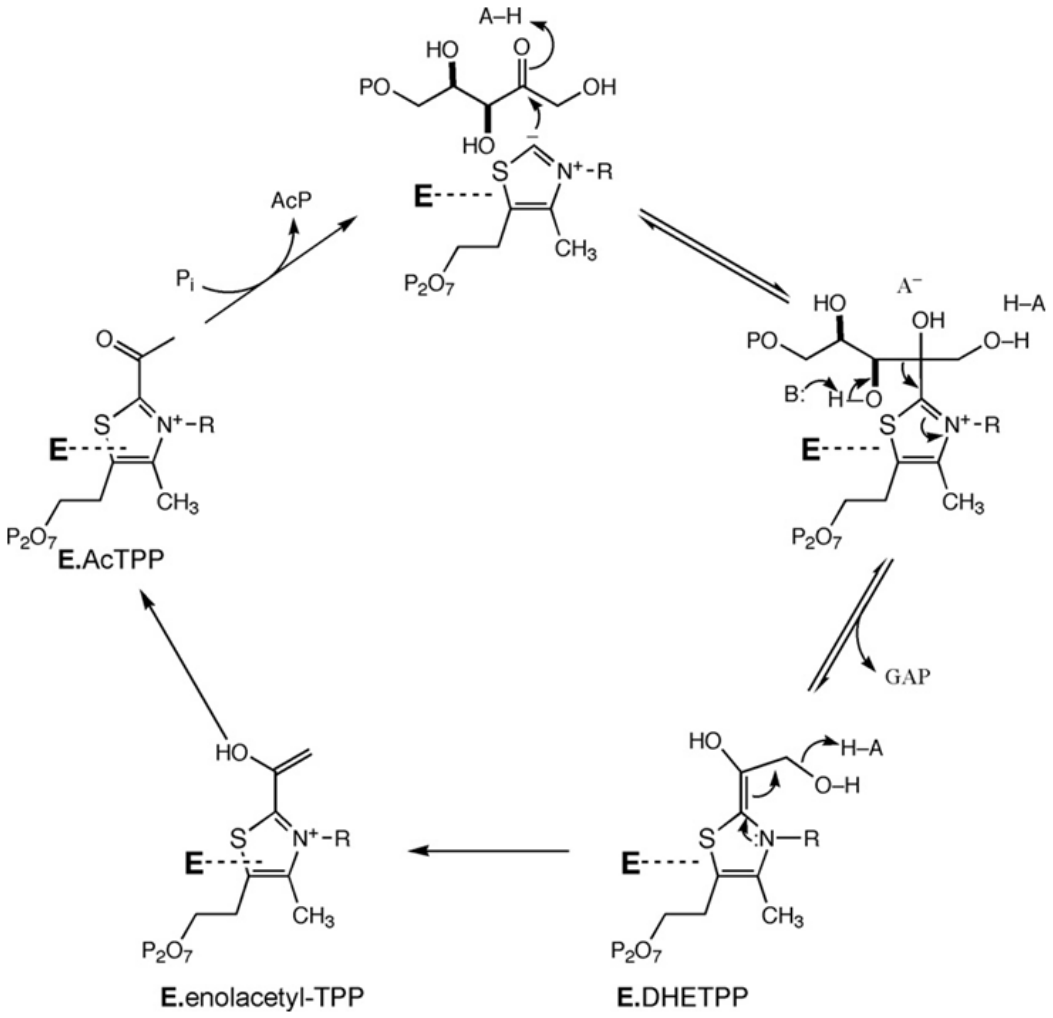

FIG 1.3 Xfp reaction mechanism. This reaction mechanism proposed by Yevenes et al. depicts Xfp catalyzed reaction for the substrate X5P (Ref 16). (Permission granted for reuse of this figure).

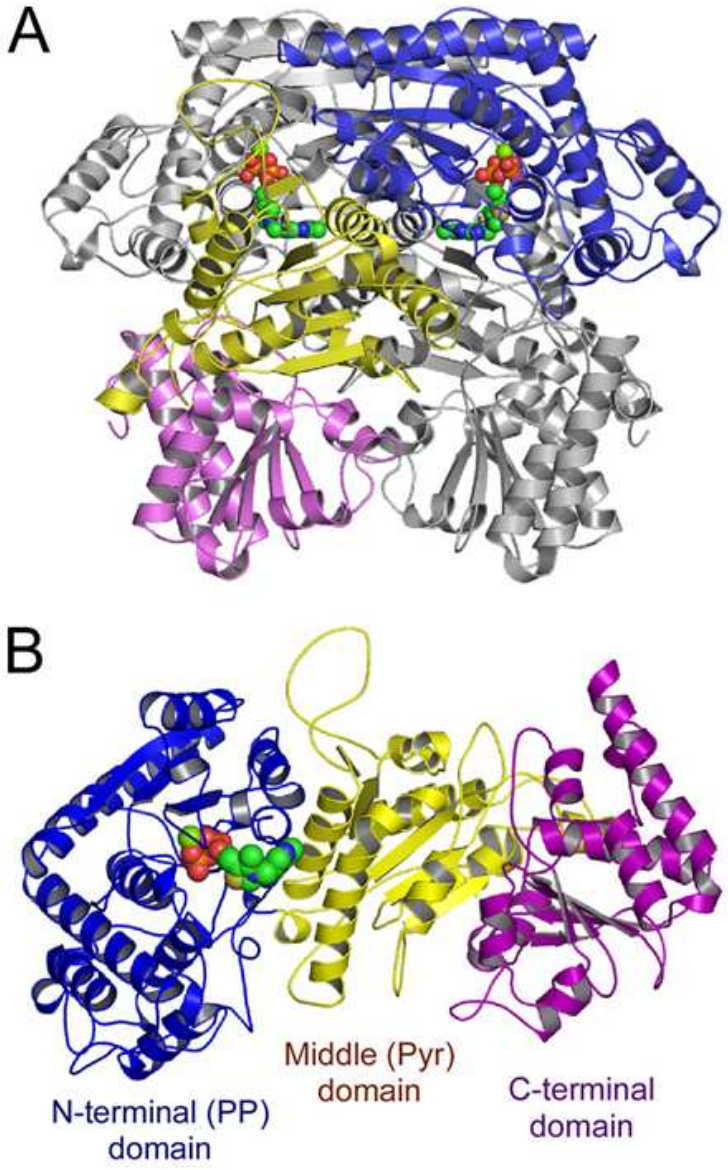

FIG 1.4 Crystal structure of *B. breve* Xfp homodimer (A) and monomer (B) with bound TPP. The monomer is separated into three domains: N-terminal (PP) domain (blue), Middle (Pyr) domain (yellow) and C-terminal domain (purple). TPP binds to the active site located between the PP and Pyr domains (Ref. 42). (Permission granted for the reuse of this figure).

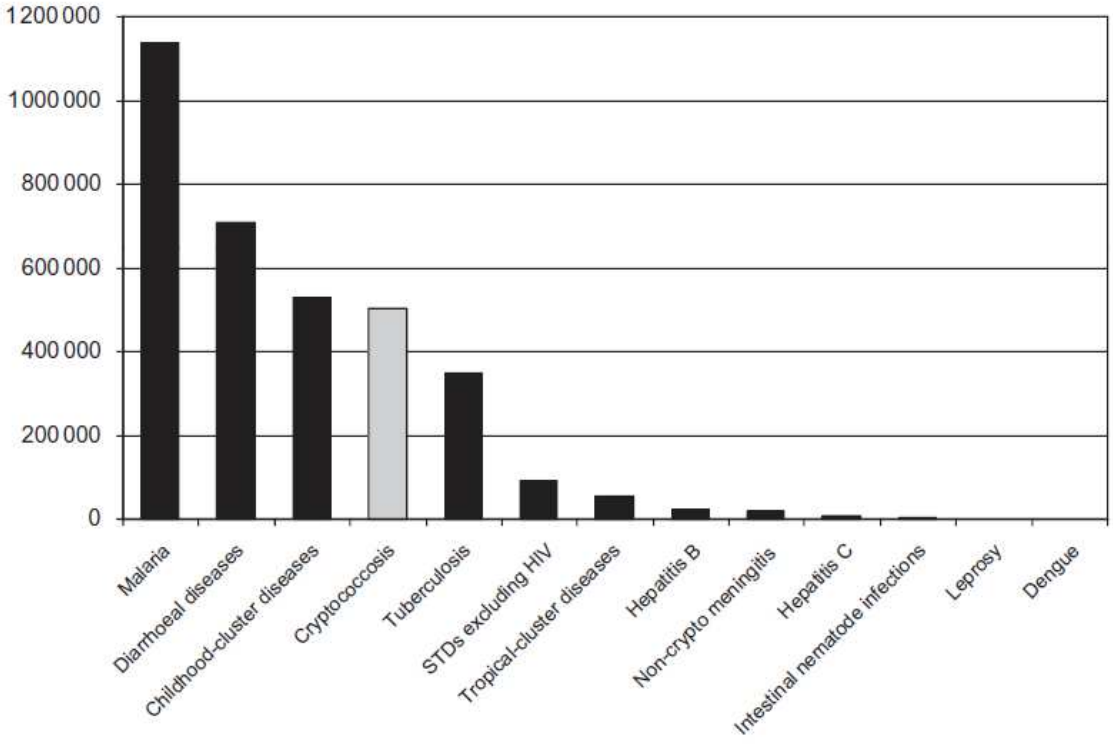

FIG 1.5 Comparison of the estimated number of deaths in Sub-Saharan Africa due to various infectious diseases (Ref 49). (Permission granted for the reuse of this figure).

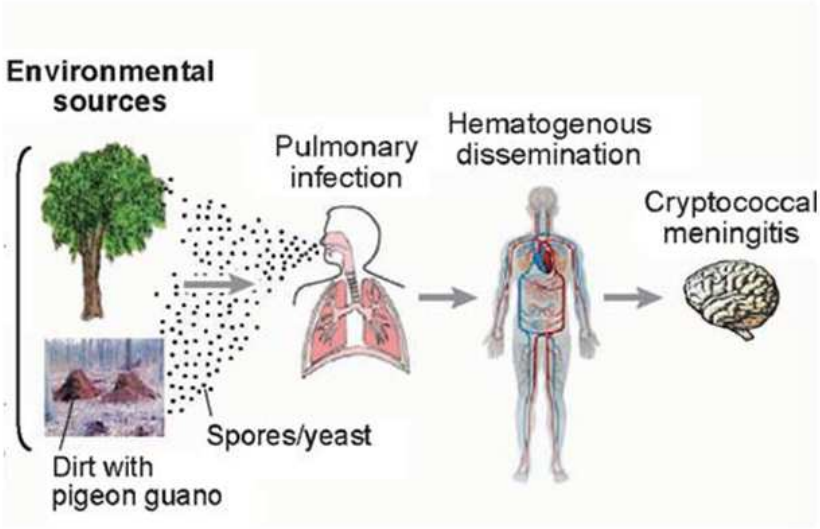

FIG 1.6 Infection pathway of *Cryptococcus neoformans* from the environment to the host. People come into contact with basidiospores from environmental sources. Spores are inhaled into the lungs where they can cause immediate pulmonary infection or simply enter a dormant form. If an individual becomes immunocompromised, the dormant form can cross the blood brain barrier through hematogenous dissemination and cause cryptococcal meningitis (Ref. 51). (Permission granted for the reuse of this figure.)

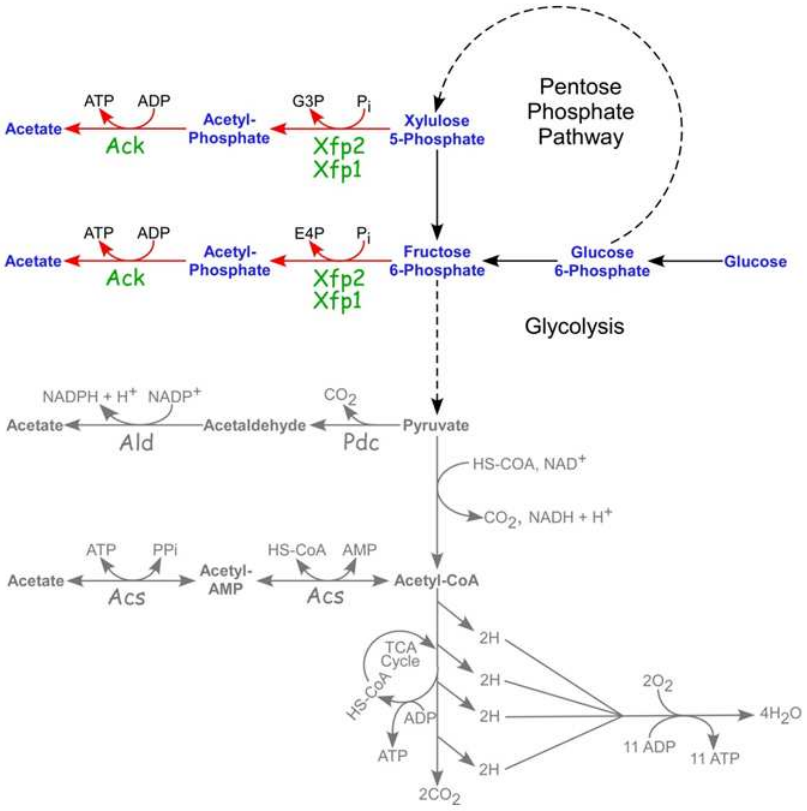

FIG. 1.7. Sources of acetate in *C. neoformans*. Acetate can be produced in *C. neoformans* via the Xfp-Ack pathway, the Pdc-Ald pathway or the enzyme Acs. (Enzyme abbreviations are indicated in the text). The Xfp-Ack pathway is highlighted at the top of this figure because it is the pathway focused on throughout this dissertation. (unpublished data, permission granted for the reuse of this figure by K. Smith).

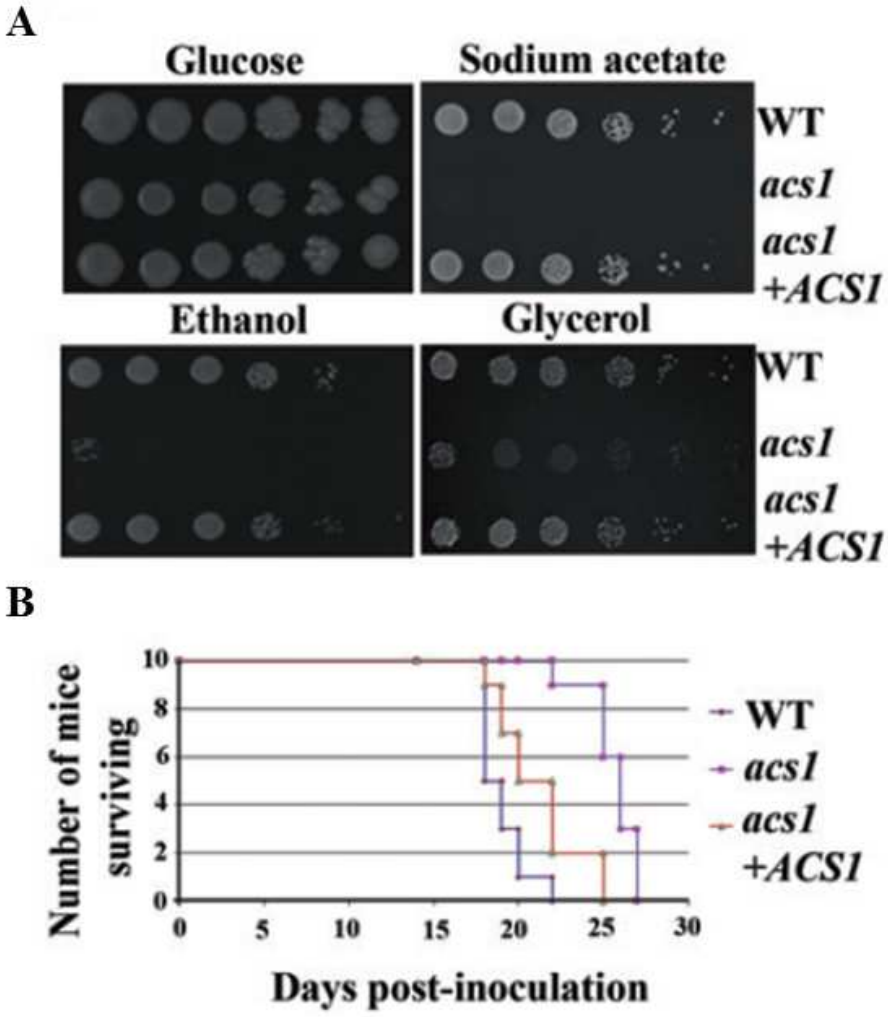

FIG 1.8 Comparison of *C. neoformans* WT, Acs1 deletion (*acs1*), and Acs1 recomplementation (*acs1* + *ACS1*) strains. Deletion of *ACS1* (*acs1*) inhibits growth on sodium acetate, glycerol and ethanol while the ability to grow on these carbon sources is regained upon *ACS1* complementation (*acs1 +ACS1*) (A). Deletion of *ACS1* (*acs1*) also results in attenuated virulence in a mouse inhalation model (B). (Ref. 70) (Permission granted for the reuse of this figure).

CHAPTER 2

BIOCHEMICAL AND KINETIC CHARACTERIZATION OF XYLULOSE 5-PHOSPHATE/ FRUCTOSE 6-PHOSPHATE PHOSPHOKETOLASE 2 (XFP2) FROM *CRYPTOCOCCUS NEOFORMANS*

Katie Glenn, Cheryl Ingram-Smith, and Kerry S. Smith

I. ABSTRACT

Xylulose 5-phosphate/fructose 6-phosphate phosphoketolase (Xfp), previously thought to only be present in bacteria but recently found in fungi, catalyzes the formation of acetyl phosphate from xylulose 5-phosphate or fructose 6-phosphate. Here we describe the first biochemical and kinetic characterization of a eukaryotic Xfp, that from the opportunistic fungal pathogen *Cryptococcus neoformans*, which has two *XFP* genes (designated *XFP1* and *XFP2*). Our kinetic characterization of *C. neoformans* Xfp2 indicated the existence of both substrate cooperativity for all three substrates and allosteric regulation through the binding of effector molecules at sites separate from the active site. Prior to this study Xfp enzymes from two bacterial genera had been characterized and were determined to follow Michaelis-Menten kinetics. *C. neoformans* Xfp2 is inhibited by ATP, phosphoenolpyruvate (PEP) and oxaloacetic acid (OAA) and

activated by AMP. ATP is the strongest inhibitor with a half maximal inhibitory concentration (IC_{50}) of 0.6 mM. PEP and OAA were found to share the same or have overlapping allosteric binding sites while ATP binds at a separate site. AMP acts as a very potent activator; as little as 20 µM AMP is capable of increasing Xfp2 activity by 24.8 ± 1.0% while 50 µM prevented inhibition by 0.6 mM ATP. AMP and PEP/OAA operated independently, with AMP activating Xfp2 and PEP/OAA inhibiting the activated enzyme. This study provides valuable insight into the metabolic role of Xfp within fungi, specifically the fungal pathogen *Cryptococcus neoformans*, and suggests that at least some Xfps display substrate cooperative binding and allosteric regulation.

II. INTRODUCTION

Cryptococcus neoformans, an invasive opportunistic pathogen of the central nervous system, is the most frequent cause of fungal meningitis resulting in more than 625,000 deaths per year worldwide (1,2). Exposure to *C. neoformans* is common, as it is an environmental fungus found in the soil and can enter the lungs through inhalation, leading to pulmonary infection. An increased rate of infection occurs in individuals with impaired cell-mediated immunity, particularly those with AIDS and recipients of immunosuppressive therapy.

Acetate has been shown to be a major metabolite released by *Cryptococcus* during infection (3-5), but the significance of this is not known. Genes encoding enzymes from three putative acetate-producing pathways and two putative acetate transporters have been shown to be upregulated during cryptococcal infection (6), suggesting acetate production and transport may be a necessary and required part of the pathogenic process.

One pathway for acetate production is composed of the enzymes xylulose 5-phosphate/ fructose 6-phosphate phosphoketolase (Xfp) and acetate kinase (Ack). Xfp catalyzes the breakdown of xylulose 5-phosphate (X5P; X5P + P_i ↔ acetyl-phosphate + glyceraldehyde 3-phosphate; EC 4.1.2.9) or fructose 6-phosphate (F6P; F6P + P_i ↔ acetyl phosphate + erythrose 4-phosphate; EC 4.1.2.22). Ack utilizes the acetyl phosphate product of the reaction to produce acetate + ATP (acetate + ATP ↔ acetyl phosphate +ADP; EC 2.7.2.1). These enzymes form a modified pathway, termed the

pentose phosphoketolase pathway, in lactic acid bacteria and bifidobacteria (7). This pathway is utilized in the heterofermentative degradation of pentoses and hexoses to the end products CO_2, ethanol, acetate and lactate (8). Xfp can convert X5P generated at the end of the oxidative phase of the pentose phosphate pathway to glyceraldehyde 3-phosphate, which can enter the glycolytic pathway, and acetyl phosphate, which Ack can convert to acetate to generate ATP.

Only the Xfp enzymes from the lactic acid bacteria *Bifidobacterium* species and *Lactobacillus plantarum* have been purified and kinetically characterized (7,9). The characterized bacterial Xfp enzymes show dual substrate specificity with X5P and F6P and follow Michaelis-Menten kinetics (7,9,10). Here we report the first biochemical and kinetic characterization of eukaryotic Xfp, the *C. neoformans* Xfp2 (Accession # CNAG_06923.7). Unlike the previously characterized bacterial Xfp enzymes, *C. neoformans* Xfp2 displays both substrate cooperativity and allosteric regulation. The enzyme is inhibited by ATP, phosphoenolpyruvate (PEP) and oxaloacetic acid (OAA) and activated by AMP.

III. MATERIALS AND METHODS

Materials

Chemicals were purchased from Sigma Aldrich, VWR, or Fisher Scientific. Oglionucleotide primers were purchased from Integrated DNA Technologies. Codon-optimized *C. neoformans XFP2* was synthesized by GenScript and supplied in the *E. coli* expression vector pET21b which provides for addition of a C-terminal His-tag for nickel affinity column purification.

Production and Purification of *C. neoformans* Xfp2

The recombinant plasmid pET21b-*XFP2* was transformed into *Escherichia coli* RosettaBlue (DE3) placI (Novagen). The recombinant strain was grown in Luria-Bertani (LB) medium with 50 µg/mL of ampicillin and 34 µg/mL of chloramphenicol at 37°C to an absorbance of ~0.8 at 600 nm, and production of the enzyme was induced by the addition of IPTG to a final concentration of 1 mM. Cultures were incubated overnight at ambient temperature and cells were harvested by centrifugation and stored at -20°C prior to protein purification.

Cell-free extract was prepared by first suspending the cells in buffer A (25 mM Tris, 150 mM sodium chloride, 20 mM imidazole, 1 mM dithiothreitol (DTT) and 10% glycerol [pH 7.4]), and passing twice through a French pressure cell at approximately 130 MPa. The cell extract was clarified by ultracentrifugation at 100,000 x g for 1 hour, and

then subjected to column chromatography using an AKTA-FPLC (GE Healthcare). Cell-free extract was applied to a 5 mL His-Trap HP column (GE Healthcare). After a 6 to 7 column volume wash with buffer A to remove any unbound protein, the column was developed with a linear gradient from 0 to 0.5 M imidazole in buffer A. Appropriate fractions determined to contain Xfp2 by SDS-PAGE and activity assays were pooled and dialyzed overnight in buffer containing 25 mM Tris, 10% glycerol and 1 mM DTT [pH 7.0]. Aliquots of purified protein were stored at -80°C. Protein concentration was determined using a modified Bradford assay with bovine serum albumin standards.

Hydroxamate Assay Measuring Acetyl Phosphate Production

Enzymatic activity was measured using the hydroxamate assay to quantitate the production of acetyl phosphate (9,11). Standard reactions consisted of 0.5 mM thiamine pyrophosphate (TPP), 1 mM DTT, 5 mM magnesium chloride, and 50 mM MES buffer (pH 5.5 for all kinetic studies), with the concentration of substrates varied. The sodium phosphate substrate was used at a pH of 5.5.

Reactions (200 µL) were initiated by the addition of enzyme and incubated at 40 °C. After 30 minutes, 100 µL of 2 M hydroxylamine hydrochloride (pH 7.0) was added and the reactions were allowed to incubate at room temperature for 10 minutes. Reactions were terminated by the addition of 600 µL of a 50:50 mixture of 2.5 % $FeCl_3$ in 2N HCl and 10% trichloroacetic acid to form the ferric-hydroxamate complex which was measured spectrophotometrically at 540nm (7,12). Reactions were performed in triplicate for all data sets.

Kinetic Analysis

Apparent kinetic parameters were determined by varying the concentration of one substrate with the other substrate held constant at a saturating level (60 mM for P_i or F6P). All substrates exhibited varying degrees of cooperativity, and kinetic parameters were determined by fitting the data to the Hill equation [Eq. 2.1] (13,14) in which V_0 is initial velocity, [S] is substrate concentration, V is maximum velocity, $K_{0.5}$ is substrate concentration at half maximal velocity and *h* is the Hill constant. Data was plotted using the scientific graphing program Kaleidagraph (Synergy Software).

$$V_0 = V + [S]^h/({K_{0.5}}^h + [S]^h) \qquad \text{[Eq. 2.1]}$$

Determination of IC_{50} Values and Allosteric Binding Site Sharing of Xfp2 Inhibitors

After determining kinetic parameters for X5P commercial availability was discontinued, so our investigations into the allosteric regulation of Xfp2 were performed only with F6P. Half maximal inhibitory concentrations (IC_{50}) were determined for all Xfp2 allosteric inhibitors by measuring the decrease in activity as a function of increasing inhibitor concentration. GraphPad Prism 5 software was used to determine IC_{50} values by fitting the data with a log [inhibitor] vs. response curve. In order to determine if any of the inhibitors bind at the same allosteric site or have overlapping allosteric sites, the IC_{50} value of one inhibitor was measured in the presence of another inhibitor.

IV. RESULTS

Optimization of reaction conditions

An *E. coli* codon-optimized *XFP2* (GenScript Inc.) was cloned into pET21b (C-terminal His tag) and the recombinant enzyme was produced and purified by nickel affinity chromatography to electrophoretic homogeneity. Optimal reaction conditions for purified Xfp2 activity were determined. The temperature optimum was found to be 37-40°C (Fig. 2.1A), the temperature that *C. neoformans* would be exposed to during infection. Xfp2 had highest activity between pH 4.5 and 6.0 (Fig. 2.1B), and pH 5.5 was used when determining kinetic parameters. Like its bacterial counterpart, *C. neoformans* Xfp2 requires the cofactor thiamine pyrophosphate (TPP), and 0.5 mM TPP was sufficient for full enzymatic activity (data not shown). Xfp2 prefers Mg^{2+} as the divalent cation, but can also utilize Ca^{2+}, Co^{2+}, Mn^{2+}, and Ni^{2+} (Fig. 2.1C).

Kinetic characterization of *C. neoformans* Xfp

In determining the kinetic parameters in the acetyl phosphate-forming direction, plots of substrate concentration versus velocity were found to be sigmoidal rather than hyperbolic as would be expected for enzymes following Michaelis-Menten kinetics. This is the first demonstration of the existence of substrate cooperative binding among Xfp enzymes which was not reported in previous characterizations of bacterial Xfps (7,9,10). Apparent kinetic parameters (Table 2.1) were determined by fitting experimental data to

the Hill equation [Eq 2.1] in which a Hill constant greater than 1.0 represents positive cooperativity and a Hill constant less than 1.0 represents negative cooperativity (15,16) Xfp2 exhibits positive cooperativity (h >1.0) for both X5P and F6P, suggesting that binding of either of these substrates causes a favorable conformational change that facilities the binding of additional substrate at separate active sites on the enzyme. Xfp2 displays negative cooperativity (h < 1.0) for P_i with an average Hill constant of approximately 0.6. The 2.6-fold higher catalytic efficiency suggests that X5P is slightly preferred over F6P.

Allosteric Inhibitors

Since we hypothesize that the Xfp-Ack pathway plays a significant role in ATP production during infection, it would seem likely that this pathway would be regulated, particularly since the F6P substrate of Xfp2 is an intermediate in glycolysis, another key ATP-generating pathway that has been shown to be critical for virulence (17). ATP along with coenzymes and intermediates from glycolysis and the tricarboxylic acid (TCA) cycle were tested to see if Xfp2 is allosterically regulated by these molecules. Of the ligands tested, ATP, phosphoenolpyruvate (PEP), and oxaloacetic acid (OAA) were found to display the most pronounced inhibition (Fig. 2.2) while citrate caused slight inhibition (data not shown). Acetyl-CoA, CoA, and pyruvic acid were also tested and had no effect on activity. Progress curves for both substrates P_i and F6P were generated in the presence of increasing concentrations of ATP (Fig. 2.3A & B), PEP (Fig. 2.4A & B), and OAA (Fig. 2.5A & B).

For each of the three inhibitors, the $K_{0.5}$ for P_i was not significantly affected (data not shown); however, the $K_{0.5}$ concentrations for F6P increased in each case. The $K_{0.5}$ for F6P increased from 15.9 ± 1.3 mM in the absence of inhibitor to 73.9 ± 3.2 mM in the presence of 9 mM ATP, 109.4 ± 6.9 mM in the presence of 15 mM OAA, and 69.3 ± 9.6 mM in the presence of 16 mM PEP. The addition of inhibitor also generated a more sigmoidal F6P progress curve that is reflected by the increase in the Hill coefficient. The Hill coefficient increased from 1.41 ± 0.11 to 4.50 ± 0.20, 2.32 ± 0.07, and 2.40 ± 0.30 in the presence of 9 mM ATP, 15 mM OAA and 16 mM PEP respectively. This suggests that the binding of ATP, PEP and OAA has a direct effect on the binding of F6P to the active site in order to more closely regulate Xfp2 activity in response to changing cellular concentrations of these effectors.

The IC_{50} concentrations, the concentration of inhibitor required to reduce activity to half its maximally inhibited value, were determined for each inhibitor using the $K_{0.5}$ concentrations of both P_i (13 mM) and F6P (16 mM) (Table 2). The IC_{50} value of 0.6 mM for ATP is much lower than those determined for PEP and OAA, which were very similar (Table 2.2). Since both molecules are similar in size and structure, it is possible that they bind at the same allosteric site. In order to test if the inhibitors share the same allosteric site, reactions were performed in which one inhibitor was held constant at its IC_{50} concentration and the concentration of the second inhibitor was varied. If two inhibitors bind at the same site (or if binding of one inhibitor occludes the binding of the second) then approximately half of the binding sites would be occupied by the first inhibitor, thereby lowering the concentration of the second (varied) inhibitor required to

inhibit activity by an additional 50%. The IC_{50} of PEP decreased by approximately half in the presence of OAA; likewise the IC_{50} value of OAA decreased by about half in the presence of PEP (Table 2.2). This suggests that PEP and OAA share the same allosteric site. Alternatively, PEP and OAA bind at separate overlapping sites in which the binding of one inhibitor prevents the binding of the second inhibitor. The IC_{50} of PEP in the presence of ATP did not change significantly suggesting that the PEP/OAA site(s) is separate from the ATP allosteric site.

Allosteric Activator

C. neoformans Xfp2 is activated by the presence of AMP (Fig 2.6). The presence of as little as 20 µM AMP resulted in elevated enzymatic activity that reached a maximum at 0.5 mM AMP. The half maximal activation concentration was determined to be 29.7 ± 1.5 µM. The effect of AMP activation on P_i and F6P progress curves was evaluated. Increasing amounts of AMP resulted in increased Xfp2 activity at all P_i concentrations without affecting the overall shape of the curve or the $K_{0.5}$ of P_i (Fig. 2.6A). Therefore, AMP does not appear to have a direct effect on the binding of P_i to the active site. The presence of AMP decreased the $K_{0.5}$ for F6P from 15.9 ± 1.3 mM in the absence of AMP to 9.1 ± 0.6 mM in the presence of 0.5 mM AMP. Increasing concentrations of AMP resulted in more hyperbolic F6P progress curves (Fig. 2.6B). The Hill coefficient decreased from 1.41 ± 0.11 in the absence of AMP to 0.97 ± 0.03 in the presence of 0.5 mM AMP, suggesting more constant affinity for the substrate F6P.

AMP not only causes activation but alleviates the effects of allosteric inhibitors (Fig. 2.7). The presence of AMP completely prevents or overrides the inhibitory effect of ATP. However, AMP cannot overcome inhibition by PEP. The results observed are consistent with AMP and PEP acting separately, with AMP fully activating the enzyme, and PEP inhibiting from this fully activated level. When ATP and PEP are both present, inhibition is slightly additive compared to the inhibition by either one alone. Activity decreased from 43.4 ± 0.7% in the presence of PEP to 32.5 ± 0.6% when both ATP and PEP are present. The level of activity observed when AMP was present in addition to PEP was similar to that when AMP was present with both ATP + PEP. In both cases, activity was in the range expected for inhibition of the fully activated enzyme by the IC_{50} concentration of PEP.

V. DISCUSSION

Here we report the first characterization of *C. neoformans* Xfp2, the first eukaryotic Xfp to be characterized. Xfp functions with Ack in heterofermentative bacteria to form a modified pentose phosphoketolase pathway. This pathway was originally thought to be present only in bacteria but has been more recently identified in euascomycete and basidiomycete fungi (18). Like *C. neoformans*, many fungi with this pathway have two *XFP* ORFs designated as *XFP1* and *XFP2*.

Unlike previously characterized bacterial Xfps, *C. neoformans* Xfp2 displays both substrate cooperative binding and allosteric regulation. Xfp2 is allosterically regulated by the activator AMP and inhibitors ATP, PEP and OAA. PEP and OAA appear to share the same allosteric binding site while ATP and AMP bind at a separate site. The simplest explanation of AMP's ability to fully overcome ATP inhibition is that they bind at the same site however our results do not conclusively rule out separate but interacting binding sites. Xfp2 activation by AMP and inhibition by ATP is consistent with Xfp2 partnering with Ack as part of a modified pentose phosphate pathway to generate ATP and acetate from X5P and F6P. The intracellular ATP:AMP ratio provides an indication of the cellular energy status and regulation of the Xfp2-Ack pathway by ATP and AMP is a way to modulate ATP production by this pathway. High ATP levels indicate the energy needs of the cell have been satisfied and thus additional ATP production via the Xfp2-Ack pathway is not necessary, whereas high AMP levels indicate an energy deficit and

the need for increased ATP production via the Xfp2-Ack pathway. A possible explanation for Xfp2 inhibition by PEP and OAA is that high concentrations of these intermediates from glycolysis and the TCA cycle respectively, are also signals that cellular energy needs have been met, and the cell can switch from glycolysis, which produces ATP and utilizes glucose, to gluconeogenesis to synthesize and store glucose.

A ping pong bi bi mechanism was originally proposed for *Lactobacillus plantarum* Xfp by Yevenes and Frey (9) in which enzyme bound TPP first interacts with F6P to form a TPP-F6P complex and release the product erythrose 4-phosphate (E4P) forming enzyme bound 2-α,β-dihydroxyethylidene-TPP (DHETPP). DHETPP undergoes a dehydration reaction to form enzyme bound enolacetyl-TPP where ketonization converts it to enzyme bound acetyl-TPP (AcTPP). AcTPP is phosphorylated and acetyl phosphate is released leaving TPP available to interact with additional F6P substrate and repeat the reaction. Therefore, the product E4P is formed by the interaction of TPP and F6P in the absence of the second substrate P_i. The crystal structure of *Bifidobacterium longum* Xfp confirmed the reaction mechanism proposed by Yevenes and Frey (19). We suspect that *C. neoformans* Xfp2 follows the same active site reaction mechanism as the bacterial Xfps but with the added complexity of allosteric regulation that influences substrate-binding affinity. Since all allosteric effectors were found to directly affect F6P binding, the binding of these effectors influences the interaction between F6P and TPP in the first step of the reaction mechanism. We found that the presence of allosteric effectors do not influence the binding of P_i which further confirms and supports the existence of a ping pong bi bi mechanism in which the interaction between TPP and F6P

to form E4P occurs in the absence of P_i and that it is this first step of the reaction that is allosterically regulated.

Acetate is the most abundant metabolite produced during cryptococcal pulmonary infection, but the role acetate plays in metabolism and infection is unknown (3-5). Genomic expression studies provide evidence that the Xfp-Ack pathway could be responsible for acetate production. Serial analysis of gene expression on *C. neoformans* cells collected from the lungs of infected mice showed elevated expression of *XFP2* (6). *XFP2* was also found to be among the genes upregulated under hypoxic conditions that occur in infected tissue (20). RNA microarray analysis of *C. neoformans* gene expression within the macrophage also indicates that Ack is expressed under this condition but Xfp2 was not present in this microarray data set (21). In addition an Xfp2 homolog is required for full virulence in the insect fungal pathogen *Metarhizium anisopliae* (22). Taken together these studies suggest that *C. neoformans* Xfp2 may play a role during infection.

C. neoformans Xfp2 shows maximal activity between 37 - 40°C which is consistent with a role of Xfp2 during *C. neoformans* infection (23). The Xfp-Ack pathway could serve as a source of ATP production under the hypoxic and acidic conditions encountered in the macrophage where ATP generation by oxidative phosphorylation is suppressed. In addition, the pH of cryptococcomas has been found to be between 5.4 and 5.6 in vivo (4). It is possible that the production and excretion of acetic acid generated by the Xfp-Ack pathway contributes to the acidic environment of

cryptococcomas. This acidic environment can aid in *C. neoformans* survival outside the macrophage by inducing neutrophil necrosis and decreasing superoxide production (4). Our studies show that Xfp2 functions best at low pH with activity decreasing as pH increases. Even in vitro assays of the bacterial Xfps were performed below neutral pH, between pH 6.0 (9) and 6.5(7), and optimal pH was not reported. The intracellular pH of *C. neoformans* during infection is unknown, but even though *C. neoformans* cells are tolerant to low pH (24), it is unlikely that Xfp2 is exposed to low pH in vivo. The presence of AMP can increase Xfp2 activity from 13.4 ± 0.7 % to 117.0 ± 2.0 % in the presence of 0.5 mM AMP at pH 7 with 100% activity considered to be the activity at pH 5.5 using K0.5 substrate concentrations (K. Glenn and K. Smith, unpublished data), so pH could provide an additional means of regulating Xfp2 activity.

The allosteric regulation that has evolved for *C. neoformans* Xfp2 versus its bacterial homolog seems to support a more complex role for this enzyme within fungal metabolism and during infection. However, allosteric regulation by PEP and OAA but not AMP and ATP may be occurring with at least some bacterial Xfps (K. Glenn and K. Smith unpublished data). We believe that Xfp2 partners with Ack to generate ATP, which is supported by the findings that Xfp2 is regulated by both ATP and AMP levels. The biochemical properties of this enzyme suggest that it utilizes its partnership with Ack to generate ATP during infection and within the human macrophage where hypoxic conditions are encountered that limit ATP production by the electron transport chain. Xfp2's involvement in *C. neoformans* metabolism especially during infection lends

support to future studies that focus on this enzyme as a possible drug target in the treatment of cryptococcal infection.

VI. ACKNOWLEDGMENTS

This work was supported by awards from the National Institutes of Health (GM084417-01A1), National Science Foundation (Award# 0920274), South Carolina Experiment Station Project SC-1700340, and Technical Contribution #6207 of the Clemson University Experiment Station.

VII. REFERENCES

1. Liu, T.-B., Perlin, D. S., and Xue, C. (2012) Molecular mechanisms of cryptococcal meningitis. *Virulence* **3**, 173-181

2. Park, B. J., Wannemuehler, K. A., Marston, B. J., Govender, N., Pappas, P. G., and Chiller, T. M. (2009) Estimation of the current global burden of cryptococcal meningitis among persons living with HIV/AIDS. *AIDS* **23**, 525-530

3. Bubb, W. A., Wright, L. C., Cagney, M., Santangelo, R. T., Sorrell, T. C., and Kuchel, P. W. (1999) Heteronuclear NMR studies of metabolites produced by *Cryptococcus neoformans* in culture media: identification of possible virulence factors. *Magn. Reson. Med.* **42**, 442-453

4. Wright, L., Bubb, W., Davidson, J., Santangelo, R., Krockenberger, M., Himmelreich, U., and Sorrell, T. (2002) Metabolites released by *Cryptococcus neoformans* var. *neoformans* and var. *gattii* differentially affect human neutrophil function. *Microbes Infect.* **4**, 1427-1438

5. Himmelreich, U., Allen, C., Dowd, S., Malik, R., Shehan, B. P., Mountford, C., and Sorrell, T. C. (2003) Identification of metabolites of importance in the pathogenesis of pulmonary cryptococcoma using nuclear magnetic resonance spectroscopy. *Microbes Infect.* **5**, 285-290

6. Hu, G., Cheng, P. Y., Sham, A., Perfect, J. R., and Kronstad, J. W. (2008) Metabolic adaptation in *Cryptococcus neoformans* during early murine pulmonary infection. *Mol. Microbiol.* **69**, 1456-1475

7. Meile, L., Rohr, L. M., Geissmann, T. A., Herensperger, M., and Teuber, M. (2001) Characterization of the D-xylulose 5-phosphate/D-fructose 6-phosphate phosphoketolase gene (xfp) from *Bifidobacterium lactis*. *J. Bacteriol.* **183**, 2929-2936

8. Kleijn, R. J., van Winden, W. A., van Gulik, W. M., and Heijnen, J. J. (2005) Revisiting the ^{13}C-label distribution of the non-oxidative branch of the pentose phosphate pathway based upon kinetic and genetic evidence. *FEBS J.* **272**, 4970-4982

9. Yevenes, A., and Frey, P. A. (2008) Cloning, expression, purification, cofactor requirements, and steady state kinetics of phosphoketolase-2 from *Lactobacillus plantarum*. *Bioorg. Chem.* **36**, 121-127

10. Suzuki, R., Katayama, T., Kim, B. J., Wakagi, T., Shoun, H., Ashida, H., Yamamoto, K., and Fushinobu, S. (2010) Crystal structures of phosphoketolase:

thiamine diphosphate-dependent dehydration mechanism. *J. Biol. Chem.* **285**, 34279-34287

11. Lipmann, F., and Tuttle, L. C. (1945) A specific micromethod for determination of acyl phosphates. *J. Biol. Chem.* **159**, 21-28

12. Racker, E. (1962) Fructose-6-phosphate phosphoketolase from Acetobacter xylinum. *Methods Enzymol.* **5**, 276-280

13. Hill, A. V. (1910) The possible effects of the aggregation of the molecules of haemoglobin on its dissociation curves. *J. Physiol.* **40**, iv-vii

14. Motulsky, H. (2004) *Fitting Models to Biological Data Using Linear and Nonlinear Regression: A Practical Guide to Curve Fitting: A Practical Guide to Curve Fitting*, Oxford University Press

15. Traut, T. (2008) *Allosteric regulatory enzymes*, Springer

16. Copeland, R. A. (2004) *Enzymes: a practical introduction to structure, mechanism, and data analysis*, John Wiley & Sons

17. Price, M. S., Betancourt-Quiroz, M., Price, J. L., Toffaletti, D. L., Vora, H., Hu, G., Kronstad, J. W., and Perfect, J. R. (2011) *Cryptococcus neoformans* requires a functional glycolytic pathway for disease but not persistence in the host. *MBio* **2**, e00103-00111

18. Ingram-Smith, C., Martin, S. R., and Smith, K. S. (2006) Acetate kinase: not just a bacterial enzyme. *Trends Microbiol.* **14**, 249-253

19. Takahashi, K., Tagami, U., Shimba, N., Kashiwagi, T., Ishikawa, K., and Suzuki, E. (2010) Crystal structure of *Bifidobacterium longum* phosphoketolase; key enzyme for glucose metabolism in Bifidobacterium. *FEBS Lett.* **584**, 3855-3861

20. Chun, C. D., Liu, O. W., and Madhani, H. D. (2007) A Link between Virulence and Homeostatic Responses to Hypoxia during Infection by the Human Fungal Pathogen *Cryptococcus neoformans PLoS Pathog.* **3**, 0225-0238

21. Fan, W., Kraus, P. R., Boily, M. J., and Heitman, J. (2005) *Cryptococcus neoformans* gene expression during murine macrophage infection. *Eukaryot. Cell* **4**, 1420-1433

22. Duan, Z., Shang, Y., Gao, Q., Zheng, P., and Wang, C. (2009) A phosphoketolase Mpk1 of bacterial origin is adaptively required for full virulence in the insect-pathogenic fungus *Metarhizium anisopliae*. *Environ. Microbiol.* **11**, 2351-2360

23. Kronstad, J. W., Attarian, R., Cadieux, B., Choi, J., D'Souza, C. A., Griffiths, E. J., Geddes, J. M., Hu, G., Jung, W. H., Kretschmer, M., Saikia, S., and Wang, J. (2011) Expanding fungal pathogenesis: Cryptococcus breaks out of the opportunistic box. *Nat. Rev. Microbiol.* **9**, 193-203

24. Levitz, S. M., Nong, S.-H., Seetoo, K. F., Harrison, T. S., Speizer, R. A., and Simons, E. R. (1999) *Cryptococcus neoformans* resides in an acidic phagolysosome of human macrophages. *Infect. Immun.* **67**, 885-890

TABLE 2.1. Apparent kinetic parameters for *C. neoformans* Xfp2

Substrate	$K_{0.5}$ (mM)	k_{cat}^{app} (sec^{-1})	$k_{cat}^{app}/K_{0.5}$ ($sec^{-1}mM^{-1}$)	*H*
F6P	15.9 ± 1.3	3.47 ± 0.10	0.22 ± 0.01	1.41 ± 0.11
X5P	6.4 ± 0.2	3.76 ± 0.05	0.58 ± 0.01	1.17 ± 0.06
P_i	13.3 ± 1.5	4.22 ± 0.13	0.32 ± 0.03	0.59 ± 0.03

TABLE 2.2. Half maximal inhibitory (IC_{50}) concentrations

Inhibitor (Varied)	Inhibitor (Constant)	IC_{50}
ATP	--------	0.61 ± 0.04
PEP	--------	8.23 ± 0.09
	OAA	4.84 ± 0.07
	ATP	9.85 ± 0.25
OAA	--------	7.50 ± 0.40
	PEP	3.71 ± 0.07

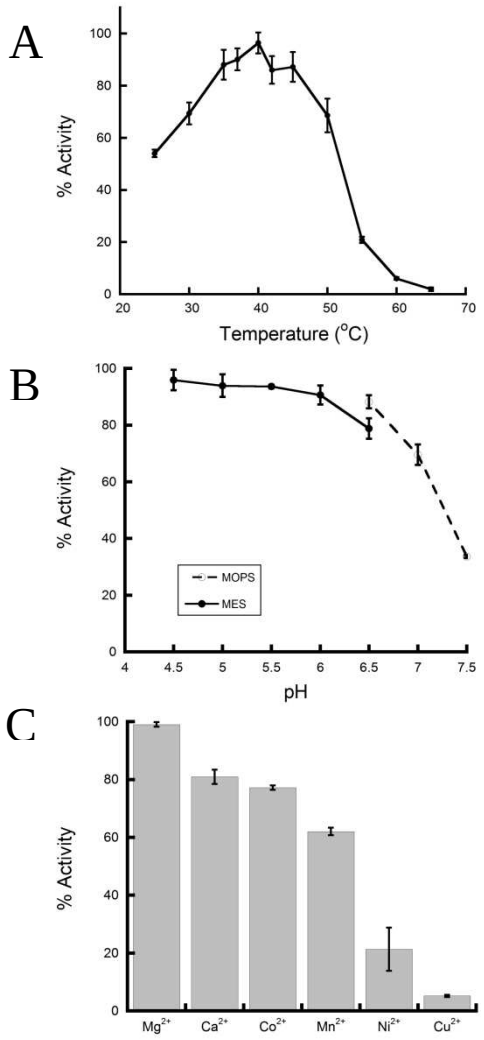

FIG 2.1. Optimization of Xfp2 reaction conditions. Xfp2 activity was determined in the presence of saturating P_i (60 mM) and F6P (80 mM) substrate concentrations for each reaction condition tested. Activities are reported as percentage of the maximal activity determined during each assay. (a) Temperature optima for Xfp2. Enzyme reactions were performed at the indicated temperatures in triplicate. (b) pH optima for Xfp2. Enzyme reactions were performed utilizing 50mM MES (●) and 50 mM MOPS (○) over a range of pH values. (c) Divalent cation metal specificity for Xfp2. Enzyme reactions were performed in the presence of 5 mM metal (as chloride salt).

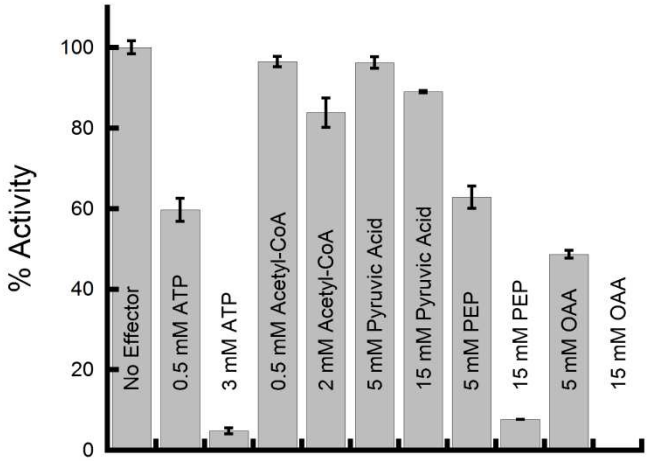

FIG 2.2. Effect of various ligands on Xfp2 activity. Various coenzymes and metabolic intermediates were tested for their effect on Xfp2 activity. Activities are reported as percentage of maximum activity with no effector present.

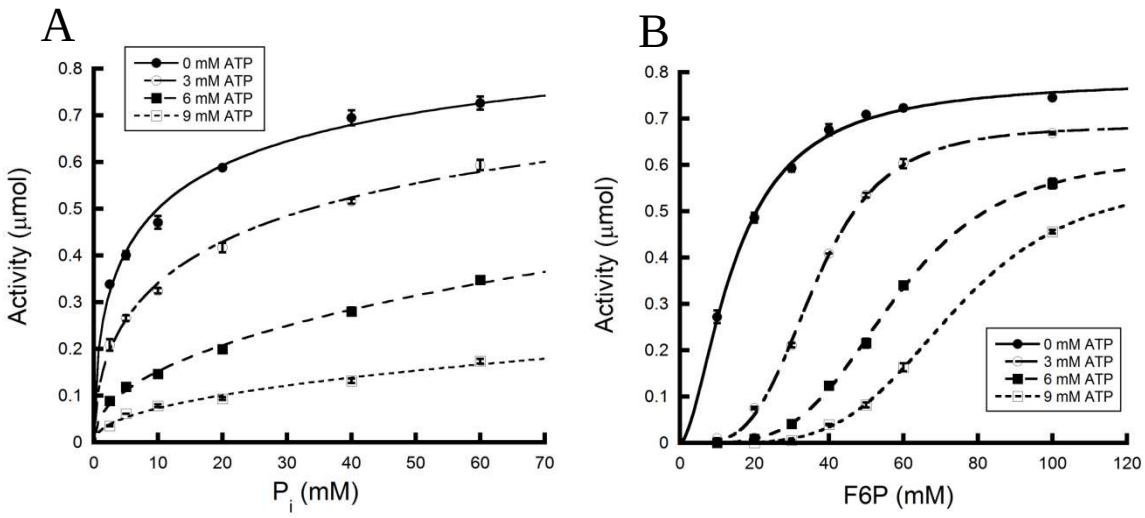

FIG 2.3. Effect of ATP on substrate progress curves. Progress curves were generated in the presence of 0 mM (●), 3 mM (○), 6 mM (■) and 9 mM (□) ATP for the substrates P_i (a) and F6P (b). Activities are reported in micromoles acetyl phosphate produced, and enzyme reactions were performed in triplicate for each substrate concentration.

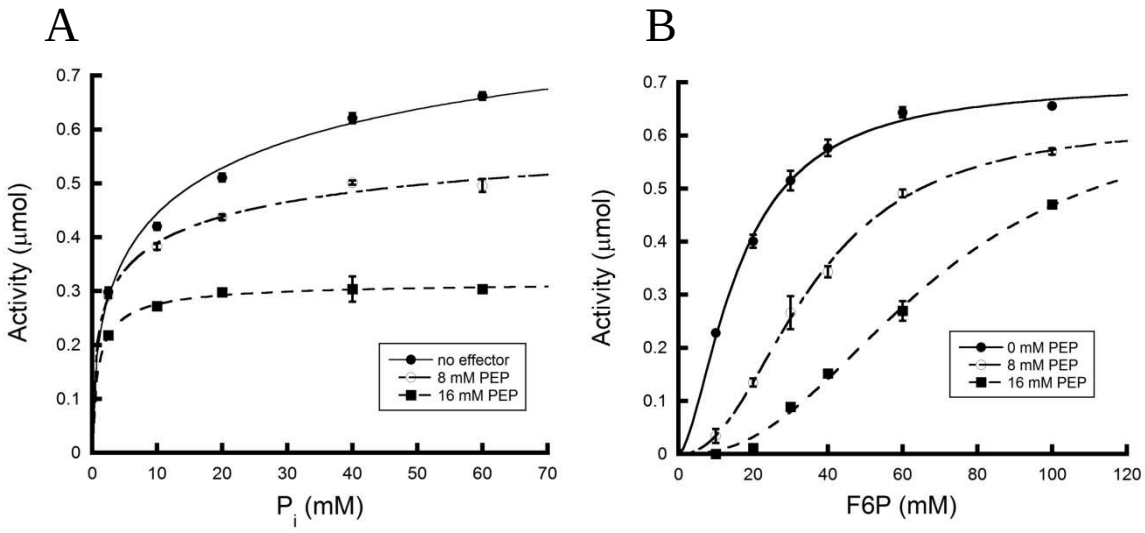

FIG 2.4. Effect of PEP on substrate progress curves. Progress curves were generated in the presence of 0 mM (●), 8 mM (○), and 16 mM (■) PEP for the substrates P_i (a) and F6P (b). Activities are reported in micromoles acetyl phosphate produced, and enzyme reactions were performed in triplicate for each substrate concentration.

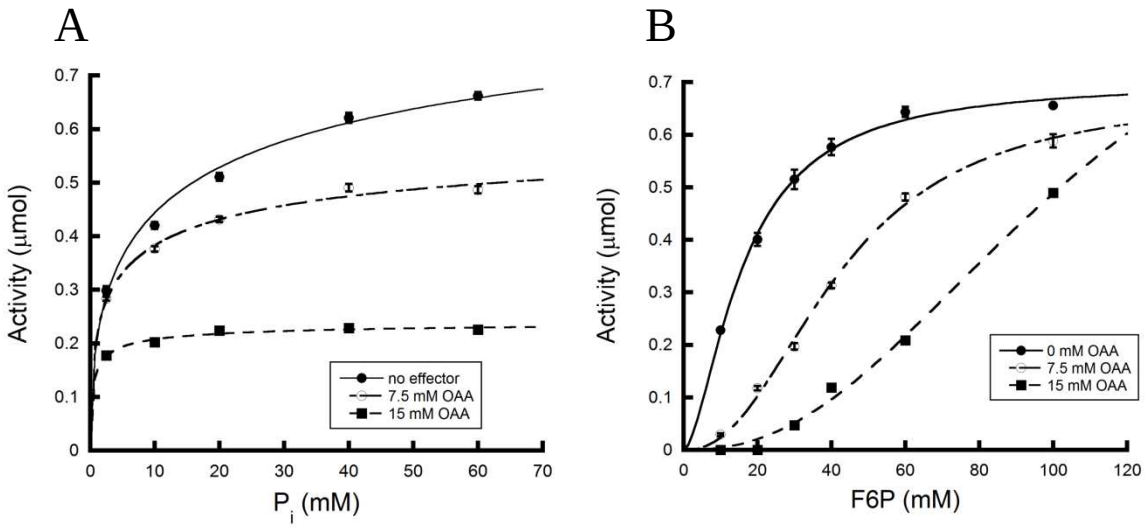

FIG 2.5. Effect of OAA on substrate progress curves. Progress curves were generated in the presence of 0 mM (●), 7.5 mM (○), and 15 mM (■) OAA for the substrates P_i (a) and F6P (b) Activities are reported in micromoles acetyl phosphate produced, and enzyme reactions were performed in triplicate for each substrate concentration.

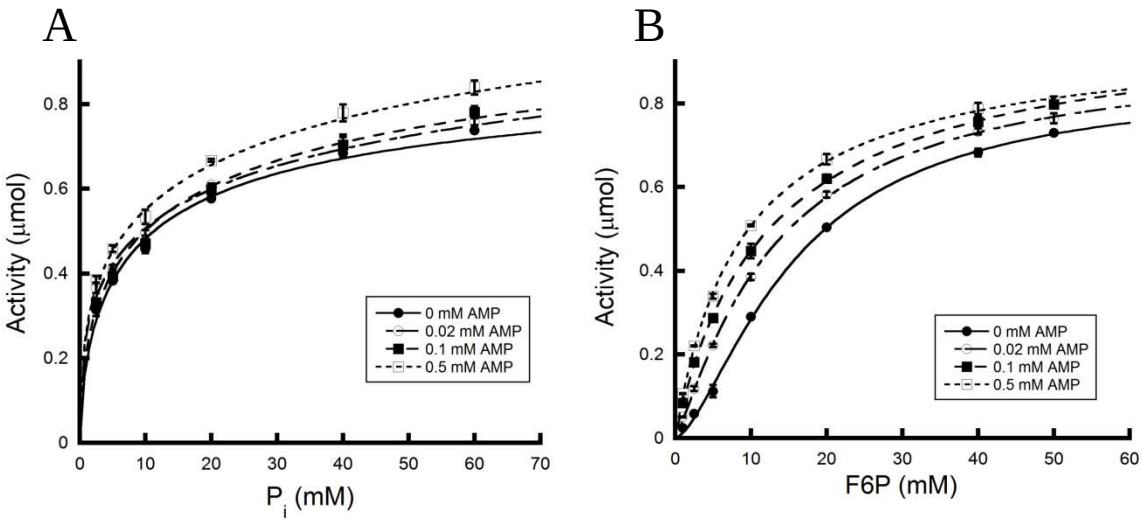

FIG 2.6. Effect of AMP on substrate progress curves. Progress curves were generated in the presence of 0 mM (●), 0.02 mM (○), 0.1 mM (■), and 0.5 mM (□) AMP for the substrates P_i (a) and F6P (b). Activities are reported in micromoles acetyl phosphate produced, and enzyme reactions were performed in triplicate for each substrate concentration.

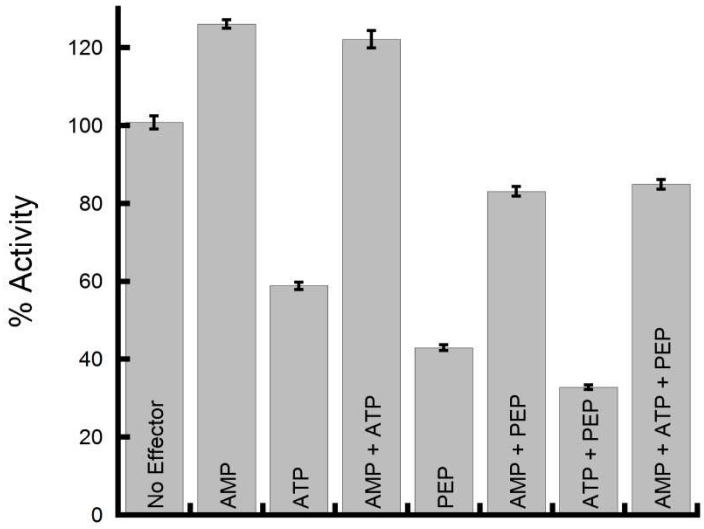

FIG 2.7. AMP activates Xfp2 activity and alleviates inhibition by allosteric inhibitors. Activities are reported as percentage of the maximum activity with no allosteric effector present. The effectors AMP, ATP and/ or PEP were added to reactions alone or in combination at final concentrations of 0.5 mM, 0.6 mM and 8 mM respectively.

CHAPTER 3

ALLOSTERIC REGULATION OF *LACTOBACILLUS PLANTARUM* XYLULOSE 5-PHOSPHATE/ FRUCTOSE 6-PHOSPHATE PHOSPHOKETOLASE (XFP)

Katie Glenn and Kerry S. Smith

I. ABSTRACT

Xylulose 5-phosphate/ fructose 6-phosphate phosphoketolase (Xfp), which catalyzes the conversion of xylulose 5-phosphate (X5P) or fructose 6-phosphate (F6P) to acetyl phosphate, plays a key role in carbohydrate metabolism in a number of bacteria. Recently we demonstrated that the fungal *Cryptococcus neoformans* Xfp2 exhibits both substrate cooperativity for all substrates (X5P, F6P and P_i) and allosteric regulation in the form of inhibition by phosphoenolpyruvate (PEP), oxaloacetic acid (OAA) and ATP and activation by AMP. Allosteric regulation has not previously been reported for the characterized bacterial Xfps. Here we report the discovery of substrate cooperativity and allosteric regulation among bacterial Xfps, specifically the *Lactobacillus plantarum* Xfp. *L. plantarum* Xfp was found to be an allosteric enzyme inhibited by PEP, OAA and glyoxylate but unaffected by the presence of ATP or AMP. Glyoxylate was also found to be an additional inhibitor to those previously reported for *C. neoformans* Xfp2. As with

C. neoformans Xfp2, PEP and OAA share the same or possess overlapping sites on *L. plantarum* Xfp. Glyoxylate, which had the lowest half maximal inhibitory concentration of the three inhibitors, binds at a separate site. This study demonstrates that substrate cooperativity and allosteric regulation may be common properties among bacterial and eukaryotic Xfp enzymes, yet important differences exist between the enzymes in these two domains.

II. INTRODUCTION

Xylulose 5-phosphate (X5P)/ fructose 6-phosphate (F6P) phosphoketolase (Xfp), a member of the thiamine pyrophosphate (TPP) dependent enzyme family, catalyzes the production of acetyl phosphate from the breakdown of xylulose 5-phosphate (equation 1a; EC 4.1.2.9) or fructose 6-phosphate (equation 1b; EC 4.1.2.22). In lactic acid bacteria and bifidobacteria, Xfp partners with either acetate kinase (Ack) to generate acetate and ATP (equation 2) or phosphotransacetylase (Pta) to generate acetyl-CoA and P_i (equation 3) (1,2). Xfp open reading frames (ORFs) have more recently been discovered in euscomycete and basidiomycete fungi as well (3). In fungi, Xfp is believed to partner with Ack since all fungi that have an Ack ORF have at least one, and in some cases two, Xfp ORFs but lack Pta (3).

$$\text{X5P} + P_i \leftrightarrow \text{Glyceraldehyde 3-phosphate} + \text{Acetyl phosphate} \quad (1a)$$

$$\text{F6P} + P_i \leftrightarrow \text{Erythrose 4-phosphate} + \text{Acetyl phosphate} \quad (1b)$$

$$\text{Acetyl phosphate} + \text{ADP} \leftrightarrow \text{Acetate} + \text{ATP} \quad (2)$$

$$\text{Acetyl-CoA} + P_i \leftrightarrow \text{Acetyl phosphate} + \text{CoA} \quad (3)$$

Xfp has been biochemically and kinetically characterized from several bacterial species, including *Lactobacillus plantarum* (referred to by Yevenes et al. as *L. plantarum* Xpk2) (2), *Bifidobacterium* spp. (1,4), *Lactococcus lactis*(5), *Leuconostoc mesenteroides* (5), and *Pseudomonas aeruginosa* (5), and more recently one fungal species,

Cryptococcus neoformans Xfp2 (6). The *Bifidobacterium* Xfp *L. plantarum*, *L. lactis*, *L. mesenteroides*, and *P. aeruginosa* Xfps displayed dual substrate specificity for both substrates X5P and F6P and followed Michaelis-Menten kinetics (1,2,4,5). *C. neoformans* Xfp2 also displays dual substrate specificity but does not follow Michaelis-Menten kinetics (6). Instead, kinetic characterization of *C. neoformans* Xfp2 indicated the existence of both substrate cooperativity and allosteric regulation. *C. neoformans* Xfp2 was found to be inhibited by ATP, phosphoenolpyruvate (PEP) and oxaloacetic acid (OAA) and activated by AMP (6). Substrate cooperativity and allosteric regulation have not been reported for any characterized bacterial Xfp (1,2,4,5).

In this paper we describe the characterization of *L. plantarum* Xfp in which kinetic parameters were determined using the Hill equation and the influence of potential allosteric effectors on *L. plantarum* Xfp activity was examined. *L. plantarum* Xfp was found to be an allosteric enzyme inhibited by PEP and OAA but unaffected by the presence of AMP or ATP. Additionally, glyoxylate was discovered to be an inhibitor of both *C. neoformans* Xfp2 and *L. plantarum* Xfp.

III. MATERIALS AND METHODS

Materials

All chemicals were purchased from Sigma Aldrich, VWR, Fisher Scientific, or Gold Biotechnology. The recombinant plasmid pET28b-*xpk2* in *Escherichia coli* BL21 (DE3) was kindly provided by Dr. Perry Frey (University of Wisconsin-Madison) for production of recombinant *L. plantarum* Xfp (2).

Production and Purification of Recombinant *L. plantarum* Xfp

BL21 (DE3) containing the recombinant plasmid pET28b-*xpk2* was grown in Luria-Bertani (LB) medium with 25 µg/mL kanamycin at 37 °C to an absorbance of ~0.8 at 600 nm. Recombinant *L. plantarum* Xfp production was induced by the addition of 1 mM isopropyl β-D-1-thiogalactopyranoside (IPTG). Cells were allowed to grow overnight at room temperature and harvested by centrifugation.

Cells were suspended in buffer A (25 mM Tris, 150 mM sodium chloride, 20 mM imidazole, 1 mM dithiothreitol (DTT) and 10% glycerol [pH 7.4]) and lysed by two passages through a French pressure cell at approximately 130MPa. Cell lysate was clarified by ultracentrifugation at 100,000 x g for 1.5 hours. The supernatant was applied to a 5 mL His-Trap HP column (GE Healthcare) and subjected to column chromatography using an AKTA-FPLC (GE Healthcare). After washing with at least seven column volumes of buffer A to remove any unbound protein, the column was

subjected to a linear gradient of 20 to 500 mM imidazole to remove all column-bound protein. Fractions determined to contain *L. plantarum* Xfp by SDS-PAGE and activity assays were pooled and dialyzed overnight against buffer containing 25 mM Tris, 1 mM DTT, and 10% glycerol [pH 7.0]. Protein concentration was determined using a modified Bradford assay (7) with bovine serum albumin as standard, and purified protein was stored at -80°C.

Production and Purification of Recombinant *C. neoformans* Xfp2

The recombinant plasmid pET21b-*XFP2* synthesized by GenScript was transformed into the *E. coli* expression strain RosettaBlue™ (Novagen). The recombinant strain was grown in LB medium supplemented with 1 % dextrose, to reduce basal level transcription from the T7 RNA polymerase gene under the control of L8-UV5 promoter in the DE3 prophage prior to the addition of IPTG, and 50 µg/mL ampicillin and 34 µg/mL chloramphenicol. At an absorbance of ~0.8 at 600 nm, IPTG was added to a final concentration of 1 mM to induce production of the enzyme. Expression was allowed to proceed overnight at room temperature, and cells were harvested by centrifugation. Recombinant *C. neoformans* Xfp2 was purified as previously described (6).

Xfp Assay

Enzymatic activity was measured using the hydroxamate assay to detect the production of acetyl phosphate (1,2,6,8). A standard 200 µL reaction contained 0.5 mM thiamine pyrophosphate (TPP), 1 mM DTT, 5 mM magnesium chloride, and 50 mM MES (at pH

6.0 for *L. plantarum* Xfp assays and pH 5.5 for *C. neoformans* Xfp2 assays) with varied concentrations of the substrates F6P and $P_{i,}$ in the form of sodium phosphate pH 6.0 for *L. plantarum* Xfp and pH 5.5 for *C. neoformans* Xfp2. Reactions were initiated by the addition of enzyme and allowed to proceed for 30 minutes at 37°C for *L. plantarum* Xfp and 40°C for *C. neoformans* Xfp2. After 30 minutes, 100 µL of 2 M hydroxylamine hydrochloride (pH 7.0) was added, and reactions were allowed to incubate at room temperature for 10 minutes to fully convert all acetyl phosphate to acetyl hydroxamate. Reactions were terminated by the addition of 600 µL of a 50:50 mixture of 2.5 % ferric chloride in 2N hydrochloric acid and 10 % trichloroacetic acid to generate the ferric-hydroxamate complex. The color change due to product formation was measured by a change in absorbance at 540 nm. All data sets correspond to reactions performed in triplicate.

L. plantarum Xfp Kinetic Analysis

To determine *L. plantarum* Xfp kinetic parameters, one substrate was varied while the other substrate was held constant at a saturating concentration (60 mM for F6P and 8 mM for P_i). Since the commercial availability of X5P has been discontinued, all kinetic parameters were determined using F6P. Data was plotted using KaleidaGraph software (Synergy), and kinetic parameters were found by applying the Hill equation (equation 4) (9,10) to the data set where V_0 is initial velocity, [S] is substrate concentration, V is maximum velocity, $K_{0.5}$ is substrate concentration at half maximal velocity and *h* is the Hill constant.

$$V_0 = V + [S]^h/({K_{0.5}}^h + [S]^h) \quad (4)$$

Determination of Inhibitor IC_{50} Values (Individually and in Combination)

The half maximal inhibitory concentration (IC_{50}) was determined for each *L. plantarum* Xfp inhibitor and an additional *C. neoformans* Xfp2 inhibitor not previously described by measuring the decrease in enzyme activity at $K_{0.5}$ substrate concentrations (11 mM F6P and 1 mM P_i for *L. plantarum* Xfp and 16 mM F6P and 13 mM P_i for *C. neoformans* Xfp2) in the presence of increasing inhibitor concentration. The IC_{50} was found by fitting the data with a log [inhibitor] vs response curve in Graphpad Prism 5 software. In order to determine if inhibitors share the same or overlapping allosteric binding sites the effect on IC_{50} of one inhibitor in the presence of another inhibitor was measured.

IV. RESULTS

Effect of pH on *L. plantarum* Xfp Activity

Recombinant *L. plantarum* Xfp was produced and purified using nickel affinity chromatography. It was previously discovered that *C. neoformans* Xfp2 activity is significantly reduced with increasing pH and that maximal activity occurs between pH 4.5 and 6.0 (6). Like *C. neoformans* Xfp2, *L. plantarum* Xfp activity decreases with increasing pH. However, the decrease in activity does not occur until pH 6.5 versus pH 6.0 for *C. neoformans* Xfp2 (Fig. 1) suggesting that *L. plantarum* Xfp is slightly more tolerant to elevated pH than *C. neoformans* Xfp2. Maximum *L. plantarum* Xfp activity occurs around pH 6.0 which was used in all kinetic assays.

Kinetic Characterization of *L. plantarum* Xfp

We have recently shown that *C. neoformans* Xfp2 displays substrate cooperativity and is subject to allosteric regulation (6), neither of which have been reported for any of the bacterial Xfp enzymes (1,4,5,11), including the *L. plantarum* Xfp (2). To establish whether substrate cooperativity exists for *L. plantarum* Xfp, apparent kinetic parameters (Table 1) were determined in the acetyl phosphate forming direction for the substrates F6P and P_i by fitting the Hill equation to plots of substrate concentration versus velocity. *L. plantarum* Xfp displays negative cooperativity for P_i as indicated by a Hill constant of 0.68 ± 0.02, similar to the Hill constant of 0.59 ± 0.03 for the *C. neoformans* enzyme (6).

The $K_{0.5}$ value of 1.0 ± 0.1 mM for P_i is similar to the K_m previously determined for the *L. plantarum* enzyme (2).

Unlike *C. neoformans* Xfp2, *L. plantarum* Xfp Hill constant of approximately 1.0 does not indicate the existence of substrate cooperativity in regards to F6P binding. F6P progress curves for *L. plantarum* Xfp were found to fit both the Michaelis-Menten and Hill equations equally well with R values around 0.99. Using the Michaelis-Menten equation K_m^{app} for F6P was determined to be 10.8 ± 0.8 mM, while a $K_{0.5}$ for F6P of 11.0 ± 1.4 mM was calculated using the Hill equation for the same data set. Both F6P $K_{0.5}$ and K_m^{app} are on the same order of magnitude as the K_m^{app} for F6P previously determined by Yevenes et al. (2).

L. plantarum Xfp is Inhibited by PEP and OAA, but Unaffected by AMP and ATP.

The same ligands examined as possible allosteric effectors of *C. neoformans* Xfp2 (6) were tested to determine their effect on *L. plantarum* Xfp activity. As with *C. neoformans* Xfp2, *L. plantarum* Xfp is inhibited by phosphoenolpyruvate (PEP) and oxaloacetic acid (OAA) (Fig. 2) and slightly inhibited by citrate (data not shown). *L. plantarum* Xfp activity was unaffected by the presence of AMP or ATP, the primary allosteric activator and inhibitor, respectively, of *C. neoformans* Xfp2. Additional ligands tested such as acetate and pyruvic acid that had no effect on *C. neoformans* Xfp2 activity also had no effect on *L. plantarum* Xfp activity.

Glyoxylate Inhibits both *L. plantarum* Xfp and *C. neoformans* Xfp2 Activity

Since PEP and OAA serve as common allosteric effectors for bacterial *L. plantarum* Xfp and eukaryotic *C. neoformans* Xfp2, various PEP analogs were tested to determine the specificity of this allosteric site for PEP and the primary chemical moiety that contributes to the allosteric inhibitory effect. Non-phosphorylated PEP analogs have previously been utilized to determine the chemical moiety that contributes to allostery in muscle pyruvate kinase (12), and each of these PEP analogs were used to test *L. plantarum* Xfp inhibition (Fig. 3a). Interestingly, glyoxylate was found to inhibit Xfp in addition to PEP and OAA. *L. plantarum* Xfp was almost fully inhibited by 8 mM glyoxylate with only 7.2 ± 1.0% activity remaining but only partially inhibited by 8 mM PEP (45.7 ± 3.4% activity remaining). Pyruvate showed no inhibition while the PEP analogs D-lactate, L-lactate, methyl pyruvate, hydroxyacetone, and glycolate displayed intermediate levels of inhibition. These same PEP analogs were used to test their inhibitory effect against *C. neoformans* Xfp2 as well, and the results were similar to those found for the *L. plantarum* Xfp. Glyoxylate also inhibits *C. neoformans* Xfp2 activity, with 8 mM reducing activity to 15.3 ± 1.0%. Similar to *L. plantarum* Xfp, pyruvate had no effect on *C. neoformans* Xfp2 activity while all other PEP analogs show intermediate inhibition between that of pyruvate and glyoxylate (Fig. 3b).

Determination of Allosteric Effector Half Maximal Inhibitory Concentrations (IC_{50}s)

The IC_{50} half maximal inhibitory concentration was determined for each *L. plantarum* Xfp inhibitor (Table 2) using $K_{0.5}$ substrate concentrations. The IC_{50} for glyoxylate was lower than those for PEP and OAA by approximately 3-fold and 5-fold, respectively. In order to determine if any of these inhibitors share the same site, the IC_{50} of one inhibitor was determined in the presence of a second inhibitor held constant at its IC_{50}. If two inhibitors share the same site or if their sites overlap, then approximately half the sites should be occupied by the inhibitor held constant thereby lowering the amount of the varied inhibitor required to reduce activity by an additional 50%.

In the presence of 10.5 mM OAA, the PEP IC_{50} decreased more than half the original value, demonstrating that the *L. plantarum* PEP and OAA binding sites are the same or overlapping, as indicted previously for *C. neoformans* Xfp2 (6). The reason the IC_{50} of PEP is reduced by more than half in the presence of OAA is most likely due to the unique inhibitory effect of OAA (Fig 4a) not seen in glyoxylate (Fig 4b) or PEP (Fig 4c) inhibition profiles. High concentrations of OAA were required to initiate *L. plantarum* Xfp inhibition followed by a sharp decrease in activity in the presence of additional OAA (Fig 4a). This inhibitory concentration threshold may suggest that PEP and OAA interact with the binding site differently or that these are overlapping instead of identical binding sites. The IC_{50} of PEP does not change significantly in the presence of 2 mM glyoxylate while the IC_{50} of OAA decreases by approximately 26%. Therefore, it appears that the

PEP/OAA site is separate from the glyoxylate site since neither PEP nor OAA IC_{50} display close to a 50% decrease in the presence of 2 mM glyoxylate.

Since glyoxylate was not previously recognized as an Xfp inhibitor (6), the IC_{50} of glyoxylate was determined for *C. neoformans* Xfp2 (Table 2). The *C. neoformans* Xfp2 PEP IC_{50} of 5.31 ± 0.13 mM, slightly lower than the 8 mM IC_{50} previously reported, (6) decreased to 4.01 ± 0.07 mM in the presence of 5 mM glyoxylate. Since the IC_{50} of PEP only decreases by about 24% in the presence of 5 mM glyoxylate, it is likely that the binding of PEP and glyoxylate occur at separate sites on *C. neoformans* Xfp2 as well.

Allosteric Inhibitors Influence F6P Binding

Progress curves of substrate concentration versus activity were generated for *L. plantarum* Xfp substrates F6P and P_i in the presence of increasing PEP concentrations (Fig. 5). The presence of PEP had the same effect on *L. plantarum* Xfp kinetic parameters as it did for *C. neoformans* Xfp2 (6). In regards to P_i, the presence of PEP had little effect on $K_{0.5}$, which remained between 1.0 ± 0.03 mM and 1.3 ± 0.30 mM at 0 mM PEP and 16 mM PEP respectively, or Hill constant, which ranged between 0.66 ± 0.01 and 0.49 ± 0.02. However, a gradual reduction in V_{max} from 1.06 ± 0.01 µmol of product formed per 30 minute reaction at 0 mM PEP to 0.80 ± 0.04 µmol at 16 mM PEP was observed. The $K_{0.5}$ of F6P increased from 9.8 ± 0.2 mM in the absence of inhibitor to 37.8 ± 0.9 mM in the presence of 16 mM F6P and the Hill constant also increased from 1.31 ± 0.01 to 1.79 ± 0.01. The presence of PEP had little effect on F6P maximal activity

with V_{max} ranging between 0.93 ± 0.02 and 0.87 ± 0.01 µmol of product formed per 30 minute reaction. Since PEP and OAA bind at the same or overlapping sites on *L. plantarum* Xfp, PEP was utilized to represent the effect of both PEP and OAA inhibition on substrate binding. The influence that PEP inhibition has on the F6P $K_{0.5}$ and Hill constant suggests that, similar to *C. neoformans* Xfp2 (6), the binding of PEP and OAA directly influences the binding of F6P to the *L. plantarum* Xfp active site. Glyoxylate binding did not significantly influence F6P $K_{0.5}$ but had a greater influence on V_{max} (data not shown).

V. DISCUSSION

Recently we determined that a fungal Xfp, *C. neoformans* Xfp2, displayed both substrate cooperativity (positive cooperativity for F6P and negative cooperativity for P_i) and allosteric regulation in the form of inhibition through the binding of ATP, PEP and OAA and activation by the binding of AMP (6). Here we report the discovery of substrate cooperativity and allosteric regulation for bacterial *L. plantarum* Xfp. This report describes the first indication that substrate cooperativity and allosteric regulation also exists among at least some bacterial Xfp enzymes. Kinetic parameters for *L. plantarum* Xfp were originally determined by Yevenes et al. by fitting substrate progress curves with the Michaelis-Menten equation to determine apparent binding constants K_m for F6P and P_i which were found to be 24 ± 4 mM and 2.9 ± 0.5 mM respectively (2). We produced the recombinant *L. plantarum* Xfp and demonstrated that this enzyme displays negative cooperativity in regards to P_i binding with a Hill constant less than one but little cooperativity in regards to F6P binding with a Hill constant roughly equal to one.

In addition to substrate cooperativity, *L. plantarum* Xfp, like *C. neoformans* Xfp2, is allosterically regulated. It is inhibited by PEP and OAA, but unlike *C. neoforamans* Xfp2 the presence of ATP or AMP had little to no effect on activity. Initially *L. plantarum* Xfp kinetic parameters did not suggest the presence of substrate cooperativity for F6P binding alone however the presence of the inhibitor PEP induces positive

cooperativity as demonstrated by the sigmoidal progress curves and increase in F6P Hill constant shown in Fig. 5. Unlike PEP, glyoxylate inhibits enzyme activity without greatly influencing F6P binding since both F6P K_m and Hill constant were not greatly altered. In regards to *C. neoformans* Xfp2 and *L. plantarum* Xfp regulation by excess PEP and OAA, the presence of these intermediates indicate the energy needs of the cell have been met. The cell can switch from glycolysis, the breakdown of glucose, to gluconeogenesis to synthesize and ultimately store glucose until it is needed, and therefore, Xfp may be inhibited by these intermediates in order to limit additional energy production through the Xfp/Ack pathway (6).

In addition to Xfp, *L. plantarum* can produce acetyl phosphate from pyruvate using pyruvate oxidase (Pox) and from acetyl-CoA using phosphotransacetylase (Pta). It has been shown that at least some Acks in heterofermentative bacteria are allosterically regulated (13). Perhaps Xfp regulation by the presence of ATP and AMP is less necessary in *L. plantarum* that has additional sources for acetyl phosphate production and may also possess an allosterically regulated Ack, though this has not been experimentally proven. Xfp regulation by ATP and AMP may have evolved in *C. neoformans* where there is no evidence of an allosterically regulated Ack (C. Ingram-Smith, A. Guggisberg, S. Henry, J. Welch, K. Laws, A. Mattison, A. Bizhanova, and K. Smith**,** manuscript in preparation) or the presence of additional acetyl phosphate producing enzymes such as Pox and Pta. Therefore, the control of ATP production by Ack in *C. neoformans* may rest solely on the production of acetyl phosphate by Xfp.

Non-phosphorylated PEP analogs were tested to determine the primary chemical moiety that contributes to PEP allosteric inhibition for both *L. plantarum* Xfp and *C. neoformans* Xfp2. Interestingly, pyruvate displayed no inhibition while glyoxylate, which differs from pyruvate by the absence of a single methyl group, inhibits *L. plantarum* Xfp more than PEP or OAA at the same concentration. Our results suggest that PEP and OAA bind to the same or overlapping sites in both *L. plantarum* Xfp and *C. neoformans* Xfp2, but glyoxylate binds at a distinct site.

Since glyoxylate is an allosteric inhibitor with presumably its own allosteric site on both *L. plantarum* Xfp and *C. neoformans* Xfp2, there is likely a metabolic connection between the presence of excess glyoxylate and the inhibition of Xfp, consequently limiting the production of acetyl phosphate from X5P and F6P. The glyoxylate cycle functions as a bypass of the decarboxylation steps of the tricarboxylic acid cycle allowing for the use of simple two-carbon compounds, such as acetate and ethanol, to generate malate from the combined action of the enzymes isocitrate lyase (Icl) and malate synthase (Mls) (14-16). The glyoxylate cycle is utilized when glucose is limiting (14), but the production of excess glyoxylate may indicate that other 2-carbon compounds, such as acetate, are prevalent. Since we hypothesize that *C. neoformans* Xfp2 partners with Ack to generate acetate and ATP, the presence of excess glyoxylate may indicate that acetate is in abundance, so glyoxylate inhibits Xfp thereby inhibiting the production of acetyl phosphate and consequently the production of acetate by Ack.

We have failed to identify genes encoding the enzymes Icl and Mls within the *L. plantarum* genome suggesting it lacks a glyoxylate cycle. However, *L. plantarum* cell free extract is capable of metabolizing glyoxylate (17). An ORF within the *L. plantarum* genome designated as 2-hydroxyacid dehydrogenase (Accession # YP_004888759) has 61% identity to a gene designated as a glyoxylate reductase (equation 5) in *Lactobacillus otakiensis*, and it has also been shown in *Rhizobium etli* that an enzyme previously labeled as 2-hydroxyacid dehydrogenase displays glyoxylate reductase activity (18).

$$\text{glyoxylate} + \text{NAD(P)H} \leftrightarrow \text{glycolate} + \text{NAD(P)}^{+} \quad (5)$$

In plants, glyoxylate reductase is believed to function as a way of removing excess reducing equivalents like NADPH (19), and glyoxylate reductase in *L. plantarum* could serve a similar purpose. A possible connection between *L. plantarum* Xfp inhibition by excess glyoxylate is that the presence of glyoxylate could indicate the presence of excess NADPH. The pentose phosphate pathway (PPP) serves as a major source of the NADPH produced in the cell. Thus, inhibiting Xfp, which utilizes PPP end products, may hinder the PPP from producing additional end products thereby also reducing the amount of NADPH produced upstream. The regulation of Xfp by glyoxylate in *L. plantarum* may serve as a means of balancing the production and utilization of NADPH by the PPP and glyoxylate reductase respectively to aid in cellular redox balance.

Concluding Remarks

Substrate cooperativity and allosteric regulation can no longer be considered a purely eukaryotic Xfp phenomenon with the discovery of its existence in at least some bacterial Xfps, specifically *L. plantarum* Xfp. However, there are differences between the degree of substrate cooperativity and the allosteric effectors that inhibit or activate eukaryotic Xfp and bacterial Xfp from *C. neoformans* and *L. plantarum* respectively. Both *C. neoformans* Xfp2 and *L. plantarum* Xfp share PEP, OAA and glyoxylate as allosteric inhibitors, but *C. neoformans* Xfp2 is also inhibited by ATP and activated by AMP while an activator of *L. plantarum* Xfp has yet to be discovered. Tighter regulation of Xfp by ATP:AMP ratios may have evolved for eukaryotic Xfps due to the lack of additional partner enzymes, compared to bacteria, that generate acetyl phosphate as a substrate for Ack. Additionally, regulation by glyoxylate appears to result from different phenomenon in *C. neoformans* that primarily produces glyoxylate through the glyoxylate cycle versus *L. plantarum* which appears to lack a glyoxylate cycle. The presence of allosteric regulation for both bacterial and eukaryotic Xfps suggests the production and utilization of acetyl phosphate is important under different environmental stresses that ultimately influence cellular metabolism.

VI. ACKNOWLEDGMENTS

We thank Cheryl Ingram-Smith for her critical reading of the manuscript.

This work was supported by awards from the National Institutes of Health (GM084417-01A1), National Science Foundation (Award# 0920274), South Carolina Experiment Station Project SC-1700340 and represents Technical Contribution #6266 of the Clemson University Experiment Station.

VII. REFERENCES

1. Meile, L., Rohr, L. M., Geissmann, T. A., Herensperger, M., and Teuber, M. (2001) Characterization of the D-xylulose 5-phosphate/D-fructose 6-phosphate phosphoketolase gene (xfp) from *Bifidobacterium lactis*. *J. Bacteriol.* **183**, 2929-2936

2. Yevenes, A., and Frey, P. A. (2008) Cloning, expression, purification, cofactor requirements, and steady state kinetics of phosphoketolase-2 from *Lactobacillus plantarum*. *Bioorg. Chem.* **36**, 121-127

3. Ingram-Smith, C., Martin, S. R., and Smith, K. S. (2006) Acetate kinase: not just a bacterial enzyme. *Trends Microbiol.* **14**, 249-253

4. Suzuki, R., Katayama, T., Kim, B. J., Wakagi, T., Shoun, H., Ashida, H., Yamamoto, K., and Fushinobu, S. (2010) Crystal structures of phosphoketolase: thiamine diphosphate-dependent dehydration mechanism. *J. Biol. Chem.* **285**, 34279-34287

5. Petrareanu, G., Balasu, M. C., Vacaru, A. M., Munteanu, C. V., Ionescu, A. E., Matei, I., and Szedlacsek, S. E. (2014) Phosphoketolases from *Lactococcus lactis*, *Leuconostoc mesenteroides* and *Pseudomonas aeruginosa*: dissimilar sequences, similar substrates but distinct enzymatic characteristics. *Appl. Microbiol. Biotechnol.*, 7855-7867

6. Glenn, K., Ingram-Smith, C., and Smith, K. S. (2014) Biochemical and Kinetic Characterization of Xylulose 5-phosphate/Fructose 6-phosphate Phosphoketolase 2 (Xfp2) from *Cryptococcus neoformans*. *Eukaryot. Cell* **13**, 657-663

7. Bradford, M. M. (1976) A rapid and sensitive method for the quantitation of microgram quantities of protein utilizing the principle of protein-dye binding. *Anal. Biochem.* **72**, 248-254

8. Lipmann, F., and Tuttle, L. C. (1945) A specific micromethod for determination of acyl phosphates. *J. Biol. Chem.* **159**, 21-28

9. Hill, A. V. (1910) The possible effects of the aggregation of the molecules of haemoglobin on its dissociation curves. *J. Physiol.* **40**, iv-vii

10. Motulsky, H. (2004) *Fitting Models to Biological Data Using Linear and Nonlinear Regression: A Practical Guide to Curve Fitting: A Practical Guide to Curve Fitting*, Oxford University Press

11. Takahashi, K., Tagami, U., Shimba, N., Kashiwagi, T., Ishikawa, K., and Suzuki, E. (2010) Crystal structure of *Bifidobacterium longum* phosphoketolase; key enzyme for glucose metabolism in Bifidobacterium. *FEBS Lett.* **584**, 3855-3861

12. Urness, J. M., Clapp, K. M., Timmons, J. C., Bai, X., Chandrasoma, N., Buszek, K. R., and Fenton, A. W. (2013) Distinguishing the chemical moiety of phosphoenolpyruvate that contributes to allostery in muscle pyruvate kinase. *Biochemistry* **52**, 1-3

13. Puri, P., Goel, A., Bochynska, A., and Poolman, B. (2014) Regulation of Acetate Kinase Isozymes and Its Importance for Mixed-Acid Fermentation in *Lactococcus lactis*. *J. Bacteriol.* **196**, 1386-1393

14. Rude, T. H., Toffaletti, D. L., Cox, G. M., and Perfect, J. R. (2002) Relationship of the Glyoxylate Pathway to the Pathogenesis of *Cryptococcus neoformans*. *Infect. Immun.* **70**, 5684-5694

15. Price, M. S., Betancourt-Quiroz, M., Price, J. L., Toffaletti, D. L., Vora, H., Hu, G., Kronstad, J. W., and Perfect, J. R. (2011) *Cryptococcus neoformans* requires a functional glycolytic pathway for disease but not persistence in the host. *MBio* **2**, e00103-00111

16. Lorenz, M. C., and Fink, G. R. (2001) The glyoxylate cycle is required for fungal virulence. *Nature* **412**, 83-86

17. Hasan, N., Nassif, N., and Durr, I. F. (1972) The metabolism of glyoxylate by a cell-free extract of Lactobacillus plantarum. *Int. J. Biochem.* **3**, 607-612

18. Fauvart, M., Braeken, K., Daniels, R., Vos, K., Ndayizeye, M., Noben, J. P., Robben, J., Vanderleyden, J., and Michiels, J. (2007) Identification of a novel glyoxylate reductase supports phylogeny-based enzymatic substrate specificity prediction. *Biochim. Biophys. Acta* **1774**, 1092-1098

19. Tolbert, N. E., Yamazaki, R. K., and Oeser, A. (1970) Localization and properties of hydroxypyruvate and glyoxylate reductases in spinach leaf particles. *J. Biol. Chem.* **245**, 5129-5136

TABLE 3.1. Apparent kinetic parameters for *L. plantarum* Xfp and *C. neoformans* Xfp2.

	Substrate	$K_{0.5}$ (mM)	k_{cat}^{app} (sec^{-1})	$k_{cat}^{app}/K_{0.5}$ ($sec^{-1} mM^{-1}$)	H
L. plantarum Xfp	F6P	11.0 ± 1.4	1.05 ± 0.05	0.10 ± 0.01	0.99 ± 0.04
	P_i	1.0 ± 0.1	1.12 ± 0.03	1.11 ± 0.09	0.68 ± 0.02
C. neoformans Xfp2*	F6P	15.9 ± 1.3	3.47 ± 0.10	0.22 ± 0.01	1.41 ± 0.11
	P_i	13.3 ± 1.5	4.22 ± 0.13	0.32 ± 0.03	0.59 ± 0.03

*Previously reported kinetic parameters (6).

TABLE 3.2. Half maximal inhibitory concentrations (IC_{50}s)

Enzyme	Inhibitor (Varied)	Inhibitor (Constant)	IC_{50} (mM)
L. plantarum Xfp	Glyoxylate	--------	1.93 ± 0.05
	PEP	--------	6.70 ± 0.12
		OAA (10.5 mM)	1.14 ± 0.12
		Glyoxylate (2 mM)	6.04 ± 0.11
	OAA	--------	10.5 ± 0.07
		Glyoxylate (2 mM)	7.78 ± 0.20
C. neoformans Xfp2	Glyoxylate	--------	4.93 ± 0.04
		PEP (8 mM)	3.13 ± 0.18
	PEP	--------	5.31 ± 0.13
		Glyoxylate (5 mM)	4.01 ± 0.07

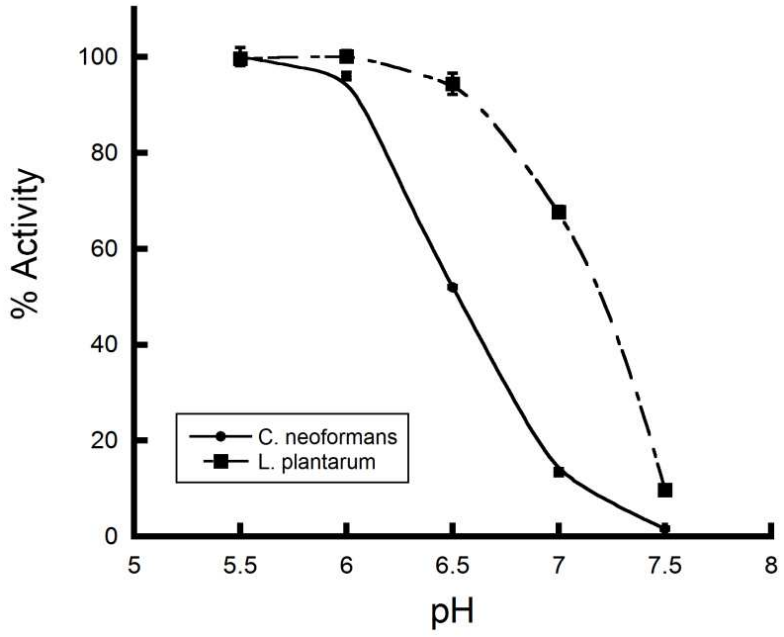

FIG 3.1. Effect of pH on *L. plantarum* Xfp and *C. neoformans* Xfp2 percent activity. Enzyme reactions were performed using F6P and P_i $K_{0.5}$ concentrations for *L. plantarum* Xfp (■) and *C. neoformans* Xfp2 (●). Activity begins to decrease at pH values above 6.0 for *C. neoformans* Xfp2 and above 6.5 for *L. plantarum* Xfp.

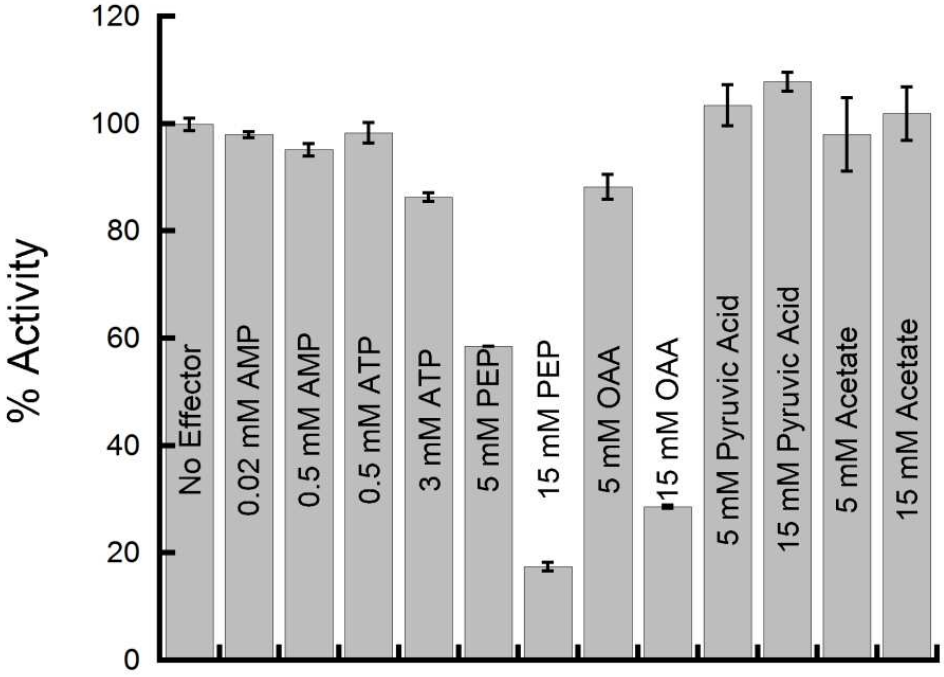

FIG 3.2. Effect of various ligands on *L. plantarum* Xfp activity. Reactions were performed using *L. plantarum* Xfp F6P and P_i $K_{0.5}$ substrate concentrations. Two concentrations of each coenzyme or metabolic intermediate were tested. Reactions were performed in triplicate. Activity is reported as percentage of activity with no ligand present.

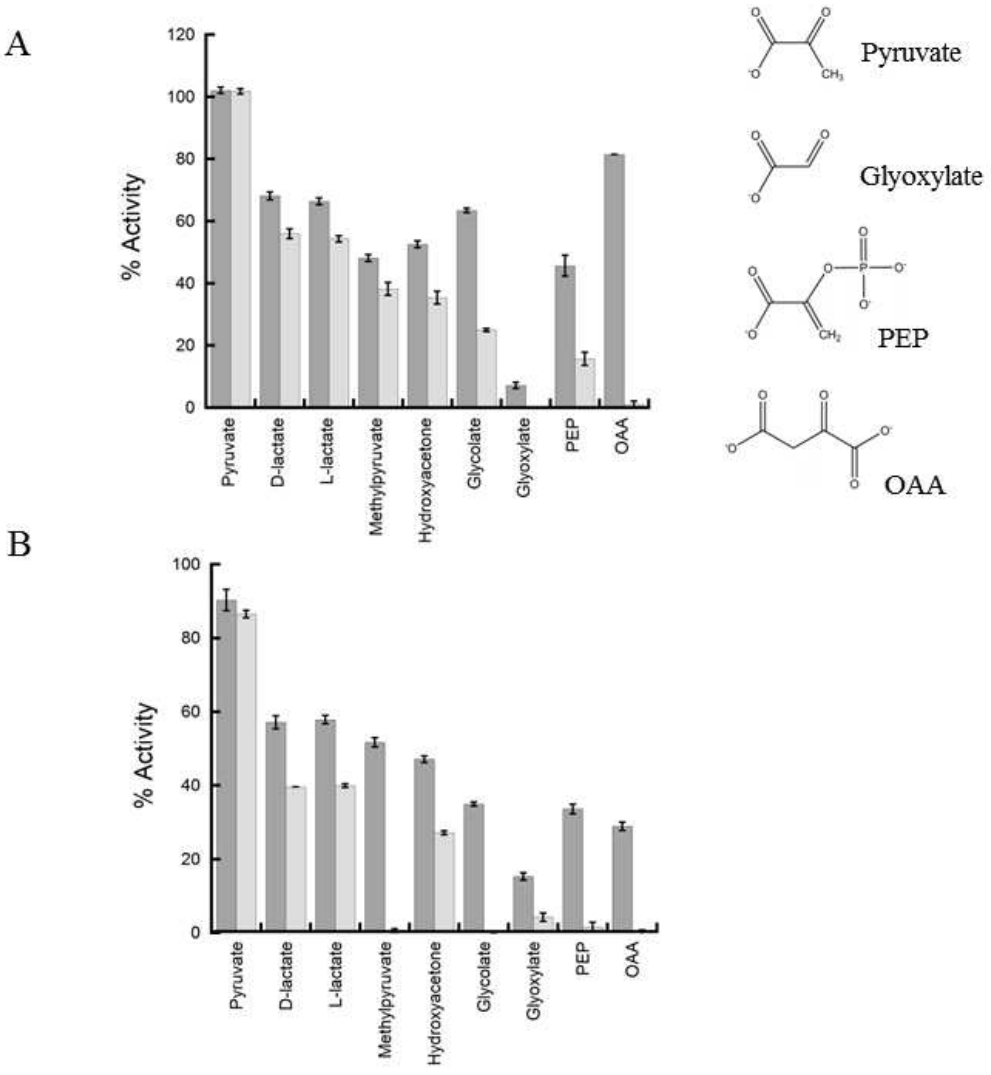

FIG. 3.3. Effect of non-phosphorylated PEP analogs on *L. plantarum* Xfp (A) and C. neoformans Xfp2 (B) activity. Reactions were performed using *L. plantarum* Xfp F6P and P_i $K_{0.5}$ substrate concentrations. Concentrations of 8 mM (dark grey) and 16 mM (light grey) for each non-phosphorylated PEP analog were tested in triplicate. Activity is reported as a percentage of activity with no ligand present.

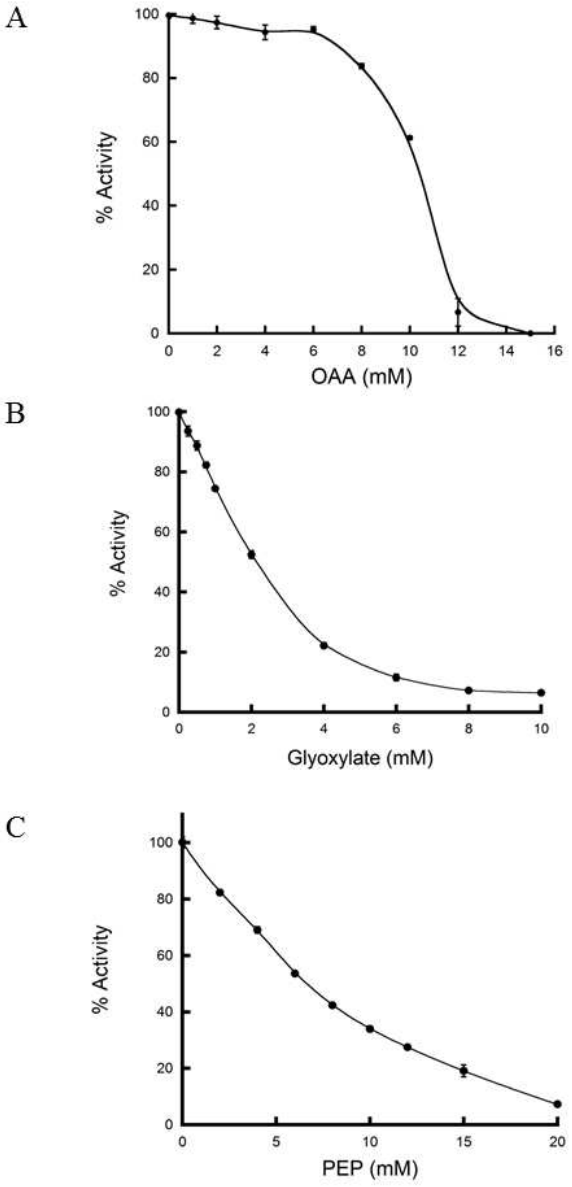

FIG 3.4. Inhibition of L. plantarum Xfp by OAA, PEP and glyoxylate. Reactions were performed in triplicate using *L. plantarum* Xfp F6P and P_i $K_{0.5}$ substrate concentrations. Activity was measured in the presence of increasing concentrations of OAA (A), glyoxylate (B) or PEP (C) and reported as a percentage of maximal activity with no ligand presence.

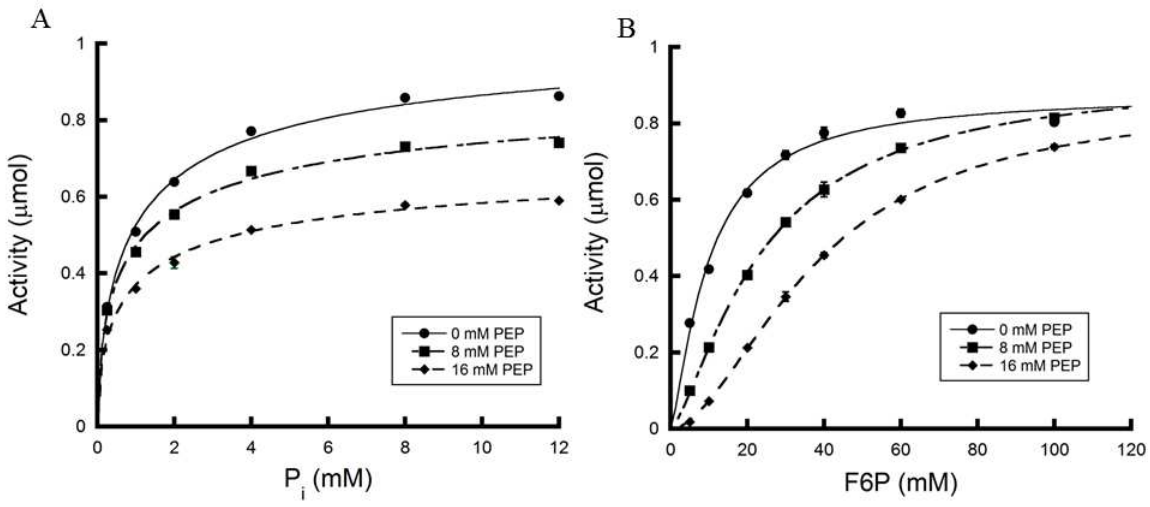

FIG 3.5. Effect of PEP on L. plantarum Xfp substrate progress curves. Progress curves were generated in the presence of 0 mM (●), 8 mM (■), and 16 mM (♦) PEP for the substrates P_i (a) and F6P (b). Reactions were performed in triplicate and activities were reported as µmol of product formed.

CHAPTER 4

INVESTIGATIONS INTO THE LOCATION OF *C. NEOFORMANS* XFP2 ALLOSTERIC SITES THROUGH COMPUTATIONAL MODELING AND SITE-DIRECTED MUTAGENESIS

Katie Glenn and Kerry Smith

I. ABSTRACT

Xylulose 5-phosphate/ fructose 6-phosphate phosphoketolase (Xfp) catalyzes the reaction converting xylulose 5-phosphate (X5P) or fructose 6-phosphate (F6P) to acetyl phosphate and glyceraldehyde 3-phosphate (G3P) or erythrose 4-phosphate (E4P) respectively. Recently we have determined that at least some fungal and bacterial Xfps are allosteric enzymes. Both *Cryptococcus neoformans* Xfp2 and *Lactobacillus plantarum Xfp* are inhibited by phosphoenolpyruvate (PEP), oxaloacetic acid (OAA), and glyoxylate, and PEP and OAA appear to share the same or possess overlapping sites on both Xfps. The *C. neoformans* Xfp2 is also inhibited by ATP and activated by AMP, but the *L. plantarum* enzyme is unaffected by these ligands. Additional studies provide evidence that ATP inhibition of *C. neoformans* Xfp2 may be dependent on ATP hydrolysis. Currently the only crystal structures that exist of Xfp are from two bacteria,

Bifidobacterium breve and *Bifidobacterium longum*. Here we describe the generation of both a monomer and dimer model of *C. neoformans* Xfp2 using the existing bacterial Xfp crystal structures. The models were used to identify possible allosteric binding sites, and ligand docking simulations were performed using PEP and OAA in an attempt to discover the location of the PEP/OAA allosteric site. Residues predicted to form hydrogen bonds with PEP and OAA were altered to the neutral residue alanine or amino acids of opposite charge, but these alterations have yet to define the PEP/OAA pocket(s). Also we discovered that AMP functions as a very potent enzyme activator capable of rescuing activity of enzyme variants displaying much lower activity than wild type.

II. INTRODUCTION

Xylulose 5-phosphate/ fructose 6-phosphate phosphoketolase (Xfp) is a thiamine pyrophosphate (TPP) dependent enzyme that catalyzes the conversion of xylulose 5-phosphate (X5P, EC 4.1.2.9; X5P + P_i → acetyl phosphate + glyceraldehyde 3-phosphate) or fructose 6-phosphate (F6P, EC 4.1.2.22; F6P + P_i → acetyl phosphate + erythrose 4-phosphate) to acetyl phosphate. Originally identified and characterized in bacteria (1-4), Xfp has more recently been found in euascomycete and basidiomycete fungi as well (5). Phylogenetic analysis show that fungal Xfps separate into two distinct clades designated as *XFP1* and *XFP2* (A. Guggisberg and K. Smith, unpublished data). All fungi in which an acetate kinase (*ACK*) open reading frame (ORF) has been identified also have an *XFP* ORF (5). Therefore, as in certain bacteria, Xfp is believed to partner with Ack (EC 2.7.2.1; acetyl phosphate + ADP ↔ acetate + ATP) in fungi as part of a modified pentose phosphate pathway to generate acetate and ATP from pentose phosphate pathway product X5P and F6P via formation of acetyl phosphate.

We purified and characterized the first eukaryotic Xfp, *Cryptococcus neoformans* Xfp2 (Accession # CNAG_06923.7) (6). Unlike previously characterized bacterial Xfp enzymes (1-4), *C. neoformans* Xfp2 displayed both substrate cooperativity (positive cooperativity in regards to F6P binding and negative cooperativity for P_i binding) and allosteric regulation. *C. neoformans* Xfp2 activity was inhibited by ATP, phosphenolpyruvate (PEP), oxaloacetic acid (OAA), (6) and glyoxylate (K. Glenn and K.

Smith, in revision) and activated by AMP (6). Previous kinetic characterizations of Xfp from bacteria do not report the presence of either substrate cooperativity or allosteric regulation for these enzymes (1-4). Recently, we purified and demonstrated that the *Lactobacillus plantarum* Xfp, initially characterized by Yevenes *et al*. (2), displayed both substrate cooperativity and allosteric regulation. We found that *L. plantarum* Xfp is an allosteric enzyme inhibited by PEP, OAA and glyoxylate but unaffected by ATP and AMP; and this enzyme also exhibits negative cooperativity for P_i (K. Glenn and K. Smith, in revision).

Currently, the structures of *Bifidobacterium breve* (3) and *Bifidobacterium longum* (7) Xfp enzymes have been solved. Analysis of these structures show that the Xfp monomer consists of 3 domains, the N-terminal (PP) domain, the Middle (Pyr) domain and the C-terminal domain, with the active site located between the PP and Pyr domains (3,7). Both structures support the ping pong bi bi reaction mechanism originally proposed by Yevenes *et al*. (2,3,7). Even though neither *B. breve* nor *B. longum* Xfp have been reported to be allosterically regulated, our studies have shown that at least one bacterial Xfp, *L. plantarum* Xfp, is an allosteric enzyme (K. Glenn and K. Smith, in revision). Here we describe the generation of a *C. neoformans* Xfp2 model from the existing *B. breve* and *B. longum* Xfp crystal structures. Since both a bacterial Xfp and C. neoformans Xfp are allosterically regulated by PEP and OAA at a shared or overlapping site (K. Glenn and K. Smith, in revision), we performed ligand docking simulations to attempt to determine the location of *C. neoformans* Xfp2 allosteric binding sites, primarily focusing on the PEP/OAA binding site.

III. MATERIALS AND METHODS

Materials

All chemicals were purchased from VWR, Fisher Scientific, or Sigma Aldrich. Oligonucleotides for site-directed mutagenesis were purchased from Integrated DNA Technologies.

Molecular Modeling

All modeling was performed using Accelrys Discovery Studio 3.5 software. The *C. neoformans* Xfp2 monomer model was built from the aligned and superimposed template structures of both *B. breve* (PDB ID 3AHC) and *B. longum* (PDB ID 3AI7) Xfp downloaded from RSCB Protein Data Bank (PDB). The *C. neoformans* Xfp2 homodimer model was built from the *B. longum* Xfp structure (PDB ID 3AI7). The monomer and homodimer model with the lowest Discrete Optimized Protein Energy (DOPE) score were chosen for further analysis. Models were prepared prior to use by other software applications using the Automatic Preparation function that prepares the protein by inserting missing atoms, modeling missing loops, removing water molecules and protonating residues based on a pH of 5.5, at which maximal *C. neoformans* Xfp2 activity occurs. Possible allosteric binding sites were determined by first identifying all possible cavities on the Xfp2 model using the Define and Edit Binding Sites From Receptor Cavities function. Ligand docking simulations were then performed for a

specified ligand using the software's LibDOCK function that docks ligands within a site based on the ligand's interaction with polar and apolar regions within that site.

Site-Directed Mutagenesis

Site-directed mutagenesis was performed on the codon-optimized *C. neoformans* Xfp2 gene using the QuikChange site-directed mutagenesis kit (Agilent Technologies, Inc.) to alter residues predicted to interact with ligands within proposed ligand binding sites of the Xfp2 model. Mutagenic primers were approximately 40 nucleotides in length with the altered base located in the center of the sequence. Mutagenesis was confirmed by Sanger-style sequencing at the Clemson University Genomics Institute.

Production and Purification of *C. neoformans* Xfp2 Variants

Confirmed Xfp2 variants were produced in the *Eschericia coli* expression strain RosettaBlue™ (Novagen) grown in LB medium supplemented with 1 % dextrose, 50 µg/mL ampicillin, and 34 µg/mL chloramphenicol. At an absorbance of ~0.8 at 600 nm, IPTG was added to a final concentration of 1 mM to induce production of the enzyme. Expression was allowed to proceed overnight at room temperature, and cells were harvested by centrifugation. *C. neoformans* Xfp2 variants were purified as previously described for wild type *C. neoformans* Xfp2 (6).

Enzymatic Assays for Xfp2 Activity

C. neoformans Xfp2 activity was determined by measuring the production of acetyl phosphate using a modified hydroxamate assay previously described (6,8). 200 µL

standard reaction mixtures were prepared as previously described (6), and only F6P and sodium phosphate pH 5.5 were used as substrates due to the lack of commercial availability of X5P. Reactions were initiated by the addition of enzyme and allowed to proceed for 30 minutes at 40°C. Afterwards, 100 µL of 2M hydroxylamine HCl (pH 7.0) was added to each reaction, and the reactions were allowed to incubate at room temperature for 10 minutes to convert all acetyl phosphate to acetyl hydroxamate. Finally, reactions were terminated by the addition of 600 µL of a 50:50 mixture of 2.5 % FeCl3 in 2N HCl and 10 % trichloroacetic acid to generate the ferric hydroxamate complex that was measured spectrophotometrically at 540 nm. Most initial tests of variant activity in the presence and absence of both PEP and AMP were performed in singlet trials. The R66A variant full kinetic analysis and all ATP hydrolysis experiments were performed in triplicate.

IV. RESULTS

Generation of *C. neoformans* Xfp2 monomer model

The *C. neoformans* Xfp2 monomer model (Figure 4.1) was built from the monomer structures of both *B. breve* and *B. longum* Xfp using Accelrys Discovery Studio 3.5 software. Like the *B. breve* and *B. longum* Xfp, the *C. neoformans* Xfp2 monomer consists of an N-terminal PP (blue), middle Pyr (white) and C-terminal (red) domain. The Define Binding Site from Receptor Cavities function was performed and located a total of 44 possible binding sites on the *C. neoformans* Xfp2 model. Ligand docking simulations showed that TPP binds to site 5 on the model which overlaps well with the TPP binding sites of *B. breve* (3) and *B. longum* Xfp (7). Therefore, site 5 (labeled with a red circle in Figure 4.1) is considered to be the location of the *C. neoformans* Xfp2 active site.

Investigations into the location of the *C. neoformans* Xfp2 PEP/OAA allosteric site based on bonds formed between ligand and evolutionarily conserved residues

The PEP and OAA molecule structures were imported into Discovery Studio 3.5 software and docked into each of the 44 possible binding sites using the LibDock function. Both PEP and OAA were successfully docked into many of the sites. Since PEP and OAA have been demonstrated to be allosteric effectors for the bacterial *L. plantarum* Xfp (K. Glenn and K. Smith, in revision) and the eukaryotic *C. neoformans*

Xfp2 (6), we hypothesize that this site may be evolutionarily conserved among both bacterial and eukaryotic Xfps. Therefore, we attempted to narrow down the number of candidate PEP/OAA binding sites by focusing on sites in which both PEP and OAA can bind and directly interact, through hydrogen bonding, with several evolutionarily conserved residues within that site. ConSurf server was used to determine if a residue is evolutionarily conserved (9,10). The ConSurf server first searches for sequences homologous to the sequence of interest and then uses multi-sequence alignment, existing structures, and phylogenetic analysis to assign residues in the input sequence a score of 1 to 9, with a score of 9 assigned to residues that are considered to be highly conserved.

Utilizing the methodology outlined above we identified two sites, site 13 and site 35, as PEP/OAA binding site candidates. The position of these sites on the *C. neoformans* Xfp2 monomer model (Figure 4.2), along with 2D diagrams that represent one of several positions in which PEP can bind within each site. In both site 13 and site 35, PEP and OAA hydrogen bond with two evolutionarily conserved residues (ConSurf scores of 8 or 9). Site-directed mutagenesis was performed to generate the individual variants R66A and K64A in site 13 and D547K and K602A in site 35 because these residues had high ConSurf scores and were predicted to directly interact with PEP and OAA by forming hydrogen bonds. All residues for which mutagenesis was performed are listed in Table 4.1 along with their ConSurf scores and binding site location.

The *C. neoformans* Xfp2 R66A variant was the only variant active enough to perform a full kinetic analysis (Table 4.2). Alteration of Arg66 to Ala primarily reduced

the overall enzyme activity demonstrated by a much lower k_{cat}^{app} compared to wild type (WT) *C. neoformans* Xfp2. The R66A variant has similar $K_{0.5}$ values to those of the WT and also retains both positive cooperativity (h>1) for F6P and negative cooperativity (h<1) for P_i (Table 4.2). Since the R66A variant was generated due to its possible interactions with PEP within a proposed PEP/OAA binding site, PEP was added to the reaction mix to determine if activity of this variant is still inhibited by the presence of PEP. All previous studies involving allosteric inhibitors have been performed using $K_{0.5}$ substrate concentrations. At $K_{0.5}$ concentrations for both substrates, the activity of the R66A variant is only around 0.027 µmol of product formed per 30 minute reaction. In the presence of 8 mM PEP, R66A activity decreases from 0.027 µmol to 0.012 µmol of product formed per 30 minute reaction. Therefore, PEP still inhibits R66A activity, but it is difficult to compare PEP's effect on R66A to WT *C. neoformans* Xfp2 at similar concentrations when the activity of the R66A variant is very low.

AMP acts as a very potent enzyme activator/stabilizer

In an attempt to increase R66A variant activity, varying amounts of AMP, the only known *C. neoformans* Xfp2 activator (6), was added to the reaction assay. As expected, like with the WT, AMP was able to increase activity of the R66A variant (Figure 4.3). Surprisingly, the addition of AMP was able to rescue R66A activity back to WT levels. Upon the addition of 2 mM AMP, R66A activity reaches 100% WT activity of the same enzyme concentration. Since AMP boosts R66A activity, PEP inhibition was tested in presence of AMP (Figure 4.4). The effect of the presence and absence of 8 mM

PEP on R66A activity was tested on reactions containing 0.02, 0.2 and 0.5 mM AMP. As shown in Figure 4.4, 8 mM PEP inhibits activity in the presence of all three concentrations of AMP suggesting that R66A is not involved in the binding of PEP.

To better understand why the R66A alteration drastically reduces enzyme activity and how AMP is capable of overcoming the effects of this mutation, a model was generated of the R66A variant using the Build Mutant function of the Discovery Studio 3.5 software. Figure 4.5 shows an overlay of the WT *C. neoformans* Xfp2 model and the R66A variant focused on the R66 residue with a red sphere marking the active site. The R66 residue is in close proximity to the active site, and therefore, may even be involved in active site mechanisms such as substrate binding or stabilizing reaction intermediates. Additionally the R66A variant is predicted to produce several structural changes, indicated by green arrows in Figure 4.5, that are also in close proximity to the active site. Therefore the R66A model suggests that the reduction in enzyme activity may be due to changes in the enzyme active site but does not provide insight as to how AMP is able to overcome such structural alterations.

C. neoformans Xfp2 is known to have optimal activity at lower pH, and activity decreases as pH approaches neutrality. Therefore, the effect of AMP on *C. neoformans* Xfp2 activity in the presence of increasing pH was tested. It was found that AMP can increase WT activity at $K_{0.5}$ substrate concentrations at elevated pH values (Figure 4.6). The addition of 0.5 mM AMP can increase Xfp2 activity by approximately 8-fold at pH 7.0.

Investigations into the location of the *C. neoformans* Xfp2 PEP/OAA allosteric site based on bonds formed between ligand and arginine residues

Utilizing PDBeMotif version 2.0c, an online service that searches the Protein Data Bank with respect to protein motifs (11), it was discovered that PEP often directly interacts and binds with arginine residues in protein active sites. Therefore, all of the putative binding sites of the *C. neoformans* Xfp2 model were explored to locate sites in which PEP could interact with an arginine residue. There are five sites (Figure 4.7) in which PEP is predicted to bind and interact with an arginine residue. Two of these sites, site 10 and site 14, overlap, and PEP is predicted to interact with the same arginine residue, Arg571. The four arginine residues, their ConSurf scores, the mutations generated, and binding site location are listed in Table 4.1.

Both R300A and R55A variants were active in the absence of the activator AMP but activity was roughly 25% lower than WT at the same concentration for R55A and 75% lower for R300A. Both variants displayed activation in the presence of 0.5 mM AMP and inhibition in the presence of 8 mM PEP. Therefore, neither residue appears to be involved in PEP binding. Purified R571A and R753A had very low concentrations (~ 0.3 mg/mL) after column purification. Both variants showed no activity for R753A and very little activity for R571A (~0.034 µmol of product formed per 30 minute reaction). However, the addition of 0.5 mM AMP resulted in some activity from R753A variant (~ 0.04 µmol of product per 30 minute reaction), but this activity was inhibited by the addition of 8 mM PEP. Interestingly addition of 0.5 mM AMP did not increase R571A

activity, but the little activity observed for this variant was inhibited by 8 mM PEP. Based on these findings it appears that neither R571 nor R753 are involved in PEP binding, however additional tests are needed to rule them out with any certainty.

Generation of *C. neoformans* Xfp2 dimer structure

The functional unit of both *B. breve* and *B. longum* Xfp is a dimer. However the only Xfp dimer structure available in PDB is that of *B. longum*. Therefore, the *C. neoformans* Xfp2 dimer model (Figure 4.8) was built from the dimer structure of *B. longum* Xfp only. The *C. neoformans* Xfp2 dimer model consists of two active sites still located between the N-terminal and middle domains of each monomer. However it has been shown that residues from both subunits comprise each active site of the *B. longum* Xfp (7), and this is most likely the case for *C. neoformans* Xfp2 as well. Therefore, it is possible that allosteric sites may consist of residues from both monomers.

ATP Inhibition may be dependent on ATP hydrolysis

Since the *C. neoformans* Xfp2 model was built from bacterial Xfps, the search for allosteric binding sites using this model has thus far centered on identifying the PEP/OAA binding sites known to exist for at least one bacterial Xfps (K. Glenn and K. Smith, in revision). Therefore, the model may not be relevant in determining the location of the ATP or AMP site because neither of these effectors allosterically affect bacterial Xfp activity. However, a non-hydrolyzable ATP analog, β,γ-methyleneadenosine 5′-triphosphate (AMP-PCP), was used to learn more about the mechanism of ATP inhibition, and to determine if it is dependent on the hydrolysis of ATP.

Unlike ATP, AMP-PCP does not inhibit *C. neoformans* Xfp2 (Figure 4.9). More interestingly, AMP-PCP resulted in slightly elevated activity compared to activity when no effector is present. Adenosine was tested to see if inhibition is dependent on the adenosine portion of ATP, but adenosine alone does not appear to contribute to inhibition. These results suggest that ATP hydrolysis may be an important factor in ATP inhibition of *C. neoformans* Xfp2. Since AMP-PCP shows slight elevation of WT activity, the effect of AMP-PCP at both pH 5.5 and pH 7.0 was tested to determine if AMP-PCP mimics AMP's ability to enhance Xfp2 activity at elevated pH. AMP-PCP can enhance WT activity at elevated pH but not to the level observed with AMP (Figure 4.10). Additionally, AMP-PCP and ATP were both added to the reaction to determine if AMP-PCP can rescue ATP inhibition. Reactions containing both AMP-PCP and ATP display intermediate activity between that of ATP and AMP-PCP presence alone (Figure 4.11) which may suggest competitive binding between both molecules to occupy the allosteric site.

V. DISCUSSION

We have recently shown that at least some Xfp enzymes from both bacteria (K. Glenn and K. Smith, in revision) and fungi (6) are allosterically regulated. Both *L. plantarum* Xfp and *C. neoformans* Xfp2 are inhibited by PEP, OAA and glyoxylate, and PEP and OAA appear to share the same or possess overlapping allosteric sites. Here we attempt to locate the PEP/OAA allosteric site through ligand docking simulations using a *C. neoformans* Xfp2 model built from known bacterial Xfp crystal structures from *B. breve* (3) and *B. longum* (7). Like with *B. breve* and *B. longum* Xfp, the *C. neoformans* Xfp2 model shows the active site to be located between the N-terminal (PP) domain and the middle (PYR) domain. The software's Define and Edit Binding Site feature located a total of 44 possible binding sites on the Xfp2 model. Sites were narrowed down using two different methodologies. The first method involved focusing on sites in which both PEP and OAA docked and formed bonds with residues deemed to be evolutionarily conserved due to their high ConSurf scores (9,10). The second method involved focusing on sites in which docked PEP interacted with arginine residues, as a search of the PDBeMotif database (11) showed that PEP often forms bonds with arginine residues within active sites.

Two possible PEP/OAA binding sites, site 13 and site 35 were first chosen due to their ability to potentially bind both PEP and OAA such that bonds were formed between the ligand and Xfp2 residues having high ConSurf scores. Except for the R66A variant,

most of the Xfp2 variants purified were not highly concentrated, so a full kinetic analysis was performed only on the R66A variant. The R66A alteration primarily caused a dramatic decrease in turnover number, k_{cat}, compared to WT Xfp2. AMP was added to the R66A reaction mix in an attempt to boost activity for PEP inhibition analysis, but surprisingly, AMP at a concentration of 2 mM was capable of rescuing R66A activity up to WT values (Figure 4.3). The R66 residue is located very close to the Xfp2 active site (Figure 4.5). Therefore, it is possible that R66 may play a role in active site reaction mechanism. In fact generating the R66A alteration using the Build Mutant Function of Discovery Studio 3.5 software shows some structural alterations in regions of the protein located close to the active site (Figure 4.5). However it remains unclear as to how AMP is able to override the structural changes induced by the R66A alteration. We hypothesize that the binding of AMP stabilizes the active R state form of the enzyme over the less active T state form. It is possible that if R66A variant destabilizes the active site then AMP's ability to induce the R state may be why AMP can completely override this amino acid change. In addition to being capable of circumventing enzyme alterations induced by amino acid changes, AMP is capable of drastically increasing *C. neoformans* Xfp2 activity at elevated pH. The ability of AMP to induce a conformational change that overrides the changes caused by a residue alteration or elevated pH shows that AMP is a much stronger activator than previously thought. However as the R66A variant is still inhibited by PEP even in the presence of AMP, this residue does not appear to be involved in PEP binding. Additionally the K602A variant from site 35 displayed some activity in the presence of AMP that was also inhibited by the presence of PEP.

Therefore, we found no evidence suggesting either site 13 or sites 35 as part of a PEP/OAA binding site.

We vitalized a second approach to identify the PEP/OAA binding site by focusing on sites in which PEP forms hydrogen bonds with the side chain of arginine residues. A search of the Protein Data Bank using PDBeMotif revealed that PEP often forms bonds with arginine residues within active sites. Therefore, all arginine residues predicted to interact with PEP through ligand docking simulations were altered. All four arginine variants displayed reduced enzyme activity; however, the activity was still inhibited by the presence of PEP suggesting that these residues are not essential for PEP binding. Additionally three of the four variants were activated by AMP; however, there was no increase in R571A variant activity in the presence of AMP. Therefore, it is possible that R571A may be involved in AMP binding. The R571 residue on the *C. neoformans* Xfp2 dimer model (Figure 4.12) is not near the active sites nor is it located near junctions between both monomers to form the dimer suggesting it is not involved in either the active site mechanism or in subunit oligomerization. The location of R571 on the C-terminal domain lends support to a possible involvement in allosteric effector binding since it has been suggested that the C-terminal domain of the phosphoketolase related enzyme transketolase may serve as a binding site for regulatory molecules (12). For now it is difficult to determine the role that R571 plays in the Xfp2 structure because activity and concentration of the R571A variant were very low. Future studies involving this variant will be dependent on the purification of additional, more concentrated enzyme.

There is no evidence that *C. neoformans* Xfp2 inhibition by ATP is dependent upon ATP hydrolysis based on the absence of a Walker motif (13) within the Xfp2 sequence. However, the effects of non-hydrolyzable ATP on Xfp2 activity were still investigated. The presence of the non-hydrolyzable ATP analog, AMP-PCP, did not inhibit *C. neformans* Xfp2 activity and actually resulted in slightly elevated activity compared to the absence of any effector. This result suggests that ATP inhibition is dependent upon ATP hydrolysis. Alternatively, AMP-PCP may actually mimic the binding of AMP rather than ATP, which would explain the slight increase in activity compared to activity in the absence of effector. Since AMP is capable of increasing *C. neoformans* Xfp2 activity at elevated pH, the effect of AMP-PCP on Xfp2 activity was tested at both pH 5.5 and pH 7.0. AMP-PCP stimulated Xfp2 activity but the stimulation was much lower than that of AMP, especially at pH 7.0. When both AMP-PCP and ATP are present, activity is intermediate to that of ATP or AMP-PCP present alone, suggesting that ATP and AMP-PCP do compete for the same allosteric site. Additional studies are required to determine if ATP inhibition is truly dependent on ATP hydrolysis.

In conclusion, the sites we identified in the *C. neoformans* Xfp2 monomer model proved not to be the PEP/OAA binding site. However, other potential allosteric sites remain to be explored. Phosphofructokinase (Pfk), the principle regulatory enzyme of glycolysis, is one of the most well studied allosteric enzymes (14). The primary allosteric effectors of Pfk are ADP, which functions as an activator, and PEP, which functions as an inhibitor. Structural studies of Pfk from *B. stearothermophilus* show that PEP and ADP both bind at a single site located at the interface between tetrameric subunits but induce

very different conformational changes (14,15). Therefore, it may be worthwhile to continue the search for *C. neoformans* Xfp2 allosteric effector sites using the dimer model, focusing on sites between subunits. We have recently shown that the bacterial Xfp from *L. plantarum* is not regulated by ATP and AMP, the primary inhibitor and activator of *C. neoformans* Xfp2 respectively (K. Glenn and K. Smith, in revision). Since the *C. neoformans* Xfp2 model was built from bacterial Xfp structures, this model is less likely to be relevant in identifying the binding sites of AMP and ATP. However, initial ligand docking simulations showed that ATP can bind in only a few predicted sites on the *C. neoformans* Xfp2 monomer, but additional binding sites will likely be revealed through ligand docking simulations with the dimer model. Our preliminary studies suggest that ATP inhibition may even be dependent upon ATP hydrolysis as *C. neoformans* Xfp2 is not inhibited by the non-hydrolyzable ATP analog AMP-PCP. AMP-PCP instead caused slight enzyme activation, suggesting that AMP-PCP may mimic AMP binding. However, we also saw evidence consistent with competitive binding between ATP and AMP-PCP for the ATP allosteric site (Figure 4.11). The AMP-PCP binding data also supports the idea of a single binding site for AMP and ATP, much like the ADP/PEP effector site of Pfk. Continued studies of the *C. neoformans* Xfp2 monomer and dimer models should reveal more information regarding the mechanisms of Xfp allosteric regulation and the location of these allosteric binding sites.

VI. ACKNOWLEDGMENTS

This work was supported by awards from the National Institutes of Health (GM084417-01A1), National Science Foundation (Award# 0920274), and South Carolina Experiment Station Project SC-1700340.

VII. REFERENCES

1. Meile, L., Rohr, L. M., Geissmann, T. A., Herensperger, M., and Teuber, M. (2001) Characterization of the D-xylulose 5-phosphate/D-fructose 6-phosphate phosphoketolase gene (xfp) from *Bifidobacterium lactis*. *J. Bacteriol.* **183**, 2929-2936

2. Yevenes, A., and Frey, P. A. (2008) Cloning, expression, purification, cofactor requirements, and steady state kinetics of phosphoketolase-2 from *Lactobacillus plantarum*. *Bioorg. Chem.* **36**, 121-127

3. Suzuki, R., Katayama, T., Kim, B. J., Wakagi, T., Shoun, H., Ashida, H., Yamamoto, K., and Fushinobu, S. (2010) Crystal structures of phosphoketolase: thiamine diphosphate-dependent dehydration mechanism. *J. Biol. Chem.* **285**, 34279-34287

4. Petrareanu, G., Balasu, M. C., Vacaru, A. M., Munteanu, C. V., Ionescu, A. E., Matei, I., and Szedlacsek, S. E. (2014) Phosphoketolases from *Lactococcus lactis*, *Leuconostoc mesenteroides* and *Pseudomonas aeruginosa*: dissimilar sequences, similar substrates but distinct enzymatic characteristics. *Appl. Microbiol. Biotechnol.*, 7855-7867

5. Ingram-Smith, C., Martin, S. R., and Smith, K. S. (2006) Acetate kinase: not just a bacterial enzyme. *Trends Microbiol.* **14**, 249-253

6. Glenn, K., Ingram-Smith, C., and Smith, K. S. (2014) Biochemical and Kinetic Characterization of Xylulose 5-phosphate/Fructose 6-phosphate Phosphoketolase 2 (Xfp2) from *Cryptococcus neoformans*. *Eukaryot. Cell* **13**, 657-663

7. Takahashi, K., Tagami, U., Shimba, N., Kashiwagi, T., Ishikawa, K., and Suzuki, E. (2010) Crystal structure of *Bifidobacterium longum* phosphoketolase; key enzyme for glucose metabolism in Bifidobacterium. *FEBS Lett.* **584**, 3855-3861

8. Lipmann, F., and Tuttle, L. C. (1945) A specific micromethod for determination of acyl phosphates. *J. Biol. Chem.* **159**, 21-28

9. Ashkenazy, H., Erez, E., Martz, E., Pupko, T., and Ben-Tal, N. (2010) ConSurf 2010: calculating evolutionary conservation in sequence and structure of proteins and nucleic acids. *Nucleic Acids Res.*, 1-5

10. Celniker, G., Nimrod, G., Ashkenazy, H., Glaser, F., Martz, E., Mayrose, I., Pupko, T., and Ben-Tal, N. (2013) ConSurf: using evolutionary data to raise testable hypotheses about protein function. *Isr. J. Chem.* **53**, 199-206

11. Golovin, A., and Henrick, K. (2008) MSDmotif: exploring protein sites and motifs. *BMC Bioinformatics* **9**, 312-323

12. Lindqvist, Y., Schneider, G., Ermler, U., and Sundström, M. (1992) Three-dimensional structure of transketolase, a thiamine diphosphate dependent enzyme, at 2.5 A resolution. *EMBO J.* **11**, 2373-2379

13. Walker, J. E., Saraste, M., Runswick, M. J., and Gay, N. J. (1982) Distantly related sequences in the alpha-and beta-subunits of ATP synthase, myosin, kinases and other ATP-requiring enzymes and a common nucleotide binding fold. *EMBO J.* **1**, 945-951

14. Traut, T. (2008) *Allosteric regulatory enzymes*, Springer

15. Schirmer, T., and Evans, P. R. (1990) Structural basis of the allosteric behaviour of phosphofructokinase. *Nature* **343**, 140-145

TABLE 4.1. *C. neoformans* Xfp2 enzyme variants.

Residue	ConSurf score	Variant	Binding Site
R66	8, e, f	R66A	13
K64	9, e, f	K64A	13
D547	9, e, f	D547K	35
K602	9, e, f	K602A	35
R571	9, b, s	R571A	10 & 14
R753	9, e, f	R753A	30
R55	2, e	R55A	17
R300	8, e, f	R300A	24

ConSurf assigns scores1-9 with 9 corresponding to a highly conserved residue along with the following descriptors e = exposed, b = buried, f = functional, and/ or s = structural

TABLE 4.2. Apparent kinetic parameters for *C. neoformans* Xfp2 R66A variant

	Substrate	$K_{0.5}$ (mM)	k_{cat}^{app} (sec^{-1})	$k_{cat}^{app}/K_{0.5}$ (sec^{-1} mM^{-1})	H
C. neoformans Xfp2 R66A	F6P	26.7 ± 1.0	0.063 ± 0.003	0.0024 ± 0.0001	2.14 ± 0.27
	P_i	17.1 ± 2.6	0.055 ± 0.005	0.0032 ± 0.0003	0.75 ± 0.05
C. neoformans Xfp2 WT*	F6P	15.9 ± 1.3	3.47 ± 0.10	0.22 ± 0.01	1.41 ± 0.11
	P_i	13.3 ± 1.5	4.22 ± 0.13	0.32 ± 0.03	0.59 ± 0.03

WT – wild type, *Previously reported kinetic parameters (6).

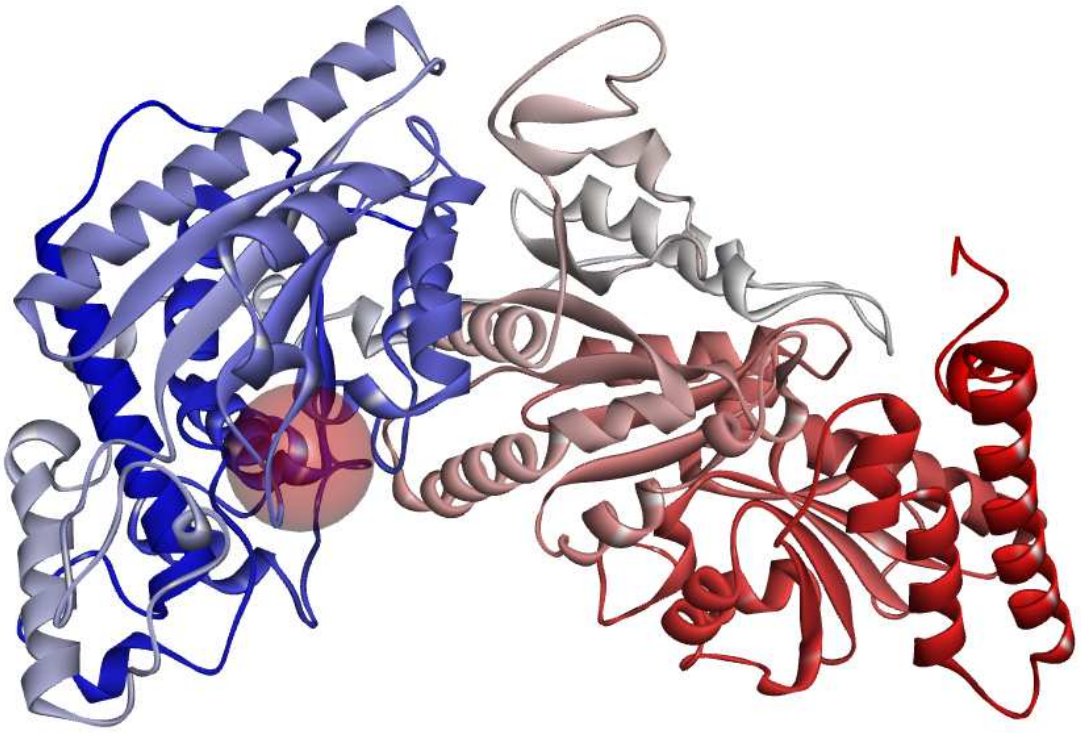

FIG 4.1. Model of C. neoformans Xfp2 monomer. Model was generated using both the *B. breve* and *B. longum* Xfp crystal structures. Model colored from N-terminal (blue) to C-terminal (red). Active site (area where TPP binds) is marked by a transparent red sphere.

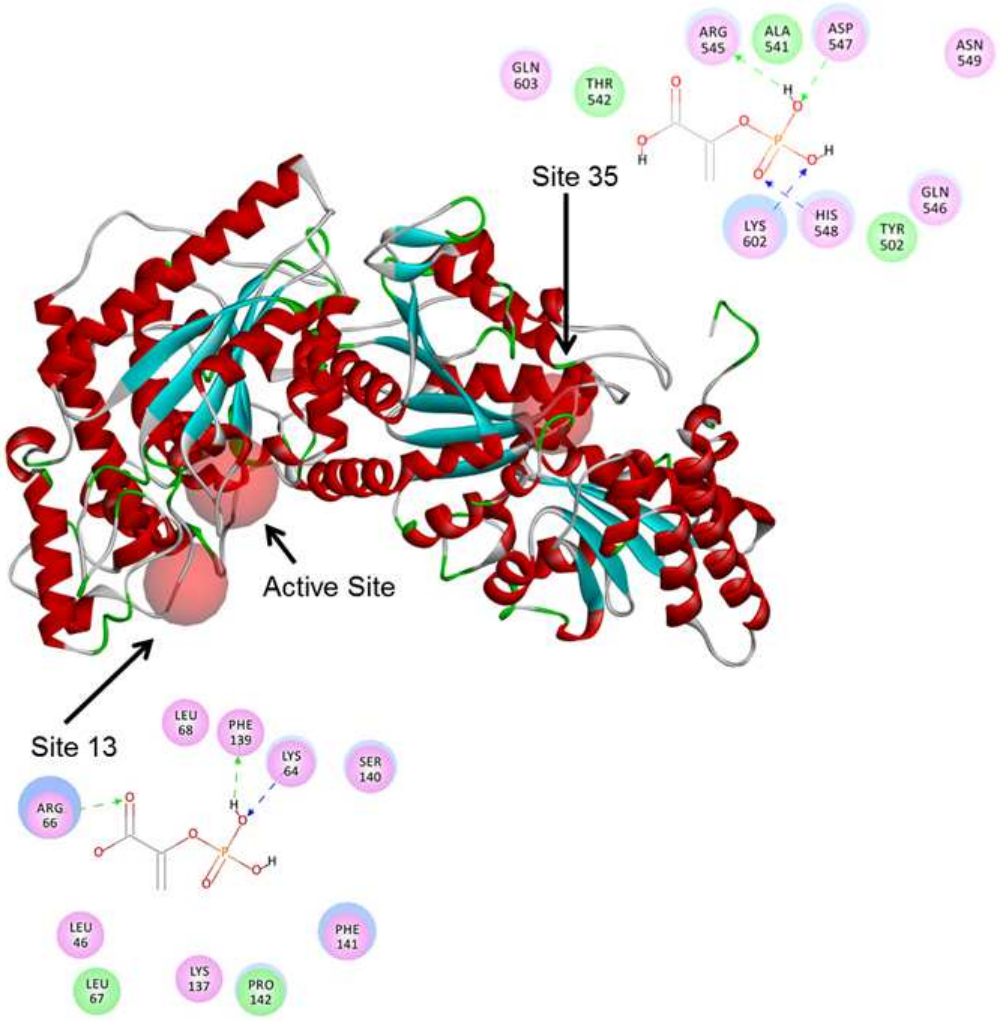

FIG 4.2. Location of the predicted PEP binding sites 13 and 35. Red spheres mark the location of sites 13, 35 and the active site on the *C. neoformans* Xfp2 monomer model. 2D diagrams depict one of several possible poses PEP can take in each site. Hydrogen bonds between PEP and site residues are indicated by green (hydrogen bond with amino acid main chain) and blue (hydrogen bond with amino acid side chain) arrows that point towards the electron donor.

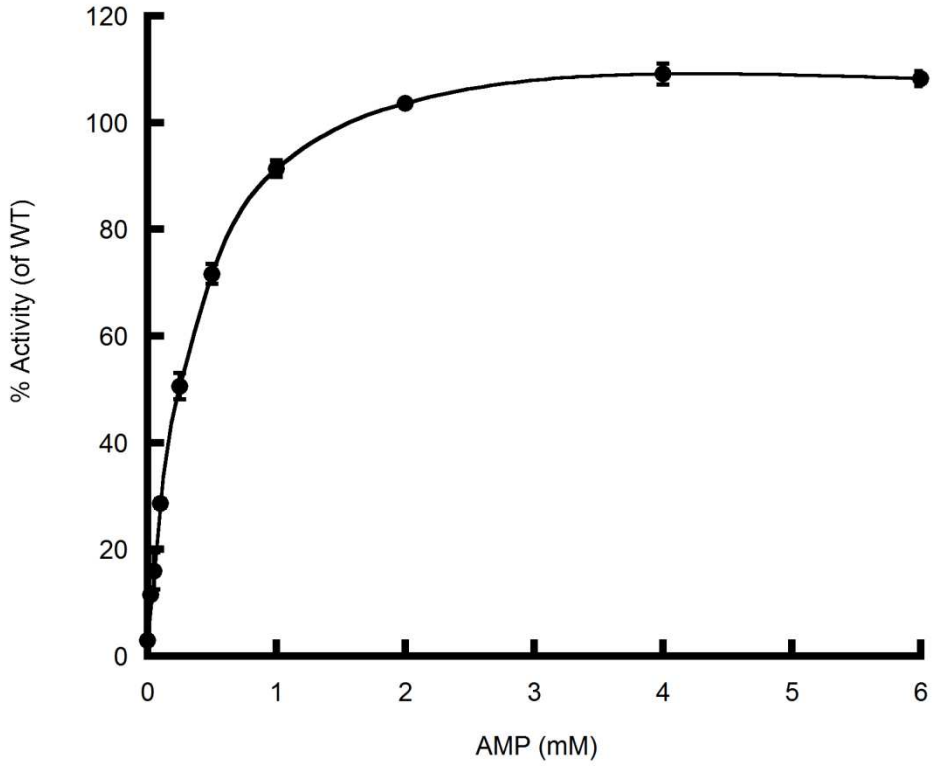

FIG 4.3. AMP activation of *C. neoformans* Xfp2 R66A variant. Reactions were performed in triplicate for *C. neoformans* Xfp2 R66A variant using WT *C. neoformans* Xfp2 F6P and P_i $K_{0.5}$ concentrations in the presence of increasing amounts of AMP. Activity was measured as a percentage of WT *C. neoformans* Xfp2 where activity with no AMP at the same enzyme concentration as the R66A variant was set at 100%.

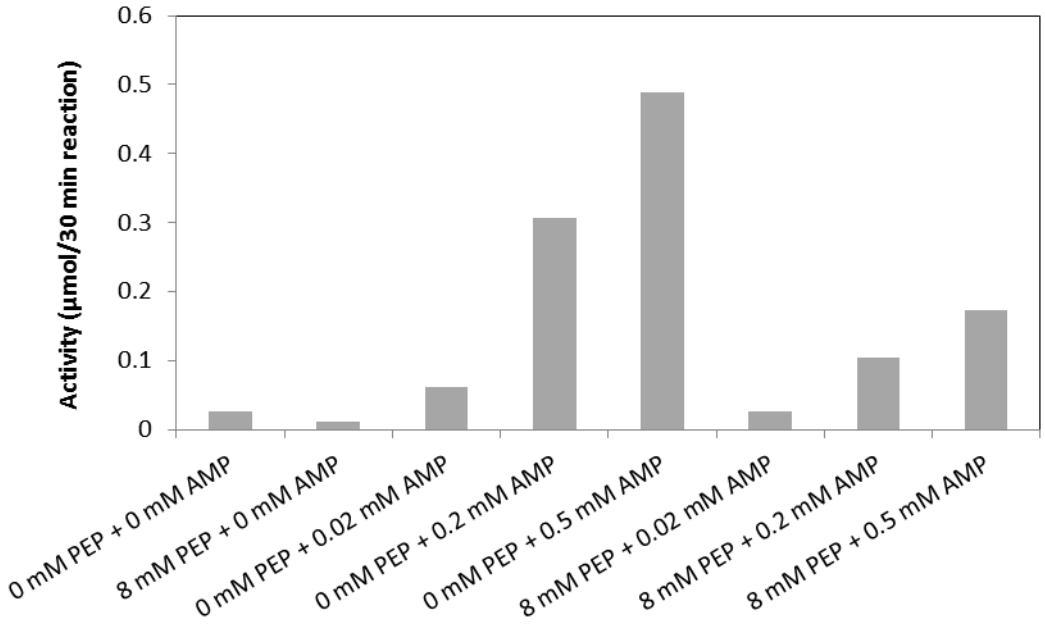

FIG 4.4. Effect of PEP on *C. neoformans* Xfp2 R66A variant activity in the presence of AMP. Reactions were performed in singlet using wild type *C. neoformans* Xfp2 $K_{0.5}$ substrate concentrations. Activity is reported as µmols of product formed per 30 minute reactions.

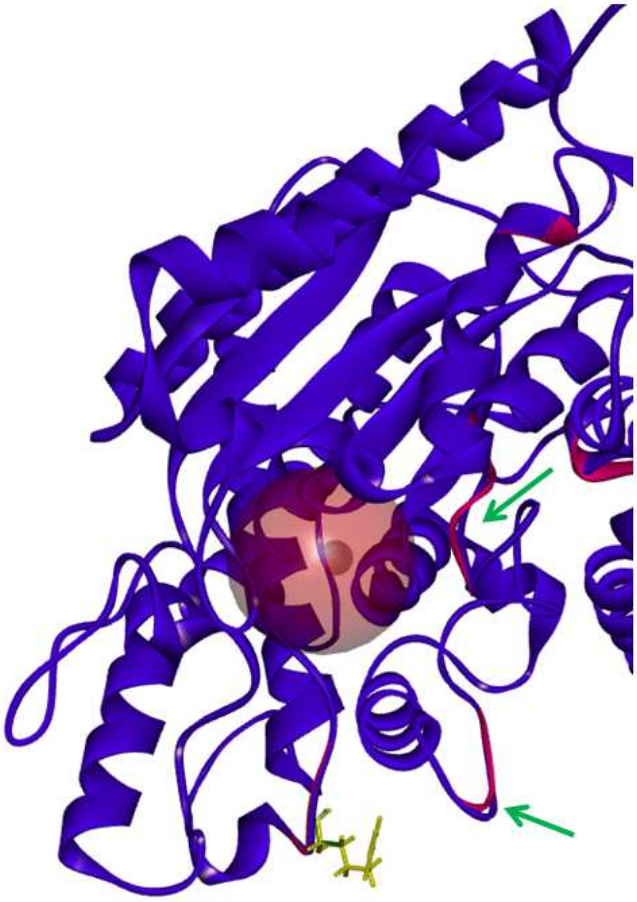

FIG 4.5. Model predicting structural effects of R66A mutation. The wild type *C. neoformans* Xfp2 model is in blue, and the R66A mutation model is in pink. R66 residue is shown in yellow. The *C. neoformans* Xfp2 active site is marked by the red sphere. Green arrows point to structural changes caused by the R66A mutation.

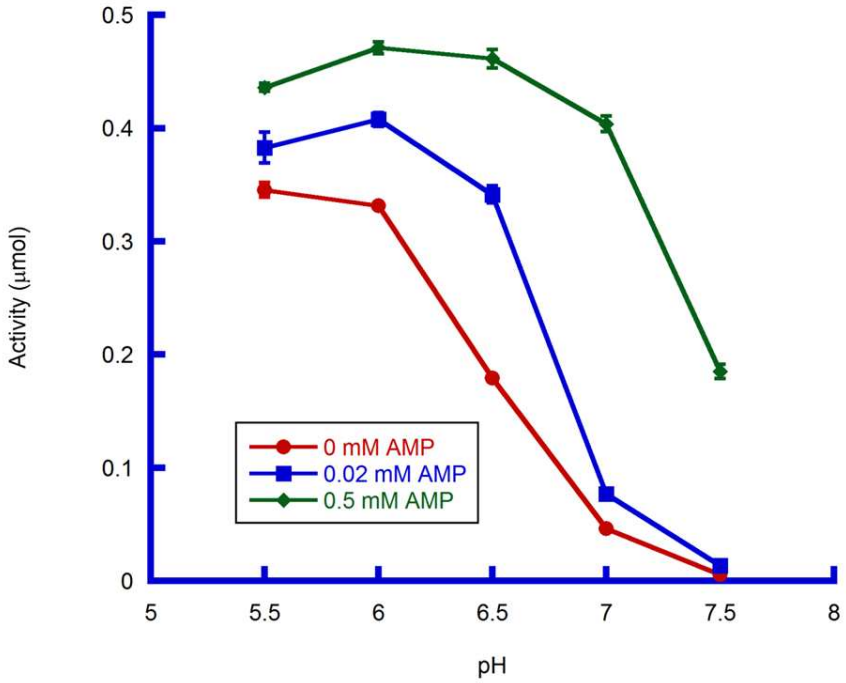

FIG 4.6. Effect of pH on WT *C. neoformans* Xfp2 activity in the presence and absence of AMP. Reactions were performed in triplicate using $K_{0.5}$ substrate concentrations, and activity is reported as µmol of product formed per 30 minute reaction. Wild type *C. neoformans* Xfp2 activity was measured as a function of increasing pH in the presence of 0 mM AMP (red), 0.02 mM AMP (blue) and 0.5 mM AMP (green).

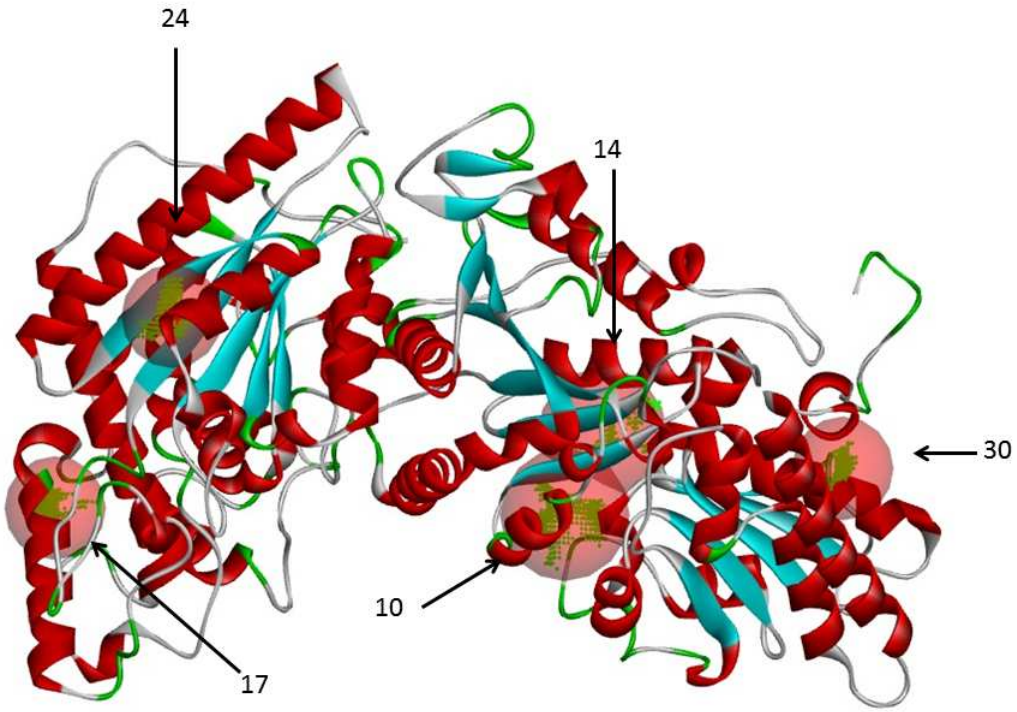

FIG 4.7. Location of sites on the *C. neoformans* Xfp2 model in which PEP interacts with arginine residues. Sites 10, 14, 17, 24, and 30, labeled with arrows and marked by red spheres on the *C. neoformans* Xfp2 monomer model, contain arginine residues that through ligand docking simulations are predicted to interact with PEP.

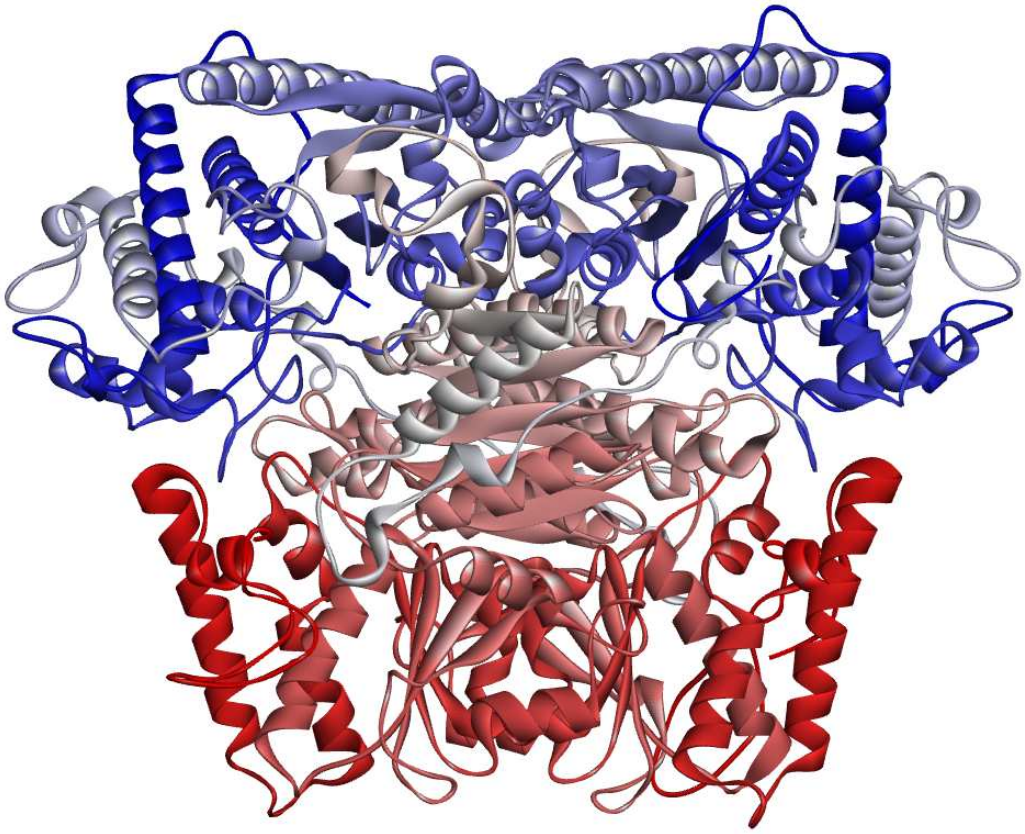

FIG 4.8. *C. neoformans* Xfp2 dimer model. Model generated from the *B. longum* Xfp dimer structure. Colors indicate the N-terminal (blue) and C-terminal (red) domains.

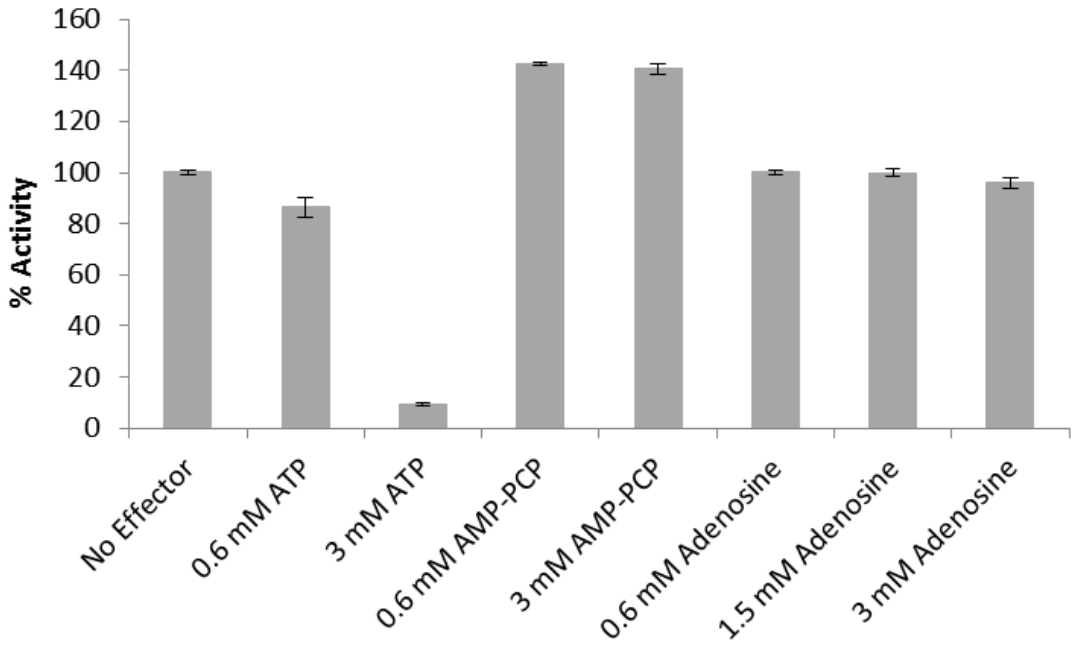

FIG 4.9. Effect of adenosine and AMP-PCP on *C. neoformans* Xfp2 activity compared to ATP inhibition. Reactions were performed in triplicate using $K_{0.5}$ substrate concentrations of F6P and P_i. Activity is reported in percentage where 100% is wild type activity with no effector present.

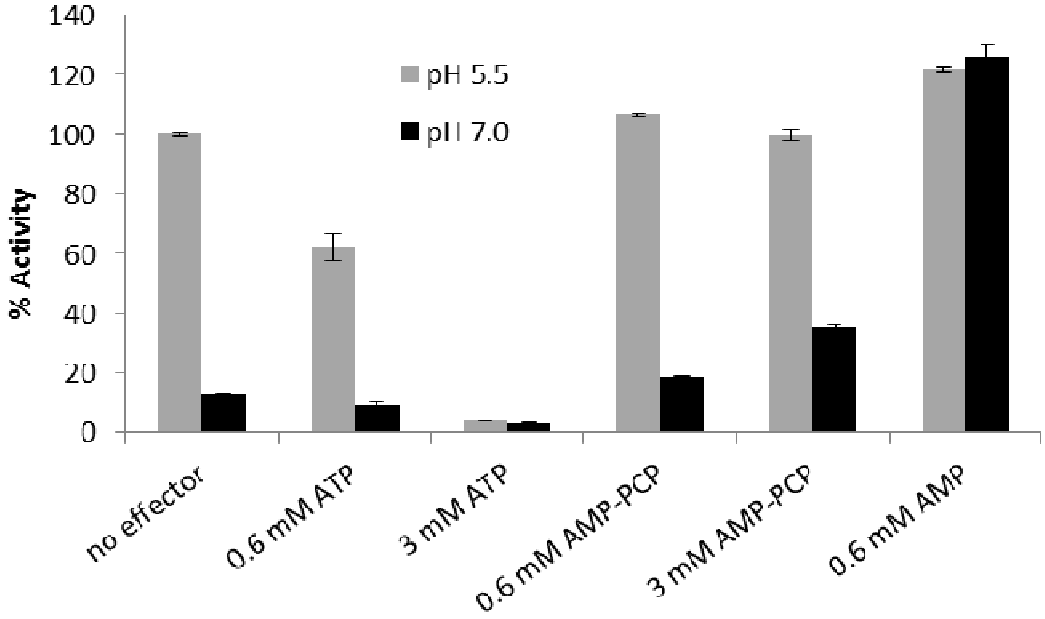

FIG 4.10. Effect of AMP-PCP on *C. neoformans* Xfp2 activity at pH 5.5 (grey) and pH 7.0 (black). Reactions were performed in triplicate using $K_{0.5}$ substrate concentrations of F6P and P_i. Activity is reported as percentage where 100% is wild type activity at pH 5.5 in the absence of effector.

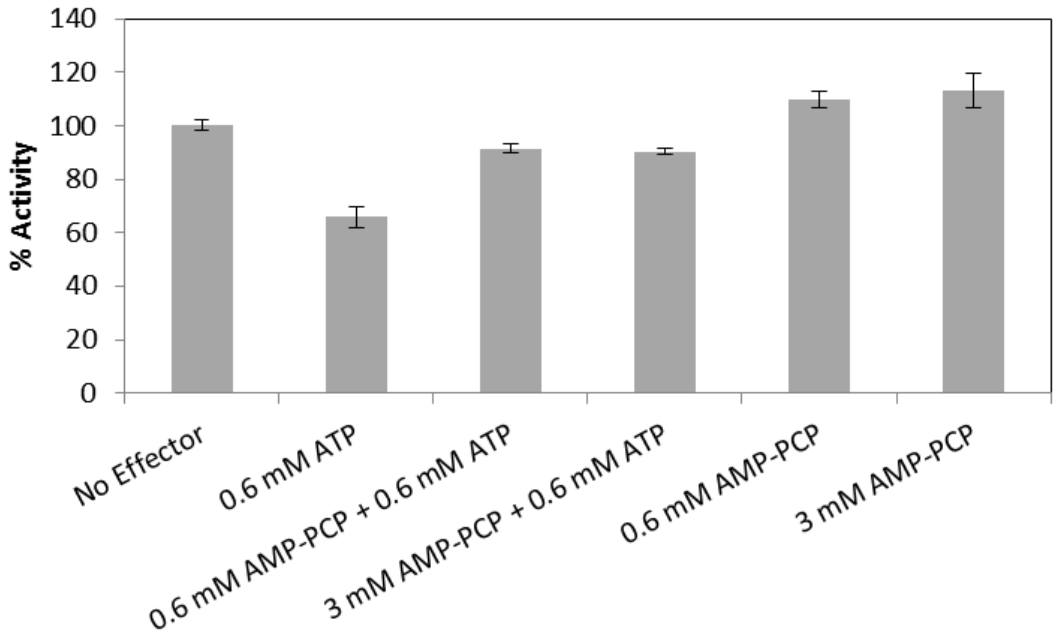

FIG 4.11 Effect of the presence of both AMP-PCP and ATP on *C. neoformans* Xfp2 activity. Reactions were performed in triplicate using $K_{0.5}$ substrate concentrations of F6P and P_i. Activity is reported in percent where 100% is wild type activity in the absence of effector.

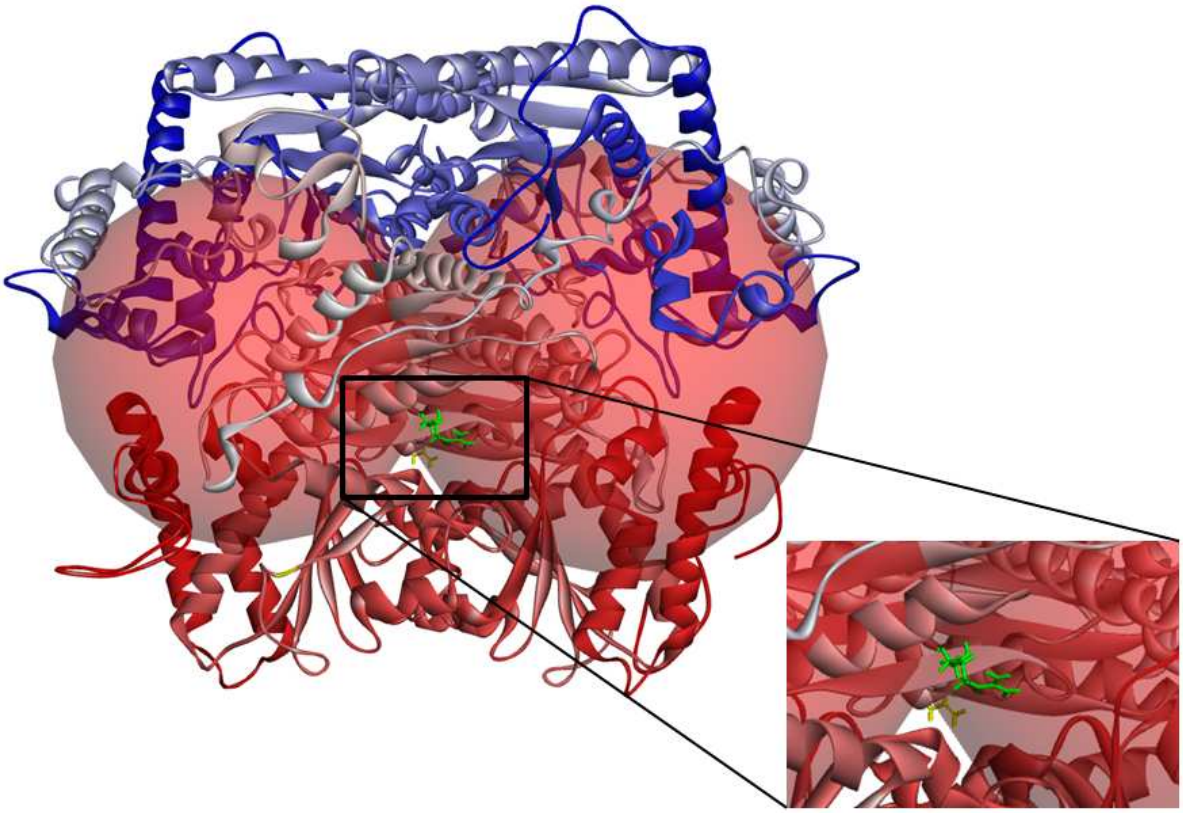

FIG 4.12. Location of R571 residue on the *C. neoformans* Xfp2 dimer model. The two large red spheres mark the two active sites of the Xfp2 dimer. The R571 residue is colored green on one of the two monomers and yellow on the other.

CHAPTER 5

CONCLUSIONS AND FUTURE WORKS

This dissertation describes the first characterization of a eukaryotic xylulose 5-phosphate/ fructose 6-phosphate phosphoketolase (Xfp) from the pathogenic fungus *Cryptococcus neoformans*. Xfp is believed to partner with acetate kinase (Ack) to produce acetate during cryptococcal infection. Studies have shown that acetate is one of the most abundant metabolites produced during cryptococcosis. In addition, Xfp and Ack have been shown in several different studies to be expressed and/or upregulated in *C. neoformans* during infection, and an Xfp2 homolog has been shown to be required for full virulence in the insect fungal pathogen *Metharizium anisopliae*. If the Xfp-Ack pathway does prove to be important during *C. neoformans* infection, this pathway could be utilized as a possible drug target as these enzymes are not present in humans.

C. neoformans Xfp2 displayed substrate cooperativity in the form of positive cooperativity for fructose 6-phosphate (F6P) and xylulose 5-phosphate (X5P) and negative cooperativity for P_i. Additionally, *C. neoformans* Xfp2 was found to be an allosteric enzyme inhibited by ATP, phosphoenolpyruvate (PEP), oxaloacetic acid (OAA) and glyoxylate and activated by AMP. Studies showed that PEP and OAA share the same or possess overlapping allosteric sites on the enzyme while ATP and glyoxylate bind at separate sites. Regulation by AMP:ATP levels seem to support a partnership between Xfp2 and Ack in producing acetate and ATP while inhibition by PEP, OAA, and

glyoxylate seem to suggest an indirect connection between the Xfp-Ack pathway and gluconeogenesis and the glyoxylate cycle respectively (Figure 5.1).

Even though bacterial Xfps have previously been characterized, there is no report that any of these enzymes display either substrate cooperativity or allosteric regulation. The *Lactobacillus plantarum* Xfp was purified and characterized specifically to determine if this enzyme displayed substrate cooperativity or allosteric regulation. *L. plantrum* Xfp displayed substrate cooperativity in the form of negative cooperativity for P_i and was found to be an allosteric enzyme inhibited by PEP, OAA and glyoxylate but unaffected by the primary *C. neoformans* Xfp2 allosteric effectors, ATP and AMP. Like with *C. neoformans* Xfp2, PEP and OAA bind at the same or overlapping sites on *L. plantarum* Xfp while glyoxylate binds at a separate site. This study provided the first evidence that at least some bacterial Xfps are allosterically regulated.

To locate the *C. neoformans* Xfp2 allosteric sites, a model of this enzyme was generated from the existing bacterial Xfp structures from *Bifidobacterium breve* and *Bifidobacterium longum*. Ligand docking simulations were performed using PEP and OAA within predicted binding sites. Several sites were investigated by performing site-directed mutagenesis on residues predicted to directly interact with PEP and OAA. Each variant generated was still inhibited by PEP suggesting that those residues, and most likely those sites, are not involved in PEP binding. Even though these studies have yet to reveal the location of the PEP/OAA binding sites, they have provided some interesting insights into other aspects of *C. neoformans* Xfp2 regulation. For example, we

discovered that AMP acts as a very potent activator. AMP was able to rescue at least some activity for most variants that showed a considerable decrease in activity. AMP was able to fully rescue activity of the R66A variant back up to wild type activity values. However, one variant, R571A, showed no increase in activity in the presence of AMP. Therefore it is possible that we have stumbled across a residue that is part of the AMP allosteric site, but additional studies will be needed to show this. In addition, the presence of AMP was able to overcome the decrease in *C. neoformans* Xfp2 activity that occurs at elevated pH values. It is possible that AMP is capable of overcoming what are typically adverse conditions, such as single amino acid mutations and elevated pH, because it induces a very stable, active R state enzyme conformation. Additionally, preliminary studies were performed using a non-hydrolyzable ATP to see if ATP inhibition is dependent on ATP hydrolysis. The non-hydrolyzable ATP did not inhibit the enzyme suggesting that inhibition by ATP may be dependent on ATP hydrolysis, but additional experiments in this area are required to determine if this is true.

Future studies should focus on gaining a better understanding of *C. neoformans* Xfp2 allosteric regulation. Ideally a crystal structure of *C. neoformans* Xfp2 in the presence and absence of allosteric effectors will eventually be obtained. However, to obtain a crystal structure, very pure, concentrated enzyme is required, and in my experience, very little enzyme following purification. Future studies should focus on ways to generate and purify more enzyme by using different expression vectors and possibly a different expression system other than *E. coli*. Until a crystal structure of *C. neoformans* Xfp2 is obtained, the models generated and described in this dissertation

provide the best resource for exploring and identifying the location of allosteric sites. However, studies utilizing the Xfp2 monomer structure have yet to reveal the location of the PEP/OAA binding site. The recently obtained dimer model shows new binding sites formed between both monomers. Therefore future studies should focus on new sites within this Xfp2 dimer model. Also additional studies are necessary to determine if ATP inhibition is dependent upon ATP hydrolysis as preliminary assays using a non-hydrolyzable ATP suggest. Future studies should involve radiolabeled ATP and thin layer chromatography analysis to determine if ATP is hydrolyzed and converted to labeled ADP by *C. neoformans* Xfp2 during inhibition.

These studies have revealed that at least some enzymes in the Xfp family from both fungi and bacteria exhibit substrate cooperativity and are allosterically regulated. The regulation of both *L. plantarum* Xfp and *C. neoformans* Xfp2 by different allosteric effectors, suggests that this enzyme plays different roles in bacteria and fungi. However, such tight regulation of Xfp by several different metabolic intermediates suggests that the production of acetyl phosphate may be an important phenomenon in both bacteria and fungi under various environmental conditions that ultimately influence cellular metabolism.

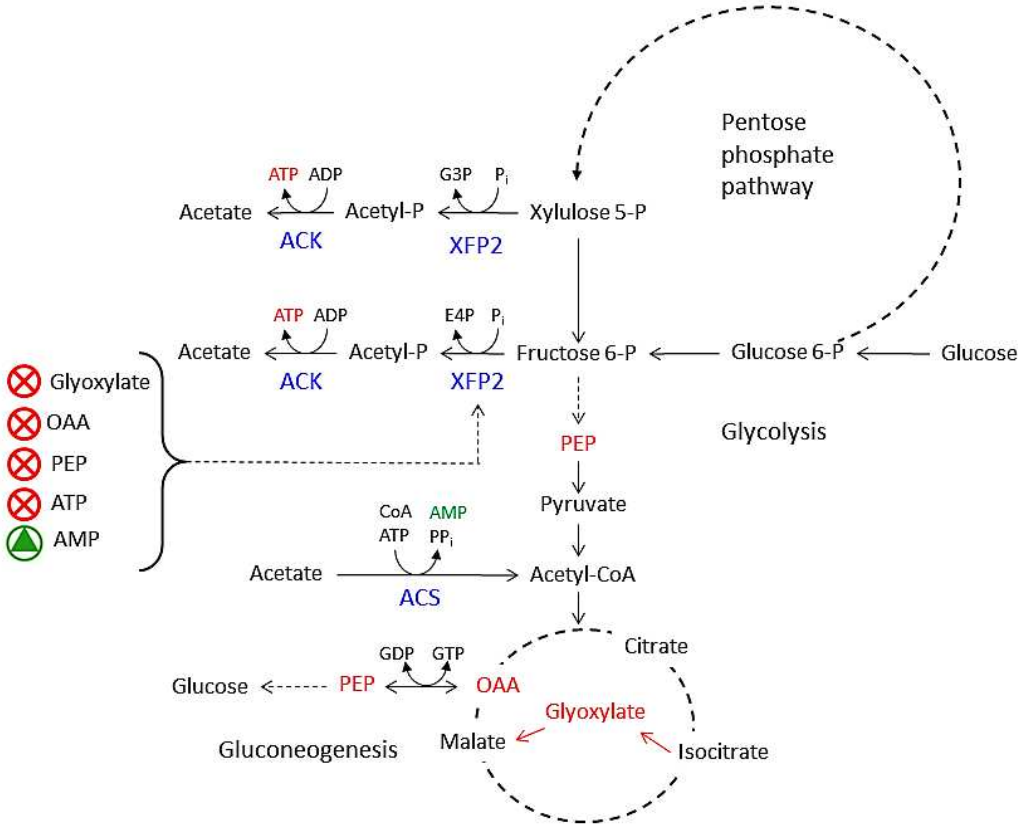

FIG 5.1. Model of how Xfp2 fits into *C. neoformans* cellular metabolism. Inhibitors are labeled in red while activators are colored green.

APPENDIX

Appendix A

A MUTATION OF *CRE1* IN *MEDICAGO TRUNCATULA* THAT SUPPRESSES SUPERNODULATION AND ROOT GROWTH WITH MINIMAL EFFECT ON CYTOKININ RESPONSES

Elise L. Schnabel, Tessema K. Kassaw, Katie F. Glenn, Kerry S. Smith

and Julia A. Frugoli

MATERIALS AND METHODS

Molecular Modeling

Discovery Studio 3.5 software (Accelrys, Inc.) was used to generate a model of the wild type *M. truncatula* cytokinin receptor sensor domain (*Mt*CRE1) based on the *Arabidopsis thaliana* histidine kinase 4 (AHK4) complexed with N6-isopentenyladenine (accession code 3T4J) from Hothorn, *et al.* (2011). The *Mt*CRE1 V97I variant model was generated using the software's Build Mutant function that creates an alteration at the specified residue and optimizes conformation of the mutated and surrounding residues. For both the wild type and V971 variant, the model with the lowest DOPE (Discrete Optimized Protein Energy) score was chosen for further analysis. The Define and Edit Binding Sites From Receptor Cavities function was used to determine the active site for

both the wild type and variant model and the site that overlaid best with the active site of AHK4 was chosen for ligand docking simulations. Ligand docking of the cytokinin ligand N6-isopentenyladenine within the active sites of both the *Mt*CRE1 wild type and *Mt*CRE1 V97I variant models was performed using the Dock Ligands function that docks ligands within a site based on the ligand's interaction with polar and apolar regions within that site.

RESULTS

A model of the membrane external portions of wild type *Mt*CRE1 was generated from AHK4 using Accelrys Discovery Studio 3.5 software (Figure 1a). The loop (amino acids 95-108) containing V97 is positioned distinct from the *Mt*CRE1 ligand binding site (Figure 1a). Alteration of V at position 97 to I (the *cre1-4* defect) does not affect positioning of surrounding residues, and inspection of the overall structures did not reveal any major structural changes between wild type *Mt*CRE1 and the V97I variant, however, the side chain of the amino acid now rotates outward from the loop (Figure 1b). Ligand docking simulations of N6-isopentenyladenine within the active site were performed for both the wild type and variant models to determine if the V97I mutation affected cytokinin binding. These ligand docking simulations did not reveal any differences between the WT and V97I variant in primary hydrogen bonding residues between N6-isopentenyladenine and active site amino acids residues (data not shown).

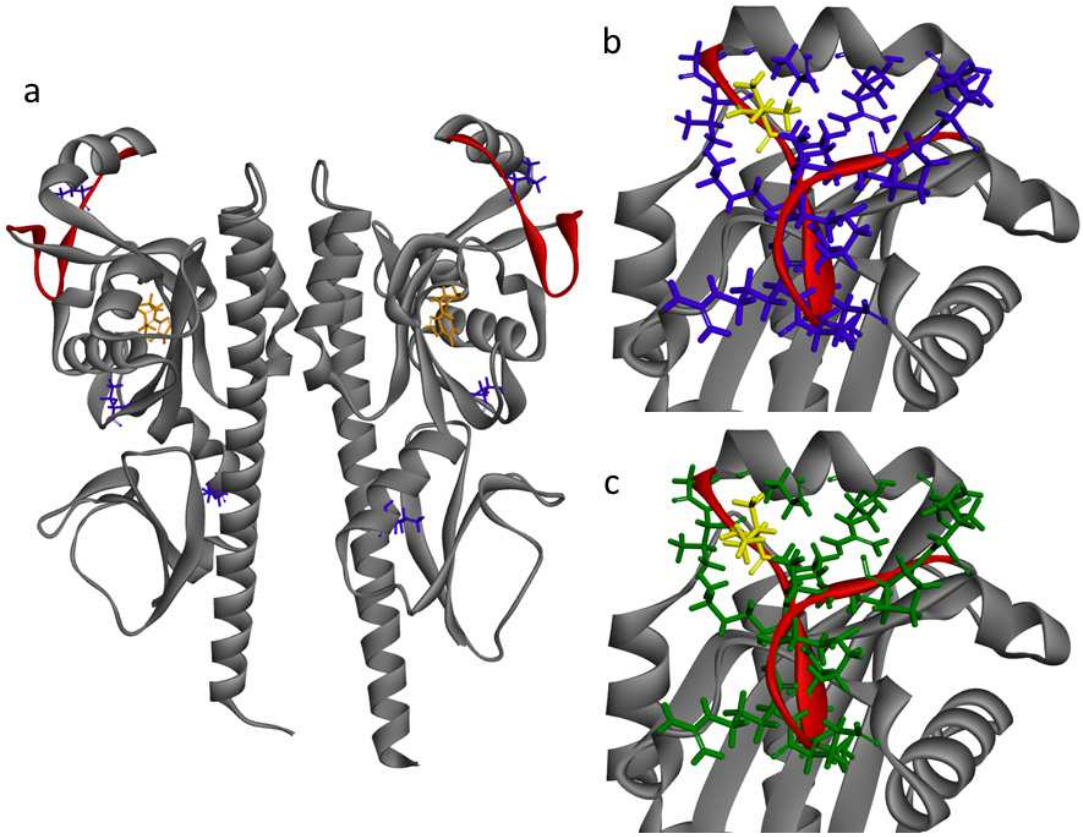

Figure A.1 The amino acid change in the *cre1-4* mutant does not affect the cytokinin binding pocket (a) Ribbon diagram of the predicted tertiary structure of the sensor domain dimer of MtCRE1 complexed with 2iP (yellow) based on the crystal structure of AHK4 (see Materials & Methods). Amino acids altered in sensor domain mutants are shown in purple *(Ljsnf2*, *Mtcre1-4*, and *Atwol-1*). The *Mtcre1-4* mutation resides in a region distal to the cytokinin binding pocket highlighted in red. (b) Close up of red region in (a) turned 90 degrees with amino acid side chains shown in purple. The yellow residue is V97. (c) The same close up but of the mutant structure with amino acid side chains in green and the V97I mutation in yellow.